An investigation of the plasma electrolytic oxidation mechanism for coating of alumina-zirconia nanocomposite

By

Nastaran Barati

Presented to the Faculty of the Graduate School of

The University of Texas at Arlington in Partial Fulfillment

of the Requirements for the Degree of

DOCTOR OF PHILOSOPHY

THE UNIVERSITY OF TEXAS AT ARLINGTON

August 2018

ABSTRACT

AN INVESTIGATION OF THE PLASMA ELECTROLYTIC OXIDATION MECHANISM FOR COATING OF ALUMINA-ZIRCONIA NANOCOMPOSITE

Nastaran Barati, PhD

The University of Texas at Arlington, 2018

Supervising Professor: Dr. Efstathios I. Meletis

Plasma Electrolytic Oxidation (PEO) is an electrochemical surface modification technique which is able to coat ceramic coatings on valve metals from either cationic or anionic species in an aqueous electrolyte. Applying high voltage in the range of 300-600 V is required to achieve crystalline phases. PEO is a clean technology which offers several benefits including high deposition rates, excellent adhesion strength and mechanical properties. One of the interesting capabilities of the PEO process is its ability to form composite coatings.

The following work aims to study the growth mechanism of nanocomposite layers coated by PEO. Two experimental routs have been explored to develop Alumina-zirconia composites on Al 7075 alloy through PEO method. In one route, Zr containing salt has been added to the electrolyte to form ZrO_2 portion of the composite. In another way, ZrO_2 portion of the composite is incorporated from zirconia nanoparticles added to the electrolyte. Potentiostatic and

galvanostatic modes have been applied for all the samples to study the best condition for composite coating formation and surface sensitive properties improvement. Effect of various coating parameters such as PEO voltage, current density, growth time, and electrolyte composition on coatings characteristics has been studied. In this dissertation, the best coating conditions to achieve desirable properties (tribological and corrosion properties) have been reported. Potentiostatic mode by introducing higher energy to the surface, resulted in high hardness and crystalline phases and therefore, better tribological properties. While, in galvanostatic mode by formation of more compact layers, corrosion protection could be achieved. The dissertation is composed of three main chapters in which the microstructural evolution studies are correlated to the surface sensitive properties.

The first part of this work focuses on formation of Alumina-zirconia nanostructured coatings on 7075 Al alloy in a DC potentiostatic mode. The composite coatings were produced in the range of 425-500V in an alkaline electrolyte containing 4g/L K_2ZrF_6. Tribological properties of coatings were investigated using dry sliding wear test against WC balls with a pin-on-disc tribometer. Wear rates were evaluated using optical profilometer. It was shown that the nanostructured alumina-zirconia composite coatings can be formed at voltages >450V. The coating thickness and roughness were in the range of 15.2-24.2 μm and 0.68-2.35 μm, respectively. The distribution of Al, Zr and O in the coatings was uniform. Increasing the PEO voltage led to porosity increment and formation of the high temperature tetragonal zirconia phase (t-ZrO_2). Significant enhancement in tribological properties for coated samples was achieved: under optimum conditions, corresponding to the PEO treatment at 500 V for 200 s, the coating wear rate of 2.62×10^{-6} $mm^3N^{-1}m^{-1}$ and friction coefficient of 0.22 were recorded that are about 120 and 3 times lower than those for the substrate.

In the second part of this work formation mechanism of compact alumina-zirconia nanocomposite coatings on Al alloy through the PEO method in DC galvanostatic mode has been studied. The layers were coated at constant current density of 0.2 A/cm^2 and 100-350 s growth time in an alkaline K_2ZrF_6 containing electrolyte. The characteristics of the coatings were investigated as a function of PEO processing time. Electrochemical properties of the layers were studied by conducting potentiodynamic polarization experiments in 3.5% NaCl solution. The results showed that under the present PEO experimental conditions, alumina-zirconia nanostructured coatings can be produced with 10-30 μm thickness and 0.4-2.35 μm roughness depending on the processing time. Phase analysis showed that the nanostructured coatings contained alumina and zirconia high temperature phases (tetragonal zirconia and a-alumina). Processing for 300 s was found to produce the most compact layer with low surface porosity (0.69%) and 26 mm thickness. This particular PEO treatment was found to reduce the corrosion rate by 2.5 orders of magnitude compared to the uncoated substrate. This significant improvement in corrosion resistance is attributed to the barrier effect of the dense layer and the presence of tetragonal zirconia. The composite coating formation mechanism in this case is oxidation of Al substrate to form alumina and oxidation of Zr^{+4} ions in the electrolyte to from zirconia.

Finally, the last part of the research is dedicated to understand the mechanism of composite formation through PEO method. Alumina-zirconia nanostructured layers were coated on an aluminum alloy by PEO technique in a direct circuit galvanostatic mode at 0.1- 0.4 A/cm^2 current density. The coatings were formed in an electrolyte containing monoclinic nano-ZrO_2 powder as a zirconia source. The microstructure of the produced coatings was studied by transmission electron microscopy (TEM), scanning electron microscopy (SEM) and X-ray

diffraction (XRD) to develop an understanding of the growth mechanism. The investigation of the coating process was complemented with voltage-time response measurements and in-situ optical spectroscopy observations. The results showed formation of various alumina-zirconia composite microstructures as a function of the current density during processing. At the higher current density, the composite layer consists of high temperature phases (tetragonal zirconia and α-alumina) in addition to monoclinic zirconia. High current density introduced larger amounts of zirconia to the coated layer due to the high energy applied to the nanoparticles in the electrolyte. TEM analysis showed formation of four sub-layers across the coating. The coating-substrate interface (sub-layer 1) contained higher amounts of alumina (both α and γ) while the amount of zirconia nanoparticles increased by moving toward the outer surface. In sub-layer 2, formation of tetragonal zirconia was observed resulting from a phase transformation of monoclinic to tetragonal zirconia. In sub-layer 3, the existence of untransformed monoclinic zirconia hints to inadequate energy for the phase transformation due to lower temperatures. At the top region of the coating, sub-layer 4, a shallow amorphous layer was formed due to quenching from the direct contact with the electrolyte. The PE process was found to be responsible for the monoclinic to tetragonal zirconia transformation, while the electrophoretic process facilitated the deposition of the original monoclinic zirconia from the electrolyte. The results showed that the coating mechanism involves a hybrid PE-Electrophoretic process.

ACKNOWLEDGEMENTS

First of all, I would like to express my sincere gratitude and appreciation to my advisor Prof. Efstathios I. Meletis for the continuous support of my Ph.D study and related research, for his patience, motivation, and immense knowledge. His guidance helped me in all the time of research and life. I could not have imagined having a better advisor and mentor for my second Ph.D study. Besides my advisor, I would like to thank the rest of my thesis committee: Dr. Rajeshwar, Dr. Aswath, Dr. Tibbals and Dr. Jiang, for their insightful comments and encouragement.

I am also grateful to Dr. Jiechao Jiang in the Characterization Center of Materials and Biology (CCMB) at the University of Texas at Arlington who gave access to the laboratory and research facilities for his valuable technical advices. I thank my fellow labmates at the Surface and Nano Engineering Laboratory (SaNEL) for all their help and support.

Most importantly, I would like to thank my family: my parents, Mom and Dad for showing faith in me and giving me liberty to choose what I desired. I salute you all for the selfless love, care, pain and sacrifice you did to shape my life. Also, I express my gratitude to my brothers, Alireza and Emad, and my sisters in law, Zohreh and Sepideh, for supporting me spiritually throughout my research and my life in general. I would not be who I am today without you all.

Last but not least, very special thank goes for my lovely husband, Dr. Mehdi Mazar Atabaki, for his continuous and unconditional encouragement and support. I am truly thankful for having him in my life. Thanks for all your patience when I was frustrated!

July 30, 2018

DEDICATION

To my devoted parents

My supportive brothers, Alireza & Emad

and

My lovely husband

Table of Contents

LIST OF TABLES

LIST OF FIGURES

Chapter 1: Introduction & Background

1.1. Introduction and Motivation

Notable properties of aluminum alloys such as high atmospheric corrosion resistance and strength-to-weight ratio lead to a wide range of applications in aerospace and automobile industry. However, beside many advantages of aluminum alloys, their shortcomings in mechanical and tribological properties are obvious. In particular, low hardness and wear resistance as well as high friction coefficient lead to certain restrictions in tribological applications [1, 2].Wear prevention accompanied with minimizing the coefficient of friction will lead to efficient tribological systems [3].Based on increasing demands for aluminum in industry, one of the ways to improve its tribological properties is modifying their surfaces by applying appropriate coatings [4-7].

Due to high strength-to-weight ratio, Aluminum alloys have seen increasing used in the automotive and aerospace industries. However, due to the aluminum alloy's low hardness and poor corrosion properties when compared to other available metals its use is limited to areas in which wear is not a significant factor [8]. While some of aluminum alloys, particularly those of the Al-Si system, have shown improved tribological properties, these alloys have yet to greatly improve aluminum's role in wear situations. The application of a hardened surface coating may be the most effective method of improving the wear performance of aluminum alloys.

As it was noted, most aluminum alloys used for tribological applications contains silicon. In these alloys, the wear resistance is attributed to the hardness of the dispersed Si containing phases in the Al-Si alloys. It has been reported that wear resistance increases with increasing Si

content up to the near-eutectic composition, after which wear resistance decreases as Si content increases [9].

Additionally, some work has been conducted on improving the performance of aluminum alloys through the addition of surface coatings. Research has been conducted on surface coatings, such as nitride and nickel coatings, as well as oFn surface coatings consisting of metal matrix composites. The benefit of these coatings is still being researched, with some coatings, particularly those consisting of Al_2O_3 [10] or Ni_3Al particles [8] created via a metal powder compaction method, showing a marked decrease in wear performance while others, particularly those containing SiC particles [10], showing an improvement in performance. In the previous cases, the Al_2O_3 or Ni_3Al particles tend to pull out of the metal aluminum matrix and act as additional abrasive, whereas the SiC particles remain fixed in the matrix and contribute to increased wear resistance. Additionally, the application of surface coatings in order to improve the surface properties of the metal is inherently difficult due to the well-known tendency of aluminum to immediate form an Al_2O_3 barrier layer upon exposure to air and/or water.

One of the prominent techniques which has been successfully applied to coat valve metals such as Al, Ti, Mg and Zr, is the Plasma Electrolytic (PE) method. This technique has been developed by Russian scientists in the 1960s [4] and is based on plasma creation in an electrolyte. This method can be used to apply a variety of coatings such as oxides, nitrides and carbides. In the case of oxide formation, this method is called Plasma Electrolytic Oxidation (PEO). The PEO is based on applying high voltages to a metal substrate immersed in an electrochemical cell, followed by plasma creation and oxidation of the substrate. This method is an environmentally friendly technique with the ability to form high temperature phases with high

growth rates and adhesion strength. Previous research efforts have been successful in improving surface sensitive properties of valve metals through this method.

Alumina is one of the attractive ceramic oxides that has been developed on the Al substrates through the PEO method [5-7]. However, the tribological performance of the PEO alumina coatings is not satisfactory. In an effort to improve properties of the latter coatings, work on alumina matrix composites has been recently initiated [11-13]. However, a fundamental understanding of the PEO process in producing composite coatings is missing at present.

Alumina-zirconia is one of the most prominent alumina-based composites with desirable mechanical properties arising from the high hardness of alumina and high fracture toughness of zirconia. These mechanical properties make alumina-zirconia coatings potentially applicable to improve tribological properties of Al substrates [14].

Another attractive feature of the PEO method is that it can provide the opportunity to incorporate components from the substrate and electrolyte to form composite coatings. This potential in addition to aforementioned advantage of this method can open new areas to produce novel composite coatings to overcome current application limitations. Thus, there is a current need to understand the PEO mechanism of producing nanocomposite coatings and fully explore the potential of this technique. In addition, the effect of PEO processing parameters on microstructure of nanocomposite coatings and its relation to resulting properties needs to be studied.

1.2. Aluminum alloy 7075

Al and its alloys are prominent for industrial applications because of their lightweight and high strength to weight ratio. The main application of these alloys is in airplane, automotive and

transportation industries. However, beside many advantages of aluminum alloys, low hardness and wear resistance as well as high friction coefficient lead to certain restrictions in their applications [15-16]. Based on increasing demands for aluminum in industry, one of the ways to improve its tribological properties is applying appropriate coatings [17-20].

1.3. Alumina- Zirconia composite

Alumina is one of the most versatile and widely used ceramic oxides based on its mechanical and thermal properties. Various crystal structures of this material lead to different properties and applications. The most stable phase of this material at room temperature is α-Al_2O_3 with hexagonal structure. There are also other phases (θ and γ) at lower temperatures which transform to α-Al_2O_3 at high temperatures. High melting temperature (2054 °C), high resistance to corrosion and electrical resistivity are some of the main properties of this material [21]. One of the alumina weaknesses that restrict its application is low fracture toughness and high friction coefficient. To overcome this limitation, composites of this material have been developed [22].

Zirconia is one of the engineering ceramics with high melting point (2370°C) and desirable mechanical properties. It can exist in three crystallographic forms, monoclinic, tetragonal and cubic. The most stable crystal structure of zirconia at room temperature is monoclinic which transforms to other phases as shown below [23]:

$$monoclinic \underset{\sim 950^{\circ}C}{\overset{\sim 1170^{\circ}C}{\rightleftharpoons}} tetragonal \overset{2370^{\circ}C}{\rightleftharpoons} cubic \overset{2680^{\circ}C}{\rightleftharpoons} liquid$$

In this case, transformation from tetragonal to monoclinic phase is accompanied by expansion which is the base of transformation toughening mechanism and therefore, high fracture toughness in this material [24-26].

Study the alumina-zirconia phase diagram at very low percentages of alumina shows formation of a solid solution in ppm range which is negligible (Figure 1-1). While, at higher amounts of zirconia, alumina and zirconia can coexist as two separate phases in a composite form. In this composite, a strategic ceramic with good tribological and mechanical properties can be achieved based on the high hardness of alumina and high fracture toughness of zirconia [27].

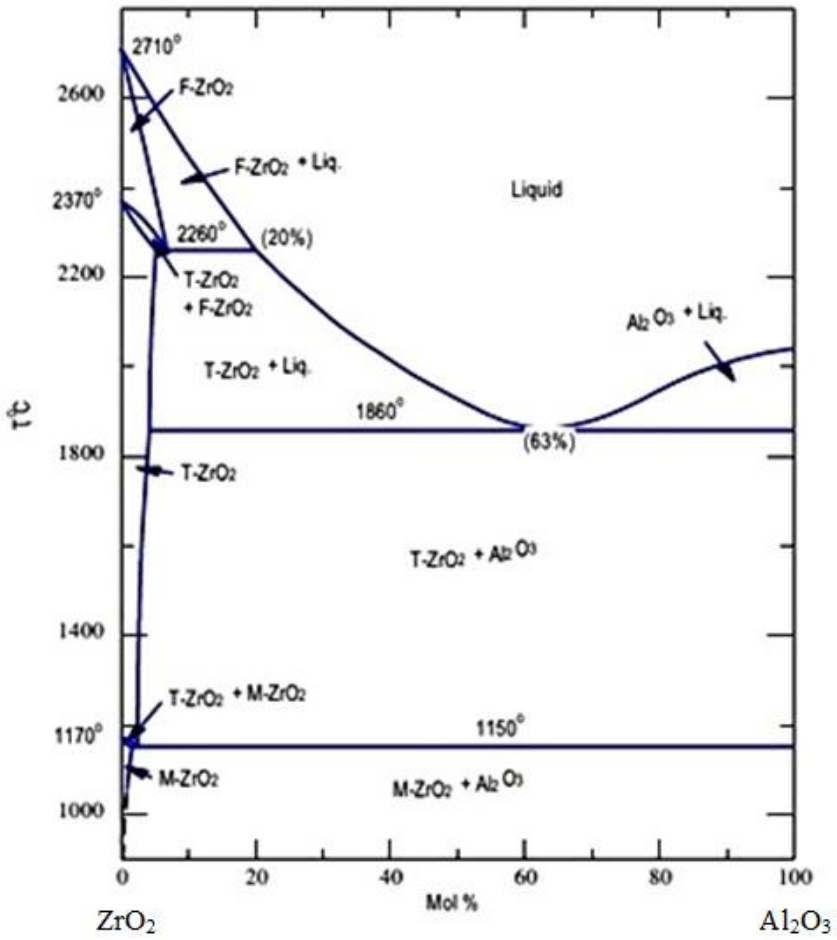

Figure 1-1Alumina-Zirconia phase diagram [21].

Tribological properties of materials are related to parameters such as hardness, fracture toughness, Young's modulus, crystal structure, etc. [28]. In addition, the materials microstructure can have critical influence on tribological properties [29]. In the case of hardness, based on the Archard equation, wear rate is inversely proportional to the hardness of the material [30]. Also, Hah, et. al. [31] have shown that in alumina based ceramics, hardness is related to particle size through the Hall-Petch relation and therefore, hardness increase due to decrease in particle size will improve wear rate in these materials. Furthermore, roughness and porosity are other parameters that affect tribological properties. It should be noticed that the effect of these parameters should take in account together. Based on the aforementioned properties of the alumina-zirconia composite in addition to characteristics affecting tribological properties, the potential of this composite for tribological properties improvement is probable [32-34].

1.4. Alumina- Zirconia coatings

Due to the prominent properties of alumina-zirconia, coating of this composite on various substrates through different methods has been studied. Thermal spraying methods such as plasma spray have been used to apply this composite as thermal barrier coatings with good corrosion and oxidation resistance [35, 36]. Other coating methods such as sol-gel, Physical Vapor Deposition (PVD) and Chemical Vapor Deposition (CVD) have been used as well with emphasis in mechanical and tribological properties investigation [37- 39].

Chen, et. al. [40] studied the formation of Al_2O_3-ZrO_2 composite coatings by air plasma spraying on titanium alloy. The microstructure, microhardness and toughness of various Al_2O_3-ZrO_2 composite coatings were studied. The result showed that in the composition close to the eutectic point of Al_2O_3-ZrO_2 pseudo-binary system, amorphous phase with denser microstructure

and lower porosity was formed due to the rapid cooling and solidification. The microhardness of the Al_2O_3-ZrO_2 coatings decreased as decreasing of the content of Al_2O_3. And the microhardness of the Al_2O_3-ZrO_2 coatings was significantly higher than that of single phase Al_2O_3coating and ZrO_2 coating due to the composites higher melting degree and denser microstructure. The Al_2O_3-ZrO_2coatings possessed considerably high toughness, which is attributed to their special microstructure. Crack deflection, crack bridging, phase transformation of ZrO_2 and stress release of micro-cracks improved the toughness of the Al_2O_3-ZrO_2 coatings [40].

In another research, Berghous, et. al. [41] studied hardness, wear resistance and fracture toughness of High Velocity Oxygen Fuel (HVOF) alumina- zirconia coated layers. Increase in wear resistance and also thermal resistivity was their main motivation for this research. Results showed higher hardness and therefore, higher wear resistance for the crystalline layers with lower porosity content. Furthermore, effect of ZrO_2 amount on tribological and mechanical properties of alumina- zirconia coatings has been studied. Based on the results, by increasing ZrO_2 amount, tribological properties have been improved. In this case, by adding zirconia to the coatings, the friction coefficient of the alumina coatings decreased from $\mu = 0.62$ to $\mu = 0.19$. Furthermore, in alumina-zirconia coated layers, the wear resistance is improved by increase in tetragonal zirconia phase (Figure 1-2) [42, 43].

Also, the mechanical and thermal properties of the alumina-zirconia composite coatings prepared by laser chemical vapour deposition have been studied. In this research it has been shpwn that the γ-Al_2O_3–t-ZrO_2 nanocomposite films exhibited high nanoindentation hardness (28.0 GPa) and heat insulation efficiency (4788 J $s^{-1/2}$ m^{-2} K^{-1}) [44]. In the case of corrosion properties, some studies showed nearly 10 times improvement in corrosion resistance of the steel

substrates by applying alumina- zirconia coatings. This corrosion properties improvement can be attributed to the chemical stability of the formed phases [45, 46].

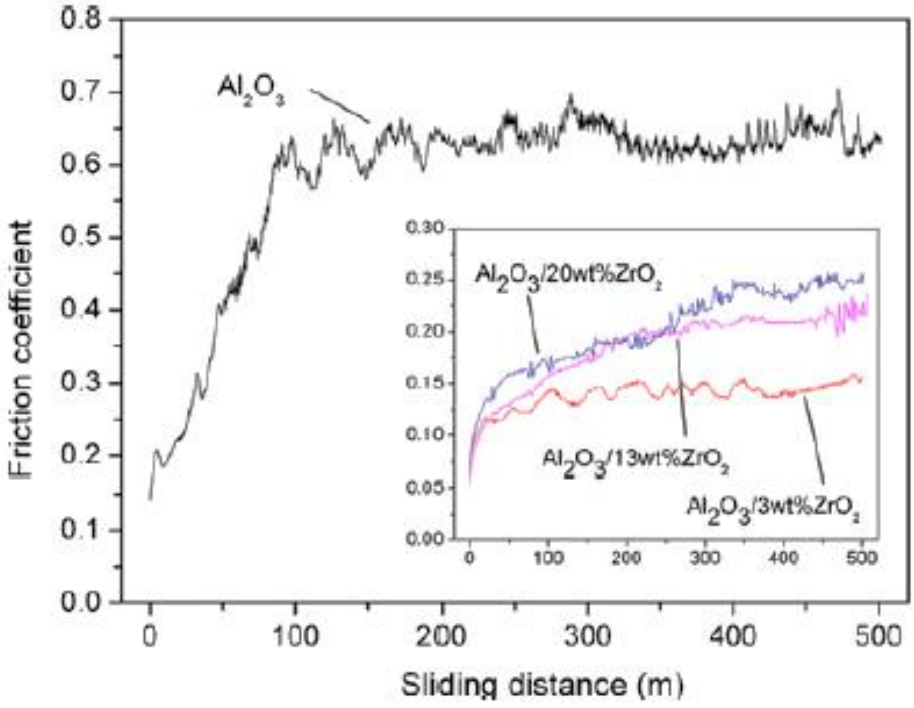

Figure 1-2 Friction coefficient improvement for alumina coatings by adding zirconia and composite formation [42].

In most of the coating methods, the layers are amorphous which need post processing like heat treatment to obtain the desirable phase composition. This phase transformation follows by expansion which results in coating detachment. Furthermore, thermal expansion mismatch of the coating and substrate and weak adhesion of the coated layers are some of the other disadvantage of the various coating methods [47].

1.5. Plasma Electrolytic Oxidation

PE is an electrochemical coating method based on plasma formation in an appropriate electrolyte. This method consists of two major categories: PEO and Plasma Electrolytic Saturation. PEO method is based on oxide formation on valve metals such as Al, Ti and Mg while PES includes carburizing, borizing and cleaning of the surfaces [48-50]. This method is similar to anodizing but taking place at higher voltages (400-700 V). An electrochemical reaction cell contains an electrolyte with controlled pH and electrical conductivity. Applying high voltages to the metal substrate serves as an anode while immersing in the electrolyte initiates electrochemical reactions. A characteristic voltage- current response of the PEO process is shown in Figure 1-3. As it can be seen, at low voltages, ohmic law exists and an oxide layer forms at the electrolyte- metal interface. At voltage U_2, the passive layer starts to dissolve, while by more voltage increasing, passivation occurs and a porous oxide layer forms again. By reaching the breakdown voltage of the oxide layer at higher voltages, dielectric breakdown and micro arcing as a result of impact ionization happens. At very high voltages, arcing could be destructive for the coated layers and therefore prevents more coating growth [50]. In the PEO process, arcing and discharges will result in high temperatures in the range of 4000-10000 K can form high temperature phases [50].

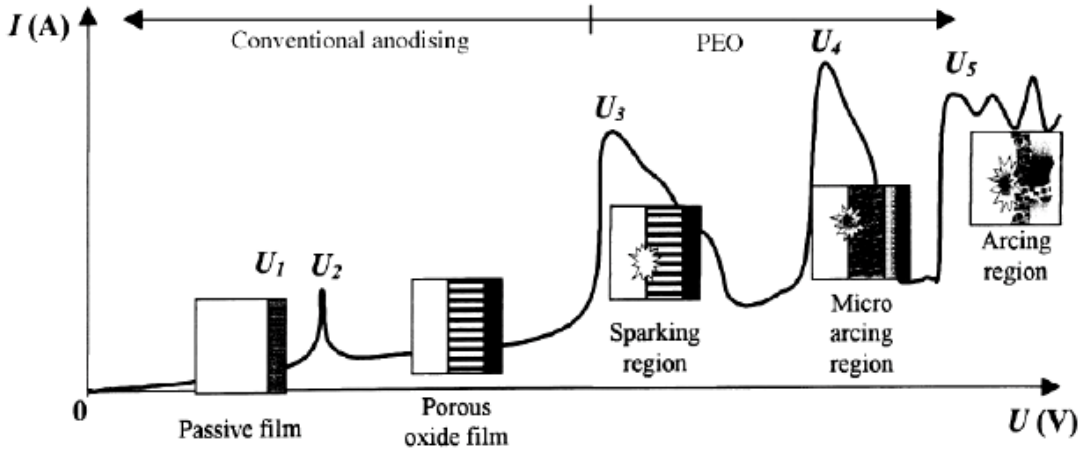

Figure 1-3 Current–voltage diagram for the PEO processes, discharge phenomena are developed in the dielectric film on the electrode surface [50].

1.6. Alumina- Zirconia coatings via PEO

One of the interesting capabilities of the PEO process is its ability to form composite coatings. Alumina-zirconia composite with high hardness, strength, wear resistance and fracture toughness is one of the most prominent engineering ceramics. Due to its properties, coating of this composite on various substrates through different methods has been studied [51-52]. Recently, PEO process has been applied to coat alumina-zirconia coatings on Mg, Zr and Al substrates [53-59].

In 2008, Yan, et. al. [53] applied alumina-zirconia coating with 90 μm thickness on zirconium substrate through PEO process. Investigation of the layers showed hardness about 1630 HV and adhesion strength of 43.5 MPa. Also tribological properties improvement in these samples has been correlated to the formation of hard α- Al_2O_3. In 2010, these researchers studied the corrosion properties of the coatings. Results showed dependency of microstructure and properties of the coatings to the electrolyte composition [54]. In another research by Malinovschi, et. al. [55], PEO process was employed in a galvanostatic regime on Zr-2.5Nb alloy to produce

Al_2O_3/ZrO_2 composite coatings. The correlation between the electrolyte concentration and the coating characteristics was studied. By optimization the electrolyte composition, significantly increased tetragonal crystal structure, particle size, hardness, and adhesion strength and corrosion resistance occurred. High concentrations of *t*-ZrO_2, found in polycrystalline zirconia provided superior mechanical and anticorrosion properties [55].

Zhang, et. al. [56] developed a nanoplate-like α-Al_2O_3 out-layered Al_2O_3-ZrO_2 coating on Zr substrate by micro-arc oxidation. The amount and crystallinity of Al_2O_3 increased gradually from inner layer to the coating surface. The coating showed noticeable improvement in wear-resistance. It indicated that the nanoplate-like α-Al_2O_3 out-layered Al_2O_3-ZrO_2 is a potential coating for particular head replacement [56].

PEO of the Zircaloy-2 has been investigated by Cheng, et. al. under a pulsed-bipolar current regime to develop coatings of high wear resistance [57]. They showed coating growth kinetics, cell potential-time responses and discharging behaviors depend significantly on the electrolyte concentration. The coatings formed in dilute aluminate electrolyte reveal a three-layered structure, with pancake structures at the coating surfaces. “Soft sparks” occur during PEO in dilute aluminate electrolyte, causing a relatively fast growth of the inner layer and resulting in a large amount of alumina-enriched material beneath the pancake structures, and hence an increased wear resistance of the coating. In contrast, more homogenous coatings, free of pancakes, result with the concentrated electrolyte. The main phase in the coatings is *t*-ZrO_2, with γ-Al_2O_3 also present in coatings formed in the latter electrolyte. The coatings formed in the concentrated electrolyte displayed a high wear resistance, even for thin coatings formed for short times, which is attributed to the relatively high alumina content of the coatings [57].

In the case of Mg substrate, alumina-zirconia coating has been applied in an alkaline aluminate electrolyte under AC currents. The coated layers showed high thermal shock and corrosion resistance [58]. Also in another effort, using silicate and phosphate electrolytes containing zirconia nanoparticles, alumina-zirconia coatings have applied on Mg substrate. In this case due to the high temperature during PEO process, monoclinic zirconia powder transformed to tetragonal zirconia [59].

Regarding aluminum and its alloys, Matykina, et. al. [60, 61] coated alumina-zirconia coatings on Al substrate by the PEO method. They used phosphate and silicate electrolytes and have investigated microstructure of the coated layers by variation of electrolyte and applied current type. Also, in 2011, in a similar research, nanoporous coatings have been prepared on Al substrate in $ZrOCl_2$ electrolyte under AC current. The main objective of this research was investigation of coating microstructure by variation of the PEO voltage. They have concluded that by increasing the PEO voltage, porosities could eliminate due to high temperatures, melting and sintering of the coated layers [62].

Literature review showed that formation of composite coating by the PEO method has been attempted by many questions remained. Due to the potential of this method to incorporate a second phase from electrolyte, composite formation by this method should be studied in detail. Furthermore, because of high potential of alumina-zirconia to improve surface sensitive properties of Al alloys, coating of this composite by PEO method can be noticed. Study the incorporation of a second phase in a PEO coated composite along with tribological behavior of the composite should be considered to develop a new model for the PEO coated Al alloys.

1.7. Objectives of this research

In this research, two experimental routes are explored to develop alumina-zirconia composite coatings. In one route, formation of the zirconia phase is attempted by addition of Zr containing salt in the electrolyte. In the second route, the zirconia phase is incorporated via addition of zirconia nanoparticles in the electrolyte. The PEO coating mechanism is investigated along with their produced microstructures. The main objectives of the present research can be summarized as development and understanding the PEO mechanism for depositing nanocomposites. Deposition of a composite coating involves the oxidation of the substrate material producing an oxide matrix and a second component/phase incorporated from "additives" in the electrolyte. The additives can have the form of ions or solid nanoparticles carrying a negative charge.

Previous studies have shown that the form of power applied to the substrate have a controlling effect in the PEO process. Thus, the effect of different ways of applying power (potentiostatic and galvanostatic) on the deposition process is investigated. Tribological and corrosion properties of all the coated layers in potentiostatic and galvanostatic modes and their relationship with microstructural evolution are investigated. The results for the samples with the best corrosion ant tribological properties have been reported. Emphasis is paid on possible competition between oxidation kinetics of the substrate and second phase deposition rate from "additives" in the electrolyte. Alumina-zirconia composite is used as a model system and in view of the above gained knowledge to:

- Investigate the coatings characteristics and their microstructure evolution as a function of processing parameters.

- Investigate the tribological behavior of the produced alumina-zirconia coatings and develop an understanding with PEO coating microstructure and tribological behavior.

In the following chapters, alumina-zirconia composite coating formation through PEO mode has been studied. Galvanostatic and potentiostatic modes have been used to study microstructural evolution of the coatings. Surface sensitive properties are correlated to the coating conditions and therefore, microstructural evolution. Mechanism of the composite formation through PEO method has been studied as well.

Chapter 2: Development of the Al_2O_3-ZrO_2 nanostructured coatings on Al substrate and understanding the microstructure and tribological behavior

2.1. Introduction

Notable properties of aluminum's such as high atmospheric corrosion resistance and strength-to-weight ratio lead to a wide range of applications in aerospace and automobile industry. However, beside many advantages of aluminum alloys, their shortcomings in mechanical and tribological properties are obvious. In particular, low hardness and wear resistance as well as high friction coefficient lead to certain restrictions in tribological applications [1, 2]. Wear prevention accompanied with minimizing the coefficient of friction will lead to efficient tribological systems [16].

Based on increasing demands for aluminum in industry, one of the ways to improve its tribological properties is modifying their surfaces by applying appropriate coatings [17,18, 63, 64]. In this regard, composite ceramic coatings with high hardness and wear resistance are potential candidates. Among them, alumina-zirconia composite coatings are one of the contestants to improve mechanical, tribological and thermal properties of aluminum substrates. For this purpose, different coating methods have been previously used [65-67].

The PEO method has been used to prepare this coating on different substrates [54, 58, 62, and 68]. As explained in detail in previous papers [50, 69, 70, 71], this method relies upon creation of plasma micro-discharges at the surface of a valve-metal electrode immersed in an appropriate electrolyte by applying a high voltage. High coating growth rate, excellent adhesion strength (caused by its formation due to the conversion of the metal substrate), high hardness and

tribological properties are some of the advantages of PEO [72, 73], which determine the potential of this method to solve the tribological weaknesses of Al substrates.

There appear to be only few studies in the field of alumina-zirconia composite coatings on Al by PEO [60-62, 68]. Tang et al. [68] have produced alumina-zirconia PEO coatings on 2A70 aluminum alloy in an alkaline electrolyte in a pulsed bipolar mode. They achieved alumina-zirconia coatings comprising α-Al_2O_3, γ-Al_2O_3 and t-ZrO_2 phases by optimizing electrolyte concentration. In this paper, just the effect of electrolyte concentration on the coating's microstructure and phase formation is reported which emphasizes to the required more studies about this coating. In this regard, investigation of PEO effective parameters such as voltage, current and coating growth time on microstructure and properties of the coatings can be substantial. Furthermore, study of the formation possibility of this coating under different PEO modes (DC, AC unipolar) can be noticed. The formation and microstructure of Zr-containing PEO coatings on Al substrates in $ZrOCl_2$ solutions were studied by Shoaei-Rad et al. [62, 74]. They produced nanoporous zirconia-alumina layers under AC-PEO conditions but didn't investigate any properties of the coatings. The fact that effects of electrolyte composition on the microstructure and phase formation were mainly reported for such coatings emphasizes the need for more studies, revealing effects of other parameters, such as electrical regimes and treatment time, on the coating microstructure and properties.

Rare numbers of reported researches in the field of alumina-zirconia PEO coatings in addition to remarkable hardness and tribological properties of this composite corroborates the need for researches on tribological properties of these coatings [75]. Therefore, formation of such composite material to improve tribological properties of Al substrates is addressed in this research. Detailed studies of the effects of applied voltage on the coating thickness,

microstructure, chemical and phase composition are carried out; surface topography, roughness and tribological properties including specific wear rate and friction coefficient of coatings are investigated as well.

2.2. Materials and methods

Rectangular samples with dimensions of 10mm×10mm×5mm made from 7075 Al alloy were used as the substrates. Before PEO treatments, the samples were polished with emery papers to achieve a surface roughness of Ra ≈ 0.1 μm, then cleaned with acetone and deionized water.

A little attention has previously been paid to the development of stable zirconium containing electrolytes, which is one of the most important aspects in achievement of uniform and homogenous coatings. Therefore, electrolyte composition was preliminary optimized to repeatedly achieve uniform PEO coatings in a potentiostatic DC mode. The coatings were prepared an aqueous alkaline suspension (pH=10.65) containing (g/L): 4 K_2ZrF_6, 6 NaH_2PO_4 and 2 KOH. The treatments were carried out for 200 s in a double walled beaker with water-glycol coolant flow to keep electrolyte temperature below 30 °C. DC voltage in the range 425-500 V was provided by a 10 kW Sorenson model SGA-3u power supply.

X-ray diffraction (XRD) analysis was used to determine coatings phase composition. The scans were performed in a grazing incidence mode with glancing angle of 10°, 2θ range from 10° to 67° and step size of 0.01°, using Bruker D8 Advance X-ray diffractometer (Cu Kα radiation, λ=0.154 nm) operated at 40 mA tube current and 40 kV accelerating voltage. The microstructure and cross-sectional morphology of the PEO-treated samples were examined using Hitachi S-4800 Field Emission Scanning Electron Microscope (FE-SEM) and Hitachi S-3000N SEM.

Energy Dispersive X-ray (EDX) spectroscopy was used for elemental analysis and mapping of coating surfaces and cross-sections. The coating thickness was measured from SEM cross sectional images. Also, quantitative studies of coating porosity were carried out using an ImageJ image analysis software. To evaluate the surface topography and roughness for a wide range of surfaces a Wyko NT-9100 optical profilometer was used.

A pin-on-disk tribometer (CSM Instruments) was used to carry out the wear tests in dry sliding conditions at room temperature and relative humidity of 4-58%. The system is similar to the pin-on-disk wear tester described in the standard ASTM G99. The samples were tested against WC/Co balls (Vickers hardness≈22GPa) of 6 mm diameter at 2N normal load and 2.5 cm/s linear speed for 20.000 laps. Friction coefficient (μ) was monitored during the wear tests and wear tracks were studied after that to determine the wear volume and specific wear rates of coated and uncoated samples using an optical profilometer. Microhardness measurements were conducted on the polished cross-sections of the coatings using a LM 300AT instrument with Vickers indenter at 100 g-force loading.

2.3 Results and discussion

In this experiment, the K_2ZrF_6 salt has been used as a zirconium precursor. The main concern about the Zr containing aqueous electrolytes is their stabilization. A great tendency for Zr^{+4} ions to from $Zr(OH)_4$, will result in $Zr(OH)_4$ precipitation and therefore creation of unstable electrolytes (Reactions 1,2,3) [68,76]. In this regard, surfactants such as poly phosphates can stabilize the electrolytes by creating surface charges. In this case, NaH_2PO_4 surfactant was used to stabilize the K_2ZrF_6 containing electrolyte by creating negative charges on the surface of

chemical species in the electrolyte (Reactions 4,5) [77]. The following reactions proceed in the electrolyte:

$$K_2ZrF_6 \rightarrow 2K^+ + (ZrF_6)^{-2} \quad (2\text{-}1)$$

$$(ZrF_6)^{-2} \rightarrow Zr^{+4} + 6F^- \quad (2\text{-}2)$$

$$Zr^{+4} + 4H_2O \rightarrow Zr(OH)_4 \downarrow + 4H^+ \quad (2\text{-}3)$$

$$NaH_2PO_4 \rightarrow Na^+ + H_2PO_4^- \quad (2\text{-}4)$$

$$H_2PO_4^- \rightarrow 2H^+ + (PO_4)^{-3} \quad (2\text{-}5)$$

Figure 2.1 represents the voltage and current responses during PEO processing of Al substrates in the potentiostatic mode. In the early stages, current-voltage variation is obeying the ohm's law to some extent. While at later stages, by starting micro arcing phenomena and increasing the oxide coatings growth rate, the current in the system will decrease as a result of resistivity of the barrier anodic oxides.

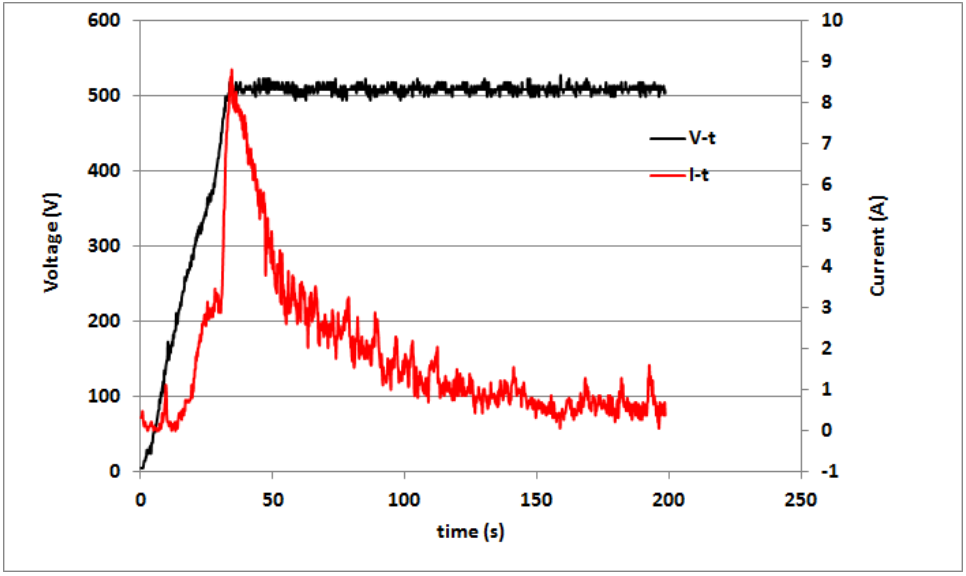

Figure 2-1 Voltage and current variations of Al substrates during PEO processing at constant voltage of 500V.

The results of phase analysis of PEO coatings on 7075 Al alloy produced at different voltages are presented in Figure 2.2 Diffraction peaks of aluminum with different intensities are detectable in all samples, indicating possible thickness/porosity variations in coatings produced at different voltages. X-ray diffraction pattern of the sample treated at 425V shows small γ-alumina peaks without evidence of crystalline zirconia phases, which is likely due to insufficient energy provided at this voltage to create crystalline zirconia. In the samples coated at voltages higher than 425V, tetragonal zirconia (t-ZrO_2) peaks appear beside those of α- and γ-alumina. ZrO_2 formation in PEO process is attributed to the movement of negatively charged $(Zr(OH)_4)^-$groups toward the positive pole (Al substrate) which led to Zr oxidation. Since the tetragonal zirconia formation temperature is about 1170 °C, based on the appearance of t-ZrO_2, discharge temperatures at different PEO voltages can be approximately estimated. Furthermore, the PEO process resulted in the formation of cubic γ-alumina and hcp α-alumina phases, which are the thermodynamically metastable and stable alumina phases, respectively. The main precursors for the metastable γ-alumina are aluminum hydroxides [73].

In alkaline solutions, the reaction of Al^{3+} ions from the substrate with OH^- ions of the electrolyte results in formation of aluminum hydroxides that under high temperature and pressures is de-hydrated to the metastable alumina phases. In addition, despite of the phosphate existence in the electrolyte, there is no evidence of any phosphorus-based crystalline phases in the X-ray patterns. Therefore, it can be concluded that the broad peak between ~ 20 to 45 degree is detectable in different samples, can be attributed to the phosphorus containing compounds in amorphous form.

In PEO coatings, formation of high temperature crystalline phases arises from reaching the melting temperatures followed by rapid quenching of melted products in discharge channels.

Hence formation of tetragonal zirconia in PEO process can be predictable, while stabilization of tetragonal zirconia at room temperature is quite notable. According to the literature, the stabilizing of *t*-ZrO_2 can be achieved by two mechanisms: one, particle size effect that in this case there exist a critical crystallite size, beyond which the tetragonal to monoclinic transformation occurs. The other one is the constraint effect in which a matrix can stabilize *t*-ZrO_2 phase, as it has been reported in the silica–zirconia materials [78]. In the case of alumina-zirconia composites, many studies showed that alumina could stabilize the tetragonal zirconia without dopants just by inhibiting the nucleation and the grain growth of zirconia [79, 80]. The stability of tetragonal phase according to this argument is attributed exclusively to the smaller surface energy of the tetragonal zirconia [81].

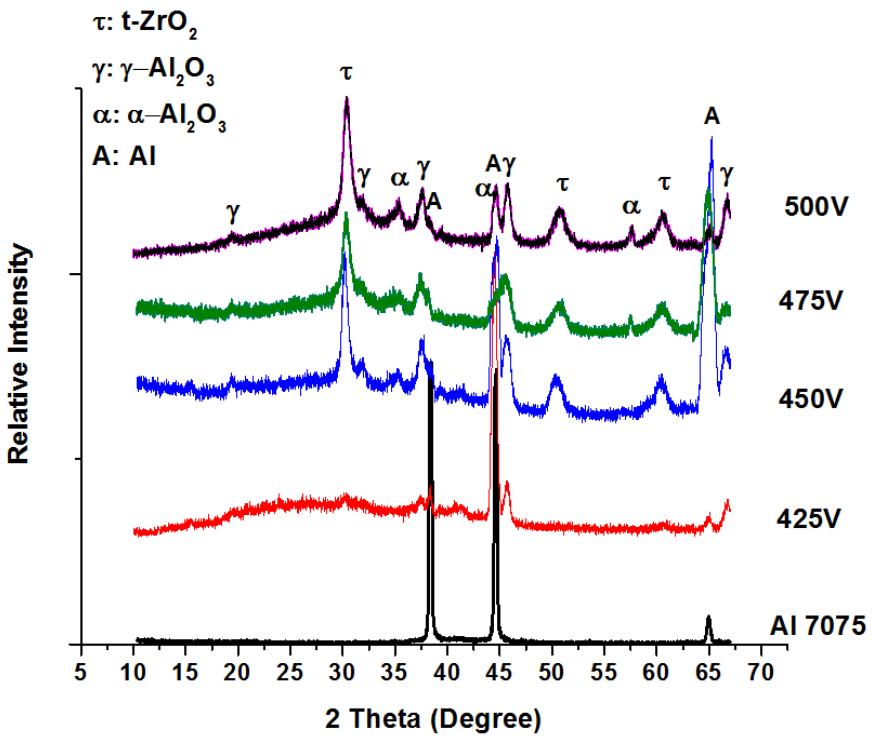

Figure 2-2 XRD patterns of the samples coated at different PEO voltages.

Figure 2-3 illustrates surface morphologies of oxide layers obtained at different PEO voltages. By increasing PEO voltage, larger pores with some cracks are developed on the surface. Increasing the pore size at higher PEO voltages can be attributed to the variation of discharge channel sizes. In the sample treated at 425 V, just some small pores have been created due to low-energy small discharges occurring on the surface. However in samples treated at higher voltages, higher energies led to stronger electron avalanches producing powerful discharges that result in larger discharge channels and therefore a coarser porosity and crack formation.

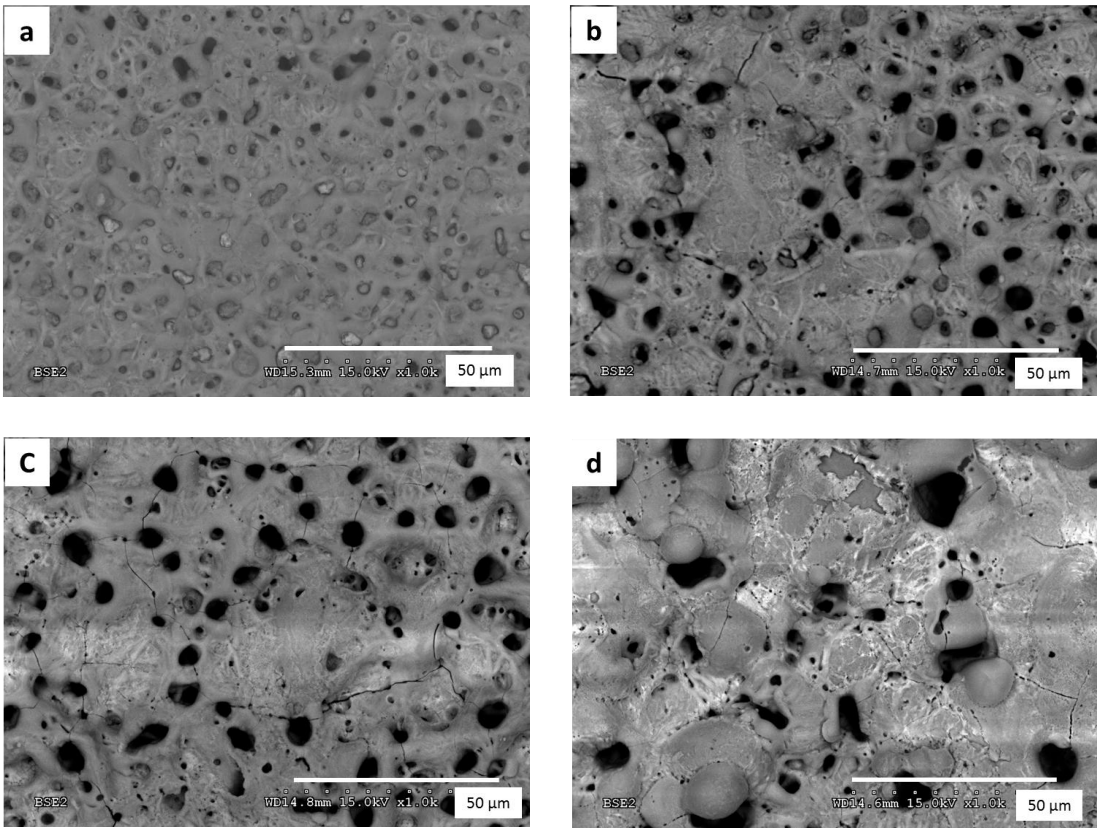

Figure 2-3 SEM images of surface morphology of PEO coatings at different voltages: (a) 425V, (b) 450V, (c) 475V, (d) 500V.

Results of quantitative analysis of coating morphology provided in Table 2-1 indicate porosity increment from 2.13% to 7.23% with increasing PEO voltage from 425V to 475V.

Applying voltages higher than 475 V led to fewer but larger pores. In this case, intensive discharging seems to have affected only some weak parts of the formed coating because of higher coating's resistance and therefore breakdown voltage.

Table 2-1 Porosity, roughness thickness and hardness of samples coated at different PEO voltages.

Voltage	425	450	475	500
Porosity (%)	2.13±0.1	11.63±0.9	11.77±0.6	7.23 ±0.3
Ra (μm)	0.68±0.1	1.41±0.3	1.55±0.1	2.35±0.1
Thickness (μm)	15.2±1.2	14±0.8	15.8±1.1	24.2±1.3
Hardness (GPa)	8.2	12.4	13.9	15.8

Results of EDX analysis of surface composition are provided in Table 2-2. Existence of Al, O, and Zr elements is evident in all coatings formed at different PEO voltages. For the coatings produced by PEO treatments of Al substrate in an alkaline electrolyte, existence of Al on the surface was predictable. The main concern was regarding Zr incorporation in the coatings, which is confirmed by both the EDX and XRD results. Only for the sample coated at 425V, notwithstanding the EDX pattern, indicating presence of 24.1 at% Zr in the surface layer, the XRD results show no evidence of crystalline zirconia phases, which can be explained by the amorphous character of Zr containing compounds in this coating. Also, the EDX results show an increase in Zr content with increasing PEO voltage which can be attributed to a higher energy provided to the surface. In this regard, higher driving forces for electrolyte anions to move toward discharge channels and get involved in chemical reactions is the main reason of Zr increment in the oxide at higher applied voltages.

Table 2-2 EDX Elemental compositions of coatings applied at different PEO voltages.

Voltage	Al (at%)	O (at%)	Zr (at%)
425	32.5	43.3	24.1
450	28.7	42.8	28.5
475	28.4	42.3	29.3
500	26	43.6	30.3

To get information about elemental distribution through the surface (especially Zr), EDX map of the coated surface has been taken (Figure 2-4). Surface EDX maps reveal a homogenous distribution of elements through the coating. The results confirmed no existence of Zr containing discrete particles in micron range to be detected with conventional SEM.

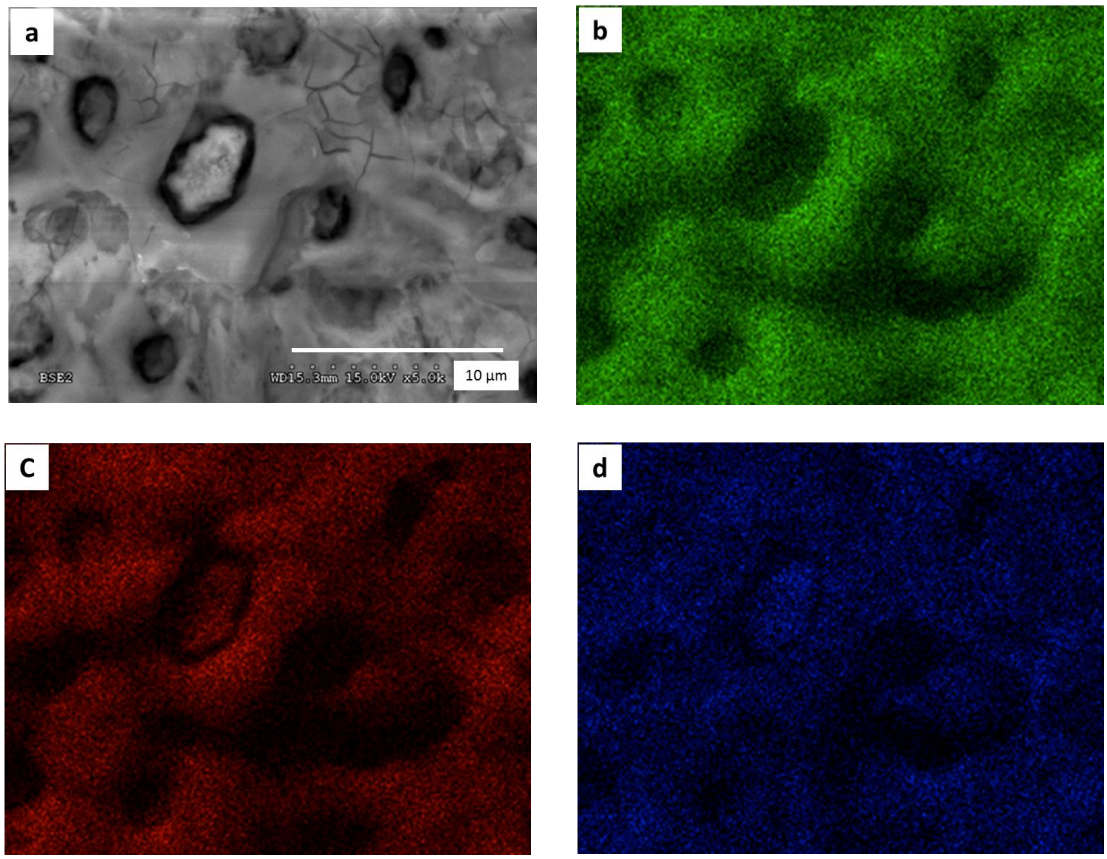

Figure 2-4 Surface EDX map of the coating formed at 475V for different elements (a) SEM image (b) Al; (c) O; (d) Zr.

Investigation of coating surface in nano-scale using FE-SEM image of the sample coated at 475 V reveals the creation of nanostructured coating with grain sizes in the range of approximately 20-40 nm (Figure 2-5).

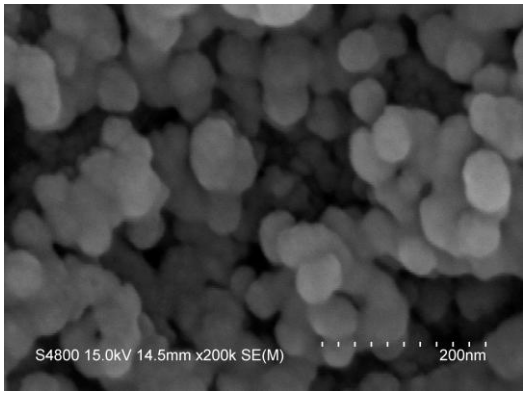

Figure 2-5 High resolution SEM image of sample surface coated at 475 V.

Figure 2-6 shows cross-sectional SEM images of the PEO coatings produced at different voltages. By increasing the PEO voltage, accretion of coating thickness is evident to some extent, while the microstructure becomes more porous and cracked. In the samples treated at higher voltages, sharp edges at the coating-substrate interface and also at the surface can be observed, which could be related to the destructive nature of powerful discharges developed under these conditions. Furthermore, larger discharge channels at higher PEO voltages can be responsible for formation of these deformed edges. The results of coatings thickness measurement using the cross sectional SEM images are reported in Table 2-1.

The coatings thickness varies in the range of 14-24 μm depending on the PEO voltage which indicates growth rate of about 7.2 μm/min for the sample coated at 500V. In comparison with normal coating growth rates of PEO layers on aluminum reported by other researchers which lies in the range of 0.2-3 μm/min, this rate is quite remarkable [82, 83]. This notable achievement can be attributed to the applying direct currents with high voltages which results in increasing the micro-discharges and intensity of plasma discharges. On the other hand, it has been proven that the coating thickness and therefore growth rate is largely influences by anions in the electrolyte system. The chemical composition of the electrolyte and presence of fluoride or phosphate species fosters the growth rate of PEO coatings [84, 85]. In the PEO process, there is a competition between the formation of oxide coating and dissolution of the coating. At higher electrolyte temperatures, the electrolyte becomes more aggressive and hence its dissolving power gets maximum and the dissolution of aluminum predominates, but at lower electrolyte temperature, the liberated heat during PEO growth is completely, uniformly and effectively cooled and dissipated from the specimen to the bulk of the solution. Hence, maximum thickness, growth rate and coating ratio were obtained using electrolytes with low temperatures [86]. In this

research, keeping electrolyte temperature as low as room temperature can be the other reason for high coating growth rates.

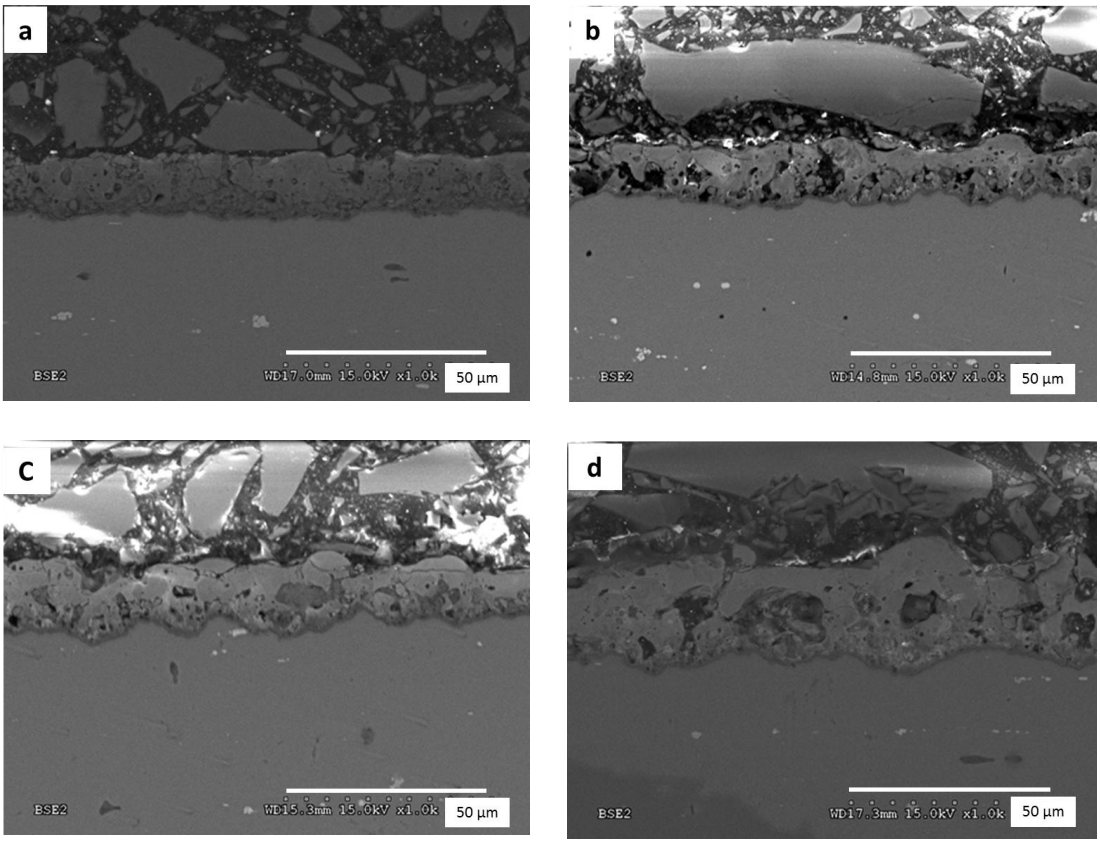

Figure 2-6 SEM cross-section images of coatings at different voltages (a) 425V, (b) 450V, (c) 475V, (d) 500V.

A typical EDX line scan across the thickness of coated sample at 475 V is shown in Figure 2-7. Distribution of Al, O and Zr elements across the coating is uniform and the elemental composition is approximately the same for different coating depths. This uniform elemental distribution in cross section indicates a simultaneous addition of different elements during the PEO process and therefore formation of a uniform coating. From the SEM image (Figure 2-7a); a barrier layer at the coating-substrate interface is notable (marked with arrows). According to the EDX line scan; this area contains high amounts of aluminum that can be referred to as a

transition region between the substrate and the coating, which confirms the creation of conversion coatings in the PEO process.

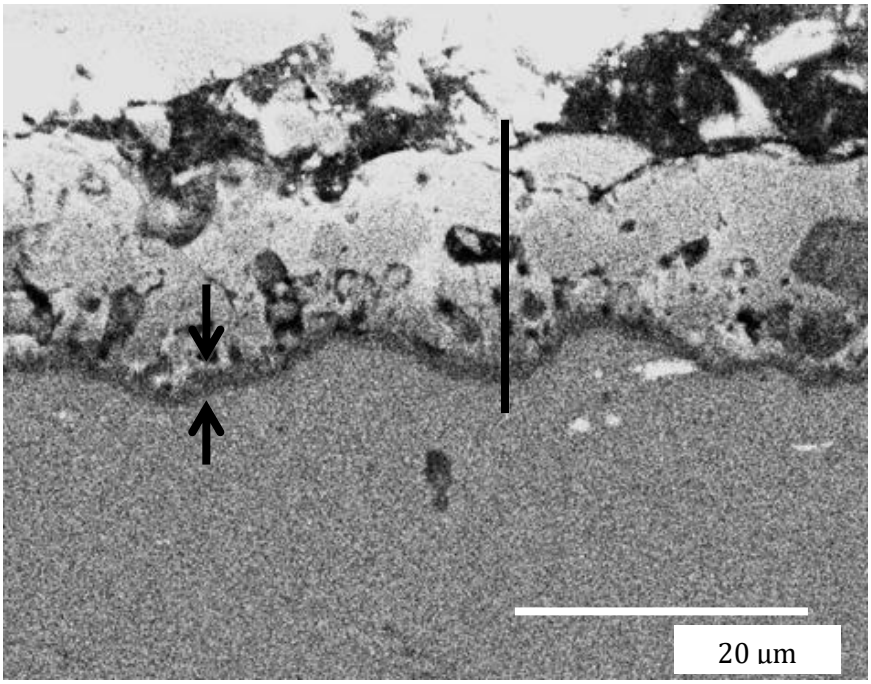

A

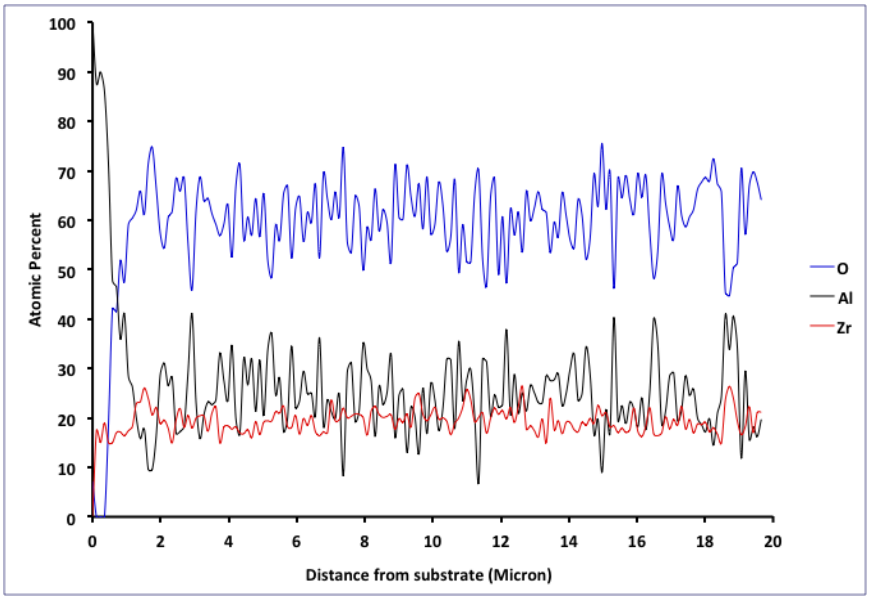

B

Figure 2-7 Cross-sectional EDX line scan analysis of sample coated at 475 V.

Plots of friction coefficient versus sliding distance (m) and corresponding number of cycles (n) obtained during pin on disc tests are represented in Figure 2-8 The mean friction coefficients (μ) of samples, summarized in Table 2-3, indicate high friction of bare Al-7075 sample (about 0.69) under 20,000 laps with 2 N sliding force. This value has decreased to 0.22 by applying alumina-zirconia PEO coating at 500 V. Three times reduction of friction coefficient for coated sample at 500 V in comparison with the bare sample implies effectiveness of obtained composite coatings for tribological applications.

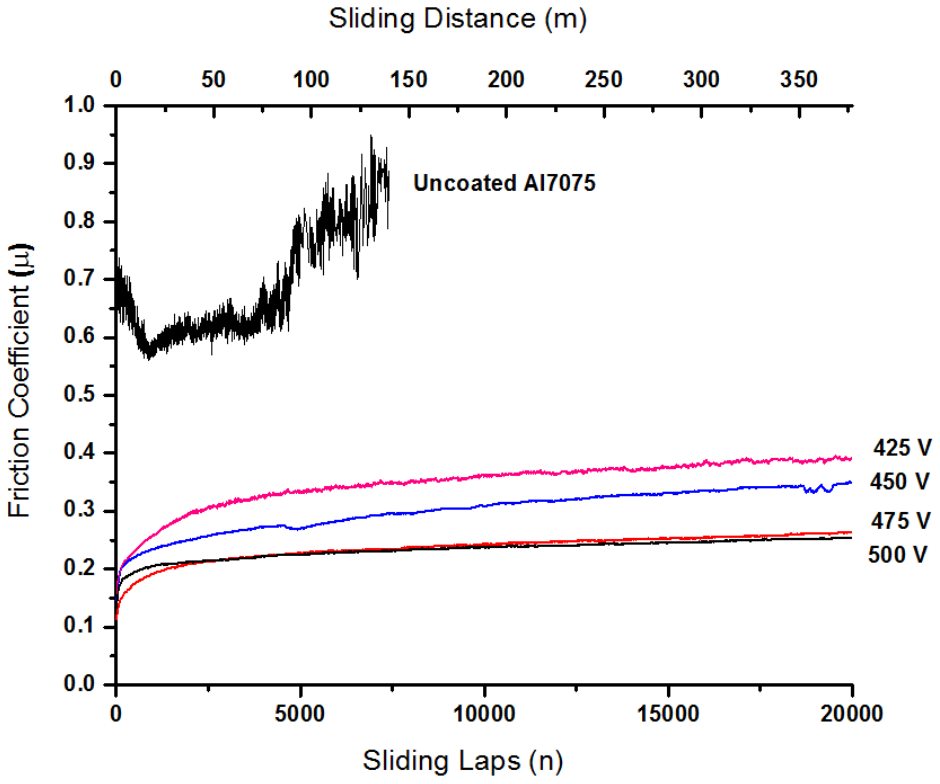

Figure 2-8 Friction coefficient of bare and PEO coated Al substrates versus sliding distance (m) and sliding laps (n).

Profilometer images of wear tracks on coated and bare samples after the wear tests are represented in Figure 2-9. The depth of the worn tracks is a good representative of wear of the

samples. To quantify this relationship, specific wear rates of samples have been calculated using equation (2-6) [87]:

$$K_w = \frac{V_w}{F.s} \left(\frac{mm^3}{N.m}\right) \quad (2\text{-}6)$$

where V_m is the wear volume measured by means of surface profilometry, F is applied load, and s is the sliding distance. Some authors indicate a limit of 10^{-6} mm^3N^{-1} m^{-1} for K_w value above which a material is no longer considered wear-resistant in unlubricated tribological applications [87]. According to the specific wear rates of the coated and bare samples in table 3, 120 times decrement of specific wear rate for coated sample at 500 V in comparison with bare aluminum is remarkable.

Table 2-3 Friction coefficients and wear rates of samples coated at different PEO voltages.

PEO Voltage (V)	Mean Friction Coefficient (μ)	Specific Wear Rate (mm^3N^{-1} m^{-1})
0 (Bare Al7075)	0.69	4.51E-04
425	0.34	4.73E-05
450	0.30	2.10E-05
475	0.23	4.92E-06
500	0.22	2.62E-06

A scrutiny of the available literature reveals that the tribological characteristics of materials are highly dependent on their composition, hardness and also surface characteristics such as roughness [16, 88]. In this research, although the coatings consist primarily of aluminum,

zirconium and oxygen, the concentrations of these elements and also the coating phase composition are strongly dependent on the coating preparation conditions.

Roughness as a major parameter was directly affecting the friction coefficient of samples. Data summarized in Table 2-1 show higher roughness for samples coated at higher PEO voltages. Therefore, the sample PEO coated at the highest voltage is expected to exhibit the highest friction coefficient. Unexpectedly, this sample shows the lowest coefficient of friction, which indicates the other possible affecting parameters discussed in the following section.

The wear behavior of most sliding couples obeys the Archard relationship in which wear volume loss is inversely proportional to the hardness of the worn surface [3]. In this research, at higher PEO voltage, both tetragonal ZrO_2 and α-Al_2O_3 phases are increasing which confirm higher hardness of coatings (Table 1-1). Furthermore, it has been proved that in addition to hardness, fracture toughness as a resistivity of material to crack propagation can be determining for materials wear resistance [89]. In alumina-zirconia composites with outstanding fracture toughness, use of zirconia particles as a reinforcing element improves wear resistance through the suppression of crack initiation and propagation due to the higher value of fracture toughness [90]. In this case, transformation of tetragonal zirconia to monoclinic phase accompanied with volume expansion can take place due to thermal stresses in combination with the mechanical stresses generated by the load during sliding. Stress induced transformation can form compressive stresses near the surface which can help the material resist crack propagation and hence reduce wear [90]. Therefore, significant improvement in wear resistance of the sample coated at the highest voltage (500V) can be attributed to the formation of hard phases accompanied with the highest amount of tetragonal zirconia phase.

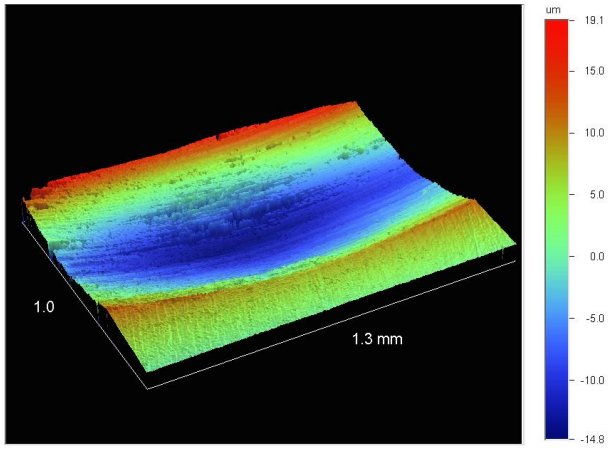

a

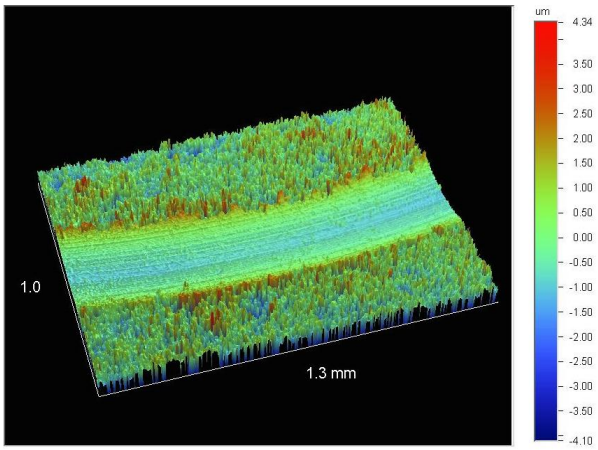

b

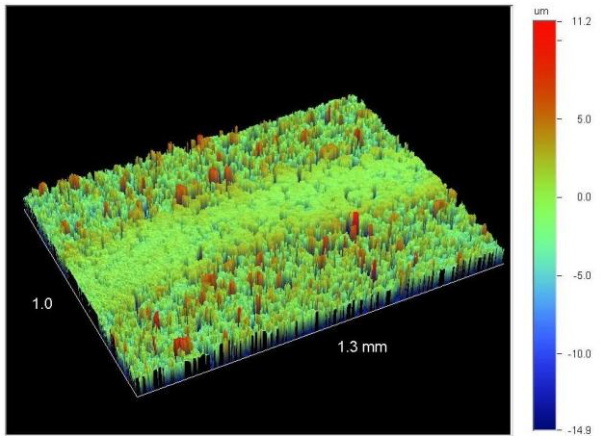

c

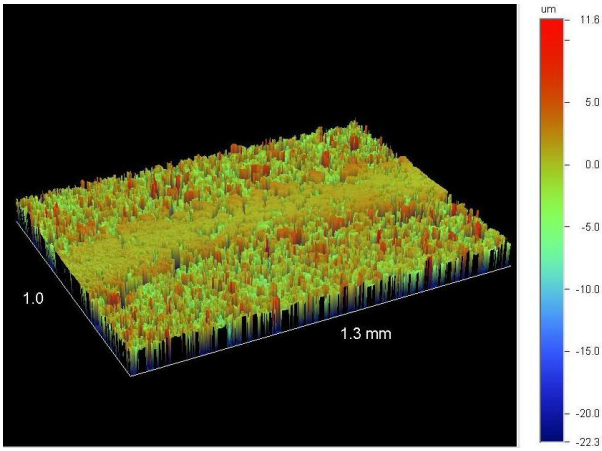

d

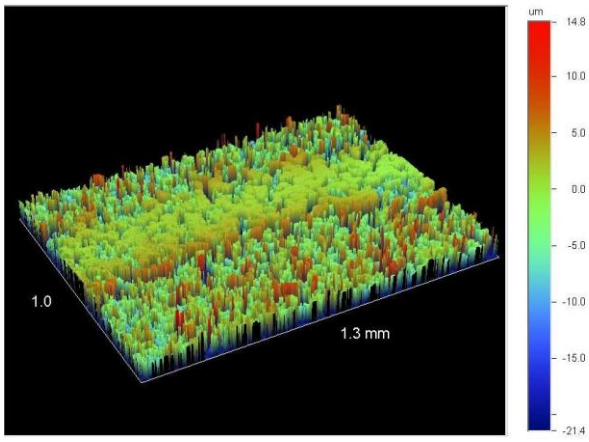

E

Figure 2-9 Profilometer images of wear tracks after sliding wear test for different samples; (a) bare Al7075, (b) coated at 425V, (c) coated at 450V, (d) coated at 475V, (e) coated at 500V.

2.4 Conclusions

Alumina- zirconia coatings were formed through DC PEO treatments in alkaline electrolytes containing K_2ZrF_6. Microstructure, surface topography and roughness, phase and chemical composition of coatings were strongly related to the PEO voltage. FE-SEM examination proved formation of composite of alumina-zirconia nanostructures with the particle size in the range of 20- 40 nm. By increasing the PEO voltage, the coating porosity and roughness were increased due to powerful discharges providing higher local energy density to the surface. The coating roughness was in the range of 0.68-2.35 μm. Tetragonal zirconia was achieved without using any stabilizer, just by optimizing the PEO conditions. Furthermore, α and γ-alumina phases were formed in PEO coatings at voltages higher than 425 V. By increasing PEO voltage, the coating thickness increased slightly with rough edges developed due to the destructive effect of powerful discharges on the surface. The alumina-zirconia PEO coatings effectively improved the tribological properties of Al alloy substrates. For the coatings produced under optimized conditions, friction coefficient of 0.22 and the mean wear rate of about 2.62×10^{-6} ($mm^3N^{-1}\ m^{-1}$) have been achieved, which are about 3 and 120 times lower than those for the Al substrate in the same pin on disk test.

Chapter 3: Microstructural evolution of Alumina- Zirconia coatings produced by Plasma Electrolytic Oxidation on Al alloy for corrosion resistance improvement

3.1 Introduction

Microstructural studies in chapter 2 led to understanding the correlation between PEO coating conditions and tribological behavior of alumina-zirconia coatings. In this chapter, due to the potential of alumina-zirconia composite to improve corrosion properties, this surface sensitive property has been studied in terms of coating condition and mechanism. After the investigation of corrosion behavior for all the coatings in galvanostatic and potentiostatic modes using variety of process parameters; in this chapter, the results for the best samples are reported. The potentiostatic mode, resulted in better corrosion behavior.

Aluminum and its alloys are prominent for their formability and high strength to weight ratio as well as high thermal and electrical conductivity [91-93]. In addition, Al alloys have good corrosion resistance in most natural environments due to passivity and creation of a thin oxide surface layer. However, the oxide layer (1-5 nm thick) deteriorates in aggressive media and restricts the extensive application of Al alloys [1, 94, and 95]. Furthermore, the presence of Zn in 7075 Al alloys deteriorates the atmospheric corrosion resistance of the alloy and limits its application [3]. To overcome this limitation, ceramic compact coatings have been applied to improve the corrosion properties of metals [96, 97, and 98].

PEO is an electrochemical coating technique, with the capability of creating well-adhered conversion coatings. PEO has been extensively applied on Al and its alloys to improve their

surface characteristics [99, 102]. Application of a high voltage during PEO results in spark discharges and complicated chemical reactions producing two types of oxide films, a compact barrier next to the interface followed by a porous film [103]. Due to the superior mechanical and physical properties of the barrier layer, the PEO coatings can protect the substrate against corrosion.

Zirconia is a promising coating material due to its high strength, chemical and mechanical stability and excellent corrosion resistance. These outstanding properties of zirconium oxide attracted significant interest from many researchers to consider PEO ZrO_2 based coatings. Luo et al. have improved the corrosion resistance of Mg substrates by about two orders of magnitude by applying alumina-zirconia PEO coatings [58]. Furthermore, literature review reveals the improvement in corrosion properties of Zr substrates by applying alumina-zirconia dense layers obtained by optimizing the electrolyte composition in the PEO process [54].

However, corrosion properties of alumina-zirconia composite layers on Al substrate by the PEO method have rarely been considered. Furthermore, it has been shown that phosphate and fluoride in the electrolyte are beneficial in improving corrosion resistance due to formation of barrier layers [50, 104]. In the present work, the growth of alumina-zirconia layers on aluminum substrates from a K_2ZrF_6 and NaH_2PO_4 containing electrolyte by PEO was investigated. The primary objective of this work was to explore the PEO method's potential to create dense layers and improve the corrosion protection of Al substrates. In this regard, DC galvanostatic PEO with different coating growth times has been applied. Detailed studies on microstructure, chemical and phase composition of the coatings were carried out. The relationship between electrochemical behavior of the layers and their characteristics was also studied.

3.2 Materials and Methods

Cylindrical 7075 aluminum alloy samples 10 mm in height and 15 mm in diameter were employed as substrates. Prior to PEO treatment, the samples were mechanically polished to achieve a mean surface roughness of Ra≈0.1 μm. Subsequently, all samples were cleaned with acetone and ethanol, rinsed in deionized water and then dried in an air stream.

A stable electrolyte containing K_2ZrF_6, KOH and NaH_2PO_4 with molar ratios of 2:2:3 was prepared by optimizing the pH value in the alkaline region (pH=10.5). Further details on electrolyte preparation procedure have been provided in a previous publication [100]. A double-walled glass container of 500 ml volume was used as the reaction cell through which cooled water/glycol mixture was pumped in order to keep the electrolyte temperature below 25°C. Stainless steel was used as the counter electrode and the 7075 aluminum alloy substrate served as the anode electrode. A Sorensen DC power supply model SGA-3u with 10 kW power was used for plasma generation. The PEO treatments were carried out in the galvanostatic mode at constant current density of 0.2 A/cm^2 and different coating growth times (100-350 s).

The voltage variation was recorded during the PEO treatment using an oscilloscope (TDS2000- Tektronix). GI-XRD was carried out utilizing a Bruker D8 Advance X-ray diffractometer using Cu Kα radiation (40 kV, 40 mA). Phase analysis was performed using the Jade software. The microstructure and cross-sectional morphology of the coatings were investigated using a Hitachi S-3000N SEM. Also, High Resolution (HR) SEM was conducted by using a Hitachi S-4800 Field Emission microscope to examine the microstructure of the composite coatings. The surface porosity of the produced layers was characterized by image analysis software (ImageJ). The thickness of the produced layers was determined through metallographic cross-sectioning. The elemental composition was investigated by energy

dispersive spectroscopy (EDS). The mean surface roughness (R_a) of the PEO coatings was measured by using a Wyko NT-9100 optical profilometer.

The electrochemical behavior of the PEO layers was investigated by conducting anodic polarization experiments. An EG &G corrosion measurement system model 273 was utilized with computer interface. The experiments were carried out in 3.5% NaCl aqueous electrolyte (pH=6.6) under ambient conditions in a three-electrode cell. Samples were mounted in an epoxy resin with only the treated surface exposed. Graphite electrodes and a saturated calomel electrode (SCE) were utilized as counter and reference electrodes, respectively. Anodic polarization measurements were conducted in a de-aerated environment by purging Ar gas. The polarization scans started at 200 mV below the open circuit potential (OCP) and were continued up to 800 mV above the OCP with a scan rate of 1 mV/s.

3.3 Results and Discussion

3.3.1 PEO coating characteristics

Figure 3-1 shows the voltage variation versus coating growth time during PEO of Al-7075 substrate at constant current density of 0.2 A/cm^2. Three different stages in the voltage-time response can be observed which are in close agreement with the previous reports about the PEO process [19].

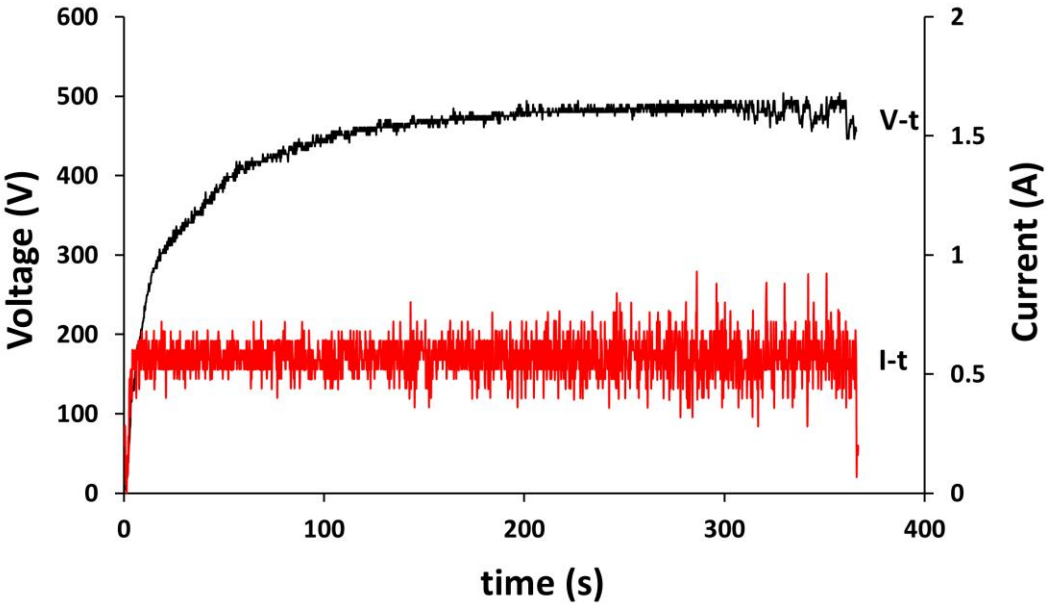

Figure 3-1 Variation of voltage and current versus PEO growth time at a current density of 0.2 A/cm^2.

An almost linear increase in the voltage at the early stage of the process demonstrates a relatively uniform growth of a passive oxide barrier layer. Meanwhile subsequent passivation-dissolution sequential steps lead to a decrease in the slope of the curve, which is followed by electrical discharges at the breakdown voltage of the oxide layer. After that, the voltage increases slightly and the voltage–time slope decreases further while a large number of small size micro discharges appear, evenly distributed over the entire surface. Following that stage, the slope remains almost constant (critical voltage). However, at longer growth times, intensive arcs appear on the surface, which can destroy the coated layer and can be verified by the observed fluctuations of voltage and current in the last stage of the treatment (Figure 3-1).

Figure 3-2 presents SEM images of alumina-zirconia layers coated at the same current density (0.2 A/cm^2), but at different processing times (100-350 s). It is evident that pores of different sizes are formed on the surface. It is also noted that the surface porosity is vanishing by

increasing the PEO growth time up to 300 s. This observation is supported with the quantitative estimation of the surface porosity of the coatings using image analysis software (Table 3-1).

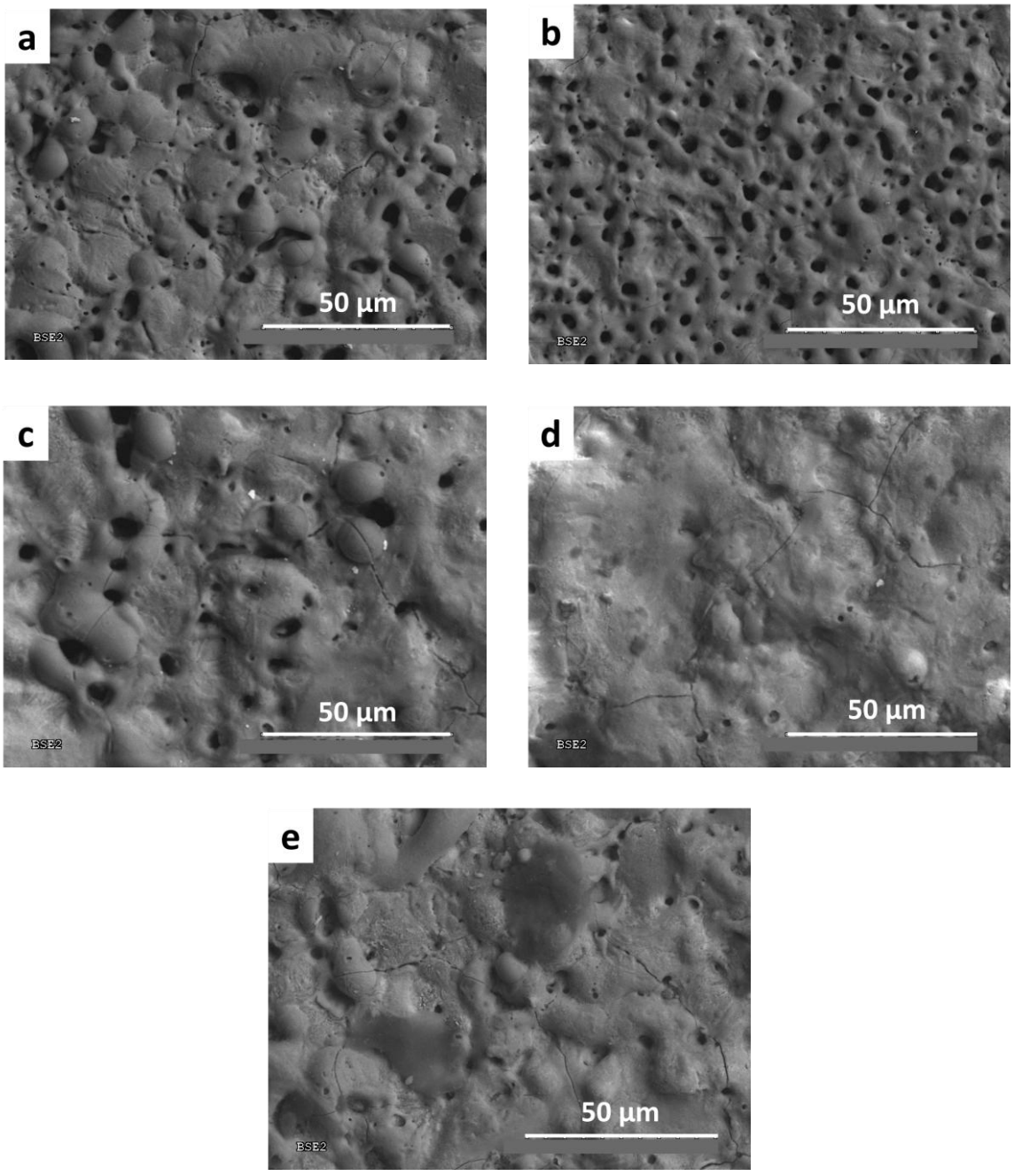

Figure 3-2 SEM images of coatings obtained at current density of 0.2 A/cm^2 and growth time of (a) 100 s (b) 200 s, (c) 250 s, (d) 300 s, and (e) 350 s.

Based on the voltage-time response (Figure 3-1), the layers coated at short growth times, just experienced the primary stages of the PEO process. In the samples coated at longer growth time, a voltage increase produced an increase in the density of intensive arcs and high temperatures. As a result, surface melting and filling in the primarily created pores occurred. According to the nature of the PEO layers, preparation of such compact layers by this method is noticeable which can be applicable in improving mechanical and electrochemical properties of the substrate material.

Table 3-1 summarizes the percentage of surface porosity, R_a and coating thickness as a function of processing time. The results suggest that under the present processing conditions, a critical growth time is reached at about 300 s. The sample processed for that period of time shows the lowest porosity and roughness while its thickness seems to have reached a maximum. Longer PEO processing simply indicates the intense arcing effect that prevails at longer times.

Table 3-1Characteristics of the alumina-zirconia layers coated at 0.2 A/cm^2 current density and different growth times.

Coating growth time (s)	100	200	250	300	350
Surface Porosity (%)	8.81	6.58	4.39	0.69	1.16
R_a (μm)	2.35	1.55	0.86	0.43	1.41
Thickness (μm)	14±3	20±4	26±4	25±7	21±6

Three-dimensional surface profiles of the PEO coated samples at different growth time are shown in Figure 3-3. The 3D surface profiles clearly show a much smoother surface for the sample treated for 300 s, Figure 3-3(c). This surface morphology is also reflected in the measured R_a values. As shown in Table 3-1, the surface roughness of the coatings varies from 0.43 to 2.35 μm in the layers coated for 300 s and 100 s, respectively. The smoother surface of the sample coated at 300 s can be attributed to the surface melting that arises from higher

temperatures during the PEO process. This surface smoothing phenomenon is valid only up to an optimum growth time. Increasing the growth time beyond that point resulted in intensive arcs that can degrade the initial coated layer and hence form rougher surfaces, Figure 3-3(d).

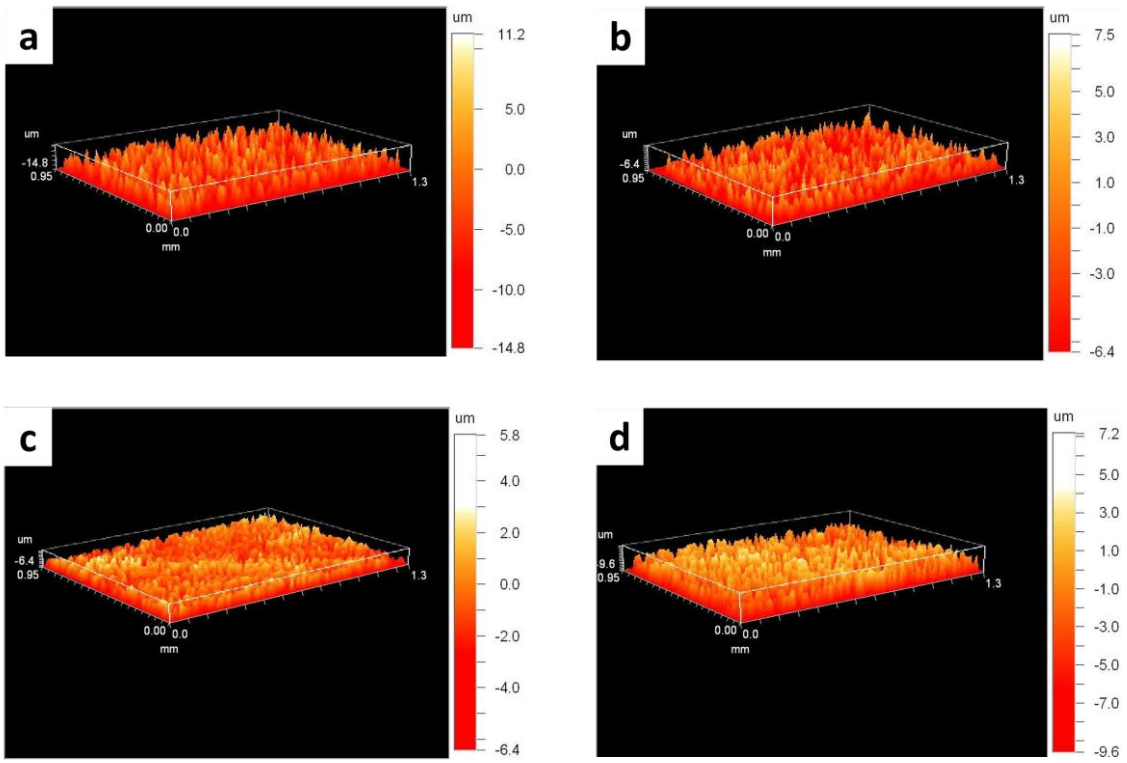

Figure 3-3 3D surface profiles of PEO coatings produced at different growth times (a) 100 s, (b) 200 s, (c) 300 s, and (d) 350 s.

The microstructure of the coating was also investigated by HR-SEM. The observations revealed that the coatings were composed of compact spherical particles with a size of about 20-40 nm (Figure 3-4). This suggests that under the present PEO conditions the produced coating possesses a nanoscale microstructure.

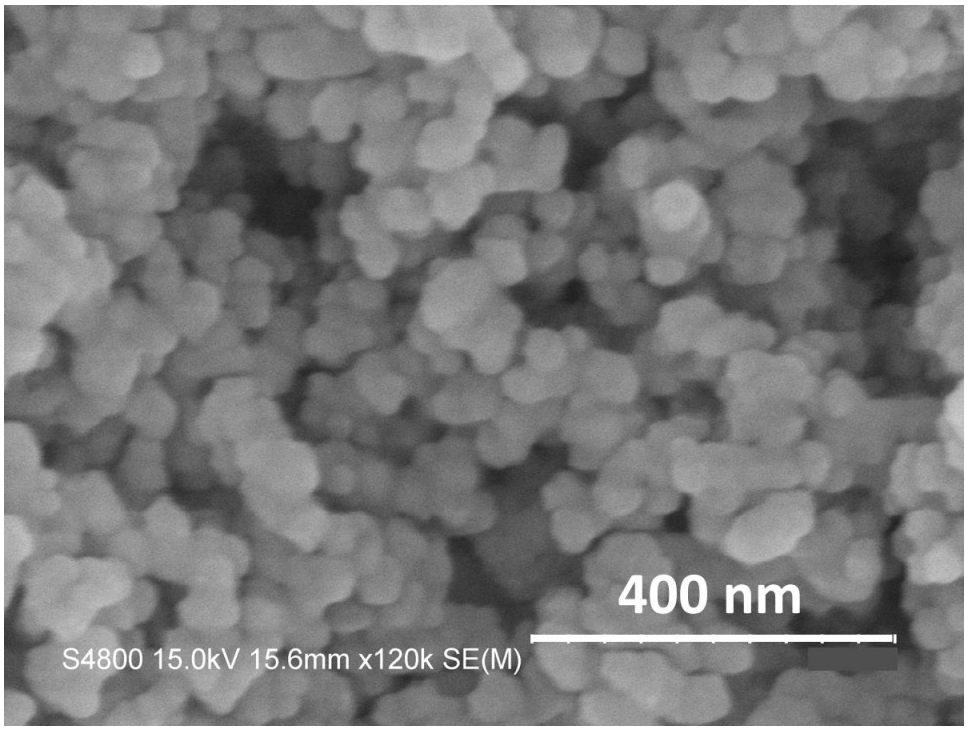

Figure 3-4 High-resolution SEM image of the PEO coating produced at 0.2 A/cm^2 current density for 300 s.

The elemental composition of the coated layers, determined by EDS analysis (composition values for three different areas of each sample at the same magnification), is presented in Figure 3-5(a). The results showed a trend with longer growth times resulting in a slight increase of the Zr content in the PEO layers. This increase is attributed to higher driving force during deposition that results in faster arrival of Zr containing ionic compounds to the surface. Furthermore, EDS line scan of the coated layer at 300 s shows rather uniform elemental distribution throughout the coating thickness (Figure 3-5(b)).

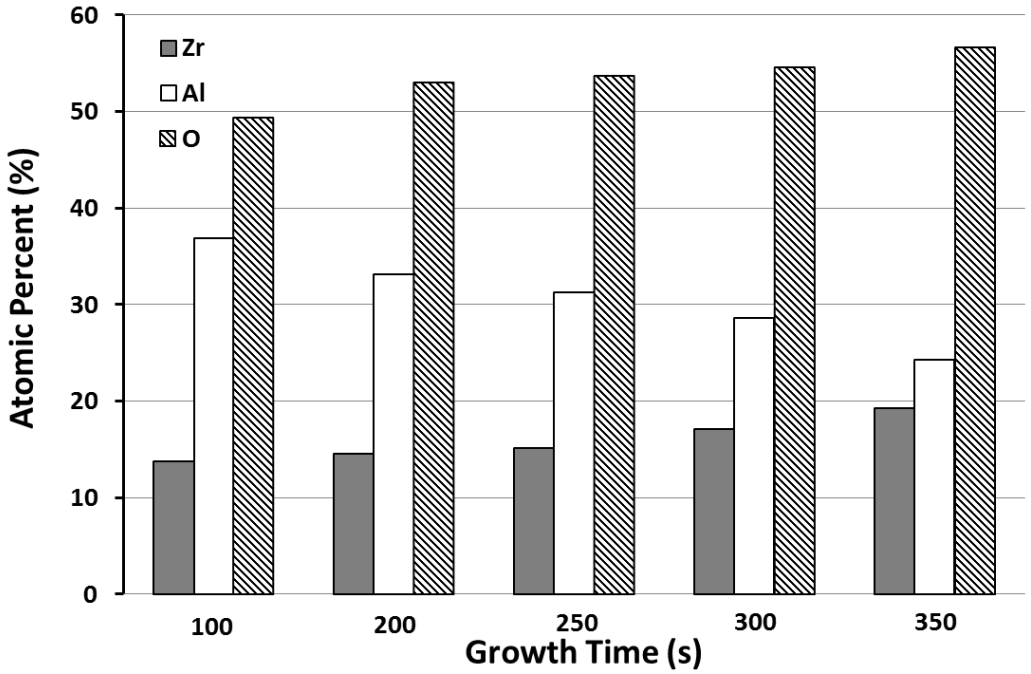

A

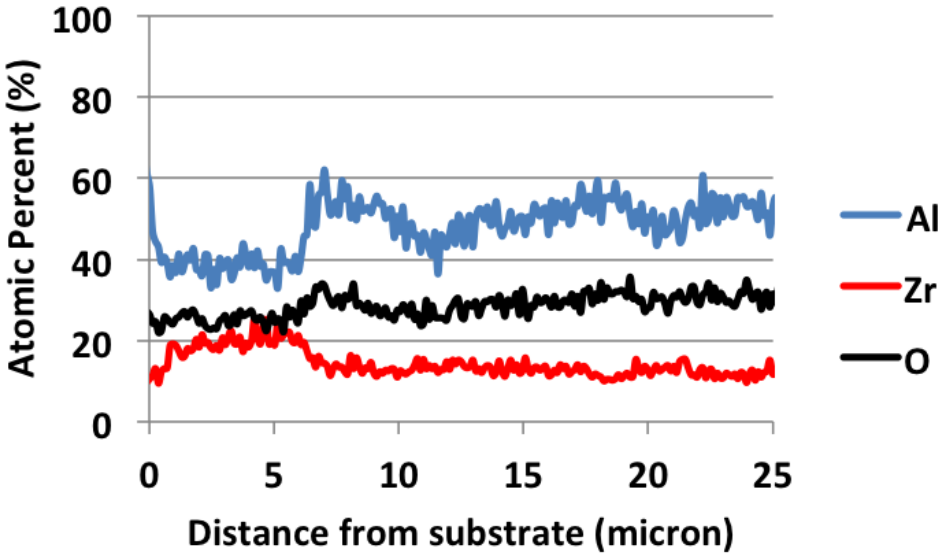

B

Figure 3-5Atomic composition of PEO coatings produced at different growth times.

Cross-sectional SEM images of the PEO coatings obtained under DC galvanostatic mode at different growth times are presented in Figure 3-6. Discharge channels in the samples coated at shorter growth times as well as porosity in most of the samples is evident. The thickness of the layers (derived from an average of 5 different lines on the cross sectional images) is listed in Table 3-1. By increasing the PEO processing time, the thickness of the coated layers increased to maximum saturation level and after that applying a longer processing time resulted in a thickness reduction. This is shown in the sample coated at 350 s. Intensive arcs degraded the coated layer with formation of rough edges, Figure 3-6(e), and resulted in a somewhat decrease in thickness.

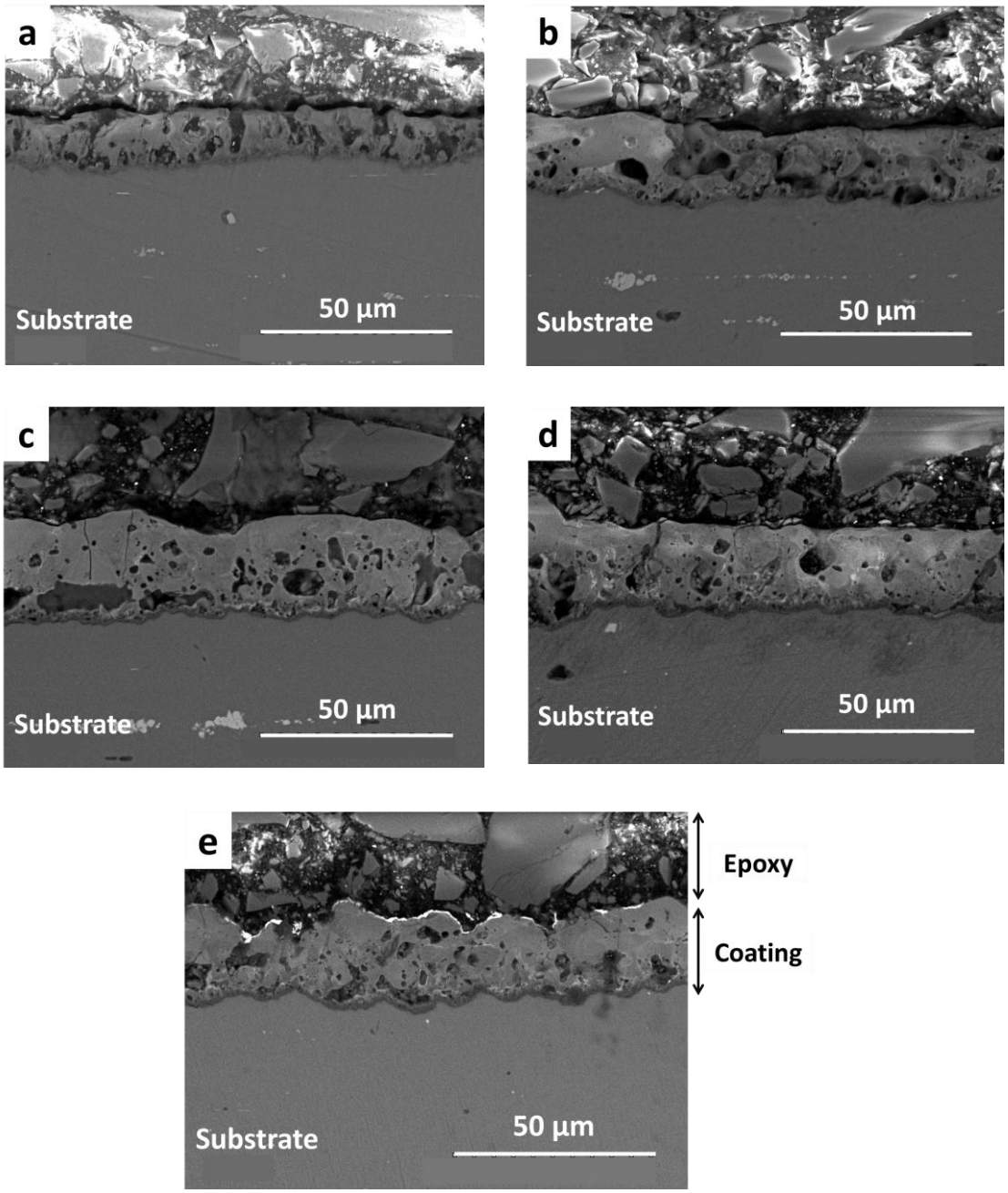

Figure 3-6 SEM cross-sectional images of the coatings formed at constant current density of 0.2 A/cm^2 and different growth times (a) 100 s, (b) 200 s, (c) 250 s, (d) 300 s, and (e) 350 s.

The various phases formed during PEO processing were investigated by XRD. The XRD patterns of the coated layers are shown in Figure 3-7. The peaks formed at 2θ angles of 35.17° and 37.66° correspond respectively to d-spacing of 2.51 Å and 2.38 Å and are attributed to the

formation of α-Al_2O_3 phase (PDF# 46- 1212). Three main diffractions observed at 2θ angles of 30.31°, 50.38°, 60.21° correspond to d-spacing of 2.95 Å, 1.81 Å and 1.54 Å and are respectively consistent with the (011), (112) and (121) of the *t*- ZrO_2 phase (PDF# 50- 1089). Stabilization of tetragonal zirconia phase in this composite is related to alumina which can stabilize the tetragonal zirconia by inhibiting the nucleation and grain growth of zirconia [100]. This effect is attributed to the constraining the grain boundaries of ZrO_2. In this case, there exists a critical crystallite size, beyond which the t-to-m transformation occurs [79].

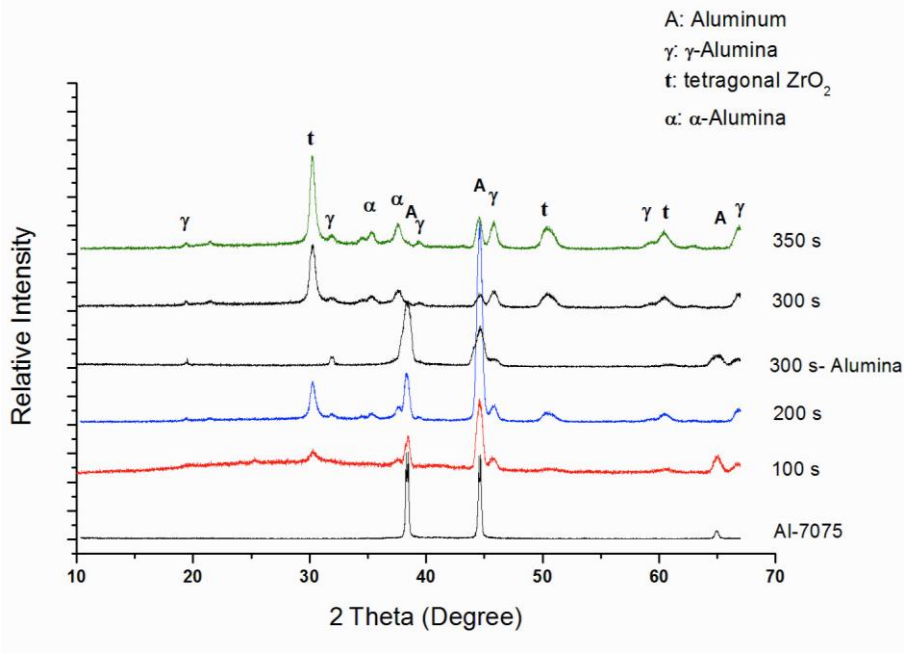

Figure 3-7 XRD patterns of the layers coated on 7075 Al alloys at 0.2 A/cm^2 current density and different growth times (100 s - 350 s).

It is also interesting to observe from the XRD pattern that by increasing the coating growth time, the intensity of the crystalline phases was increasing. Intensive arcs with high energy and temperature at the surface can be the main reasons of improved crystallinity. In addition, by increasing the coating growth time, the substrate peaks are vanishing, which implies

an increase in the thickness of the coated layers. Furthermore, Crystallite size of the tetragonal zirconia was determined according to the Scherrer equation [105], which was in the range of 12-25 nm which is consistent with HR-SEM results.

3.3.2 Corrosion Properties

The potentiodynamic polarization results of the as-received and PEO coated 7075 Al alloy are presented in Figure 3-8 The corrosion potential (E_{corr}), corrosion current density (I_{corr}), anodic/cathodic Tafel slopes (β_α and β_c) and polarization resistance (R_p) obtained by Tafel extrapolation are summarized in Table 3-2. The polarization response showed lower anodic current densities and corrosion rates for all PEO processed samples compared to the Al alloy (AA 7075). It is important to note that all the alumina/zirconia coatings showed at least a two orders of magnitude lower corrosion current density than 7075 Al alloy.

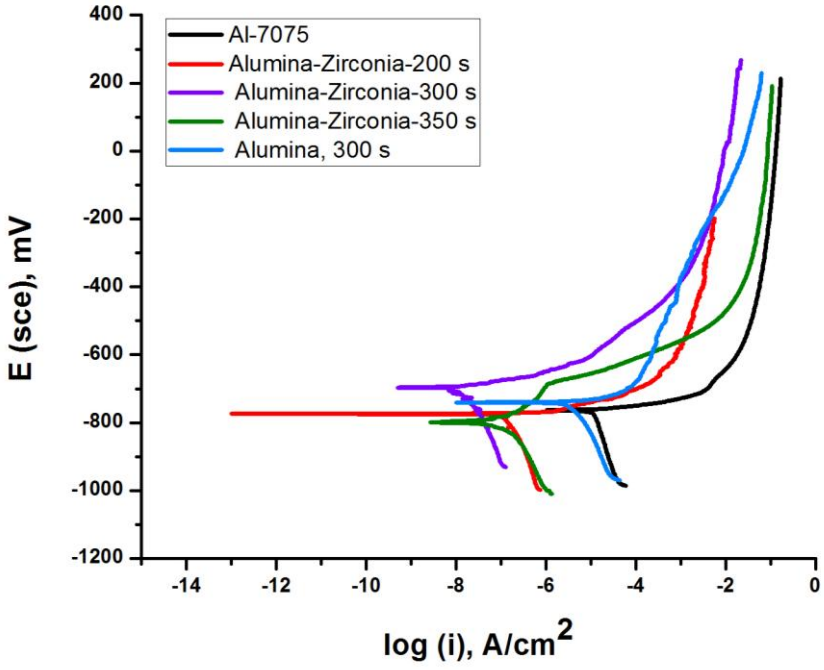

Figure 3-8 Potentiodynamic polarization curves of alumina-zirconia and alumina PEO coatings in 3.5 wt.% NaCl solution.

Table 3-2 Electrochemical parameters of the unprocessed and PEO coated Al alloy.

Coating growth time (s)	Coating	E_{corr} (mV/sce)	I_{corr} (Acm^{-2})	β_c (mV/decade)	β_α (mV/decade)	Polarization resistance ($k\Omega cm^{-2}$)
0*	-	-768.2	9.7×10^{-6}	331.2	213.3	5.79
200	Alumina-Zirconia	-781.2	1.9×10^{-7}	401.0	187.1	289.12
300	Alumina-Zirconia	-701.9	2.1×10^{-8}	316.3	97.6	1515.49
300	Alumina	-745.8	2.2×10^{-6}	226.4	189.0	20.34
350	Alumina-Zirconia	-799.0	1.6×10^{-7}	250.3	44.3	102.28

*Al-7075 substrate

To discuss this remarkable improvement, it should be noted that the electrochemical behavior of coatings is affected by several factors including coating microstructure, phase composition and density. It is generally believed that a compact PEO coating with less defects, higher thickness and stable composition would be beneficial to provide a favorable corrosion protection. In NaCl corrosive media, these parameters can affect the diffusion rate of Cl^- within the coating. On the other hand, higher surface roughness and porosity can provide active regions such as cavities and pores in which Cl^- can easily penetrate the surface resulting in coating breakdown [106]. Therefore, less micro-defects and more compact structures are beneficial for suppressing the Cl^- transfer during the corrosion process. Polarization resistance, as an electrochemical property, is mainly affected by microstructure, surface morphology and phase composition. In the present experiments, the variation of porosity content, roughness and thickness of coatings (Table 3-1) is in close agreement with the observed electrochemical properties of the PEO treated samples.

The PEO coating at 300 s in particular showed the best behavior with 2.5 orders of magnitude lower corrosion current density than 7075 Al alloy. The significantly better corrosion

resistance of this coating can be attributed to the highest thickness, lowest roughness and porosity content compared to the 200 s and 350 s PEO coatings, Table 3-1.

Besides the above described microstructural coating characteristics, formation of chemically stable α-Al_2O_3 and t-ZrO_2 phases by the PEO treatment can also possibly have contributed to the improvement of the corrosion resistance. From the coating chemical composition viewpoint, increase in the Zr content by increasing coating growth time has been resulted in better corrosion protection. In order to investigate the role of zirconia in the corrosion resistance improvement, anodic polarization experiments were conducted on PEO alumina coating without the presence of zirconia, Figure 3-8. This alumina coating has been produced by PEO under the exact same condition as the optimum alumina-zirconia layer (300 s growth time, 0.2 A/cm^2 current density).

The results showed lower polarization resistance and significantly higher corrosion current density (by two orders of magnitude) in the aforementioned alumina coating compared to its counterpart alumina-zirconia coating (300 s growth time). XRD patterns (Figure 3-7) show formation of γ- alumina, t-zirconia and α-alumina phases in the alumina-zirconia coated sample compared to the γ- alumina phase (with lower corrosion resistance) for alumina coated sample. The results clearly demonstrate a major role played by zirconia in the corrosion resistance process. Similar findings have been reported by other researchers regarding the role of zirconia in delaying pitting corrosion in saline containing environments [107].

It is well known that residual stresses are introduced into coatings by PEO processing [108]. Once the PEO coating is penetrated by Cl^-, pitting corrosion occurs and the residual stress can be released by cracking [8]. In the present study, pitting corrosion was observed by SEM in the coatings after corrosion testing, Figure 3.9 (c, and d). It is important to note that after

corrosion testing, the PEO alumina coating showed pitting and evidence of major surface cracking, Figure 3.9 (c). On the other hand, such cracking was absent from the alumina-zirconia coating, Figure 3.9 (d). In this regard, formation of *t*-ZO_2 seems to have been beneficial in improving coating integrity and thus, reduce Cl^- penetration. This can be attributed to the high fracture toughness of *t*-ZrO_2 improving the crack propagation resistance and impacting the corrosion behavior of the alumina-zirconia coating. In addition, the lower elastic modulus of t-ZrO_2 (~205 GPa) compared to Al_2O_3 (~400 GPa) [109] may have also contributed to its ability to accommodate higher residual stresses and improve cracking resistance. These two mechanical factors, i.e., higher fracture toughness and lower modulus for *t*-ZrO_2 compared to alumina, seem to be the main reasons for the improved corrosion resistance of the zirconia containing coatings.

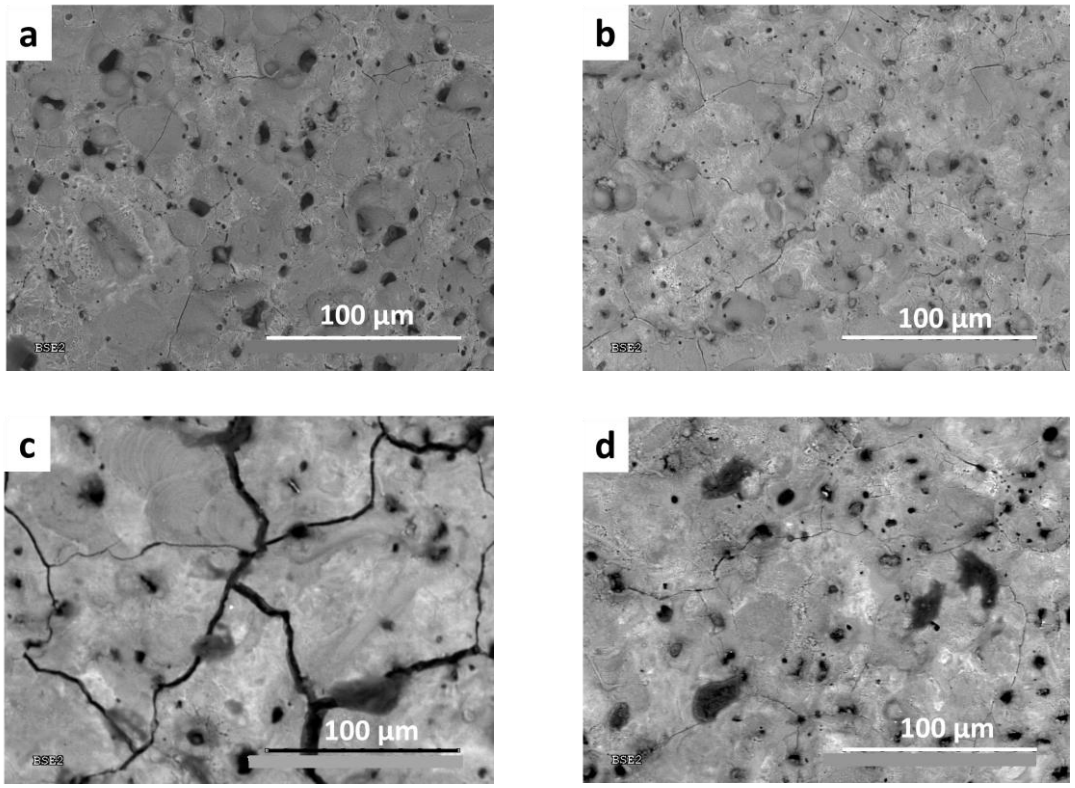

Figure 3-9 SEM images of the PEO alumina and alumina/zirconia coatings, respectively, (a and b) before and (c and d) after anodic polarization testing. Both coatings were produced at 0.2 A/cm^2 current density and 300 s growth time.

3.4 Conclusion

Alumina-zirconia coatings were produced by PEO treatment of 7075 Al alloy under galvanostatic mode (0.2 A/cm^2 current density). The results showed that coating characteristics strongly dependent on the PEO processing time. Increasing the growth time up to an optimum level was found to increase coating thickness, decrease roughness and porosity and lead to formation of high temperature phases (t-ZrO_2 and α-alumina). The treatment with 300 s growth time exhibited more compact microstructure with negligible surface porosity amount (0.69%), the lowest roughness (0.86 μm) and high thickness (~26 μm). All alumina/zirconia coatings reduced significantly the corrosion rate compared to 7075 Al alloy with the 300 s PEO coating showing a reduction by 2.5 orders of magnitude. The superior corrosion resistance offered by the alumina/zirconia coatings can be attributed to the improved mechanical properties induced by the presence of t-ZrO_2 (higher toughness and lower elastic modulus).

Chapter 4: Investigation of the Al_2O_3-ZrO_2 nanocomposites coated on aluminum alloy by plasma electrolytic-electrophoretic hybrid process

4.1 Introduction

PEO is a surface treatment method to form conversional coatings on valve metals such as aluminum (Al), titanium (Ti) and magnesium (Mg) alloys. By using appropriate electrolytes in this process, oxidation of both metal substrate and electrolyte components can take place. The coating is typically crystalline containing high temperature phases due to exposure to elevated temperatures (up to 2000 K) aroused from the plasma formation and surface arcing. This technique has been successfully used to improve the wear resistance and corrosion properties of Al, Ti and Mg alloys [1-3].

In recent efforts to produce desirable characteristics, the PEO method has been combined with other coating processes such as sol-gel, electrophoretic deposition (EPD) and laser surface melting [4-6]. Among the coating methods, the EPD has been used in many research efforts [7-9]. EPD is a colloidal process through which charged particles dispersed in a liquid medium are attracted to an oppositely charged conductive substrate by applying an electric field [9]. In this process, the particles attracted to one of the electrodes form a coherent deposit. A densification step, such as sintering or curing, needs to follow in continuation to EPD for obtaining a fully dense material [10]. Combination of this method with PEO can result in incorporation of particles from the electrolyte into the coating. Meanwhile, the PEO process can oxidize the metal substrate and form high temperature phases.

Alumina-zirconia is one of the most widely used composite structural ceramics. Due to the insolubility of alumina and zirconia over a wide temperature range from room temperature to typical sintering temperatures, Al_2O_3-ZrO_2 composites can form. This composite has the potential to combine the high hardness of alumina with the excellent toughness of tetragonal zirconia. It has been shown that the combination of high hardness alumina (19.3 GPa in the dense form) with low thermal conductivity (2.2–2.6 W/mK in the dense form) and high fracture toughness zirconia (11 $MPa.m^{1/2}$) contributed to the observed high wear resistance of this composite [11]. Alumina-zirconia ceramics have attracted significant attention for cutting tools, wear resistant elements and corrosion resistance applications. The present authors reported the superior tribological and corrosion properties of alumina-zirconia composite coatings compared to the coated surface separately either with alumina or zirconia phases [12, 13]. Despite the superior properties of this composite and its formation by the PEO method, there are only a few reports in the literature on alumina-zirconia coatings by PEO [14, 15]. Furthermore, regarding the formation of composites by the PEO method, there is a major research interest to explore the formation mechanism of this nanocomposite.

The aim of the present work was to study the mechanism of alumina-zirconia coating formation from a nano zirconia containing electrolyte. The alumina matrix of the composite formed from the conversion of the Al 7075 substrate via the plasma electrolytic process. The expectation of zirconia incorporation in the layers has been investigated by adding zirconia nanoparticles in the electrolyte. Different composite microstructures were produced as a function of the PEO current density. The produced coatings were analyzed using transmission electron microscopy (TEM), optical spectroscopy (OS), scanning electron microscopy (SEM) and X-ray

diffraction (XRD). The voltage-time, V-t, response during PEO processing was recorded to offer an additional insight in the nanocomposite formation mechanism.

4.2 Experimental

The PEO treatment was applied on Al-7075 disk samples of 15 mm in diameter and 10 mm thick. All samples were polished with emery papers and 0.3 μm Al_2O_3 slurry as the final step to achieve a roughness of $R_a \approx 0.1$ μm. Afterwards, the samples were ultrasonically cleaned in distilled water and then in acetone and ethanol.

A direct current (DC) power supply (Sorenson model SGA-3u) with a maximum output of 600 V/17 A was utilized for the PEO processing. A double walled beaker was used as the reaction container with water-ethylene glycol coolant flowing to keep the electrolyte temperature below 30 °C. The Al alloy substrates were coated in an electrolyte containing a dispersion of monoclinic (m) zirconia nanoparticles and KOH with 2:1 molar ratio (pH = 12). The as-received monoclinic zirconia nanoparticles (Sigma-Aldrich) were analyzed by High-resolution (HR) TEM (Hitachi H-9500) operated at 300 kV with a point resolution of 0.18 nm. The particle size of the as-received zirconia powder was in the range of 20-30 nm, Figure 4-1 Analysis of the zirconia powder showed d spacing of 2.63 Å, 2.84 Å and 3.14 Å corresponding to the (200), (111) and (-111) planes of the m-ZrO_2 phase. The PEO treatments were performed under galvanostatic mode, constant growth time of 250 s and current densities from 0.1 A/cm^2 to 0.4 A/cm^2. A Tektronic TDS 2000 oscilloscope was used to monitor the variation of voltage and current during PEO processing.

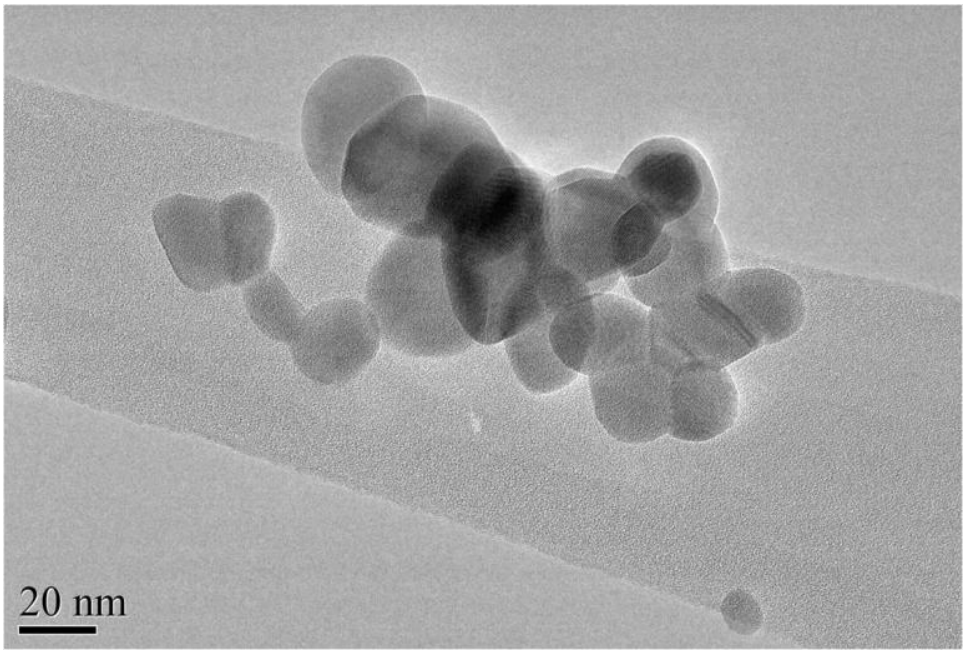

Figure 4-1 TEM micrograph showing morphology of the as-received zirconia particles.

Grazing Incident (GI) XRD analysis was conducted to determine the phases present in the coated layers. A Bruker D8 Advance X-ray diffractometer (Cu Kα radiation, λ = 0.154 nm) was used operated at 40 mA tube current and 40 kV accelerating voltage. The XRD scans were performed under a glancing angle of 10°, 2θ range from 10° to 67° and step size of 0.01°. A Hitachi S-3000N SEM was used to examine the surfaces and cross-sections of the coatings. Energy dispersive X-ray spectroscopy (EDS) was utilized to identify the chemical composition of the coatings. The microstructure of the coatings was studied by HRTEM. Electron-transparent cross-sections (TEM foils nominally 100 nm thick) were prepared from 3 mm diameter disks with the film/substrate interface oriented normal to the disk. The disks were first thinned mechanically and polished to about 10 mm thickness. Argon ion milling at 2.5 keV incident energy was conducted for final thinning of the disks.

To study the ionic involvement of the elements during the PEO process, light emission spectroscopy was used. The emitted light from the surface plasma interaction during PEO processing was collected using an optical emission spectroscope (USB4000 Ocean Optics). An optical fiber was located close to the specimen surface to optimize the intensity of the collected light. Emission spectra were studied in the wavelength range 200-900 nm with a spectral resolution of 0.4 nm.

4.3 Results and Discussion

The surface morphology of the PEO coatings obtained under various current densities (0.1-0.4 A/cm^2) is shown in Figure 4.2. As can be seen, increasing the PEO current density results in surface morphology changes and development of larger pores due to the higher energies and arcing intensity. It can also be observed in the electron backscattered images that the surface portion of the white areas increases with increasing current density. This is indicative of the presence of heavier elements (higher atomic number), i.e., higher incorporation of zirconia, at higher current densities.

This can be emanating from higher driving force on the zirconia particles to move from the electrolyte toward the coating. Hence, a higher deposition rate of nanoparticles on the surface should be expected. Hairline cracks were also observed on the surface of the coatings that are attributed to the local-thermal shocks arising from the significant temperature differences between the coating and the electrolyte.

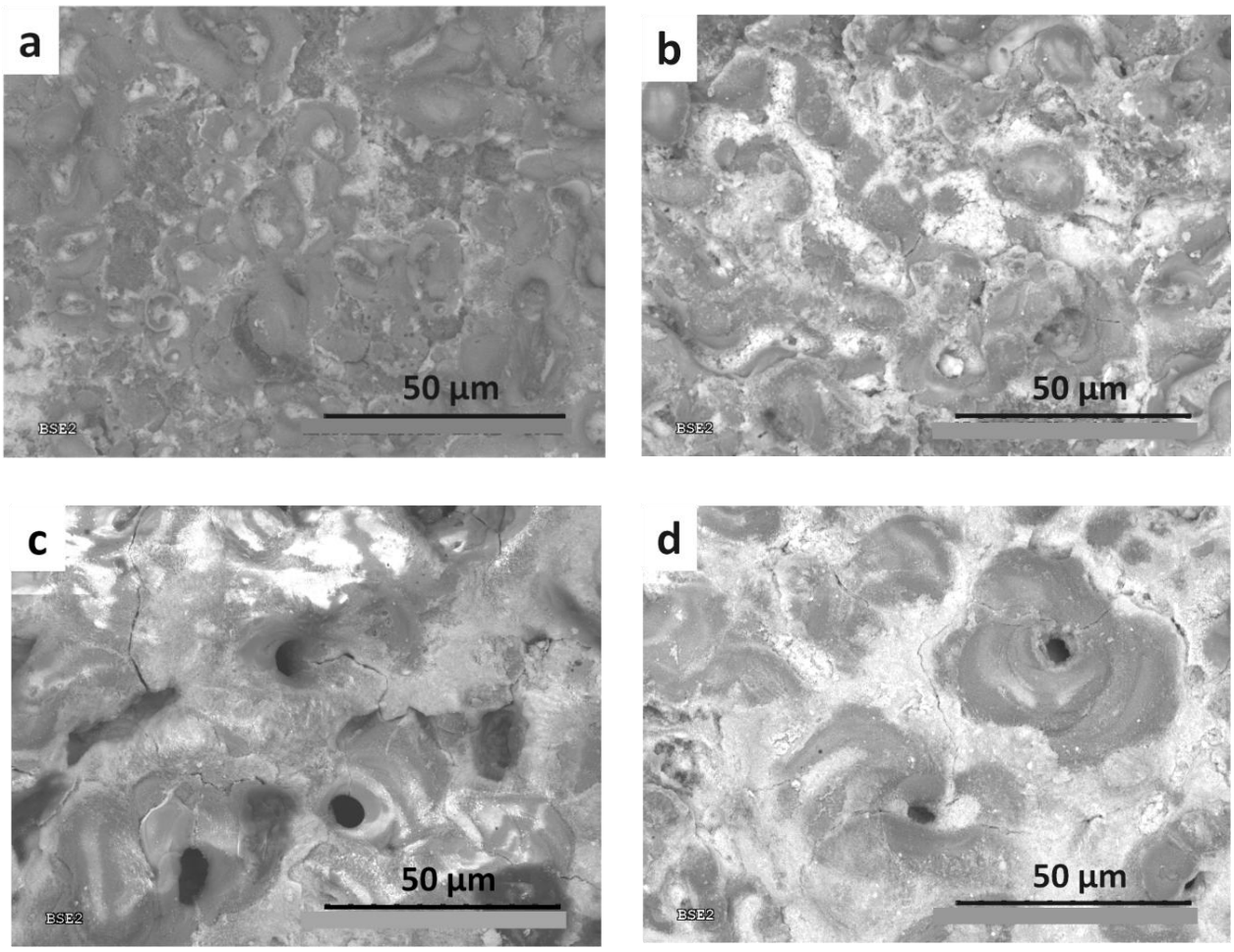

Figure 4-2 SEM surface morphology of the samples coated at (a) 0.1 A/cm^2, (b) 0.2 A/cm^2, (c) 0.3 A/cm^2 and (d) 0.4 A/cm^2.

Figure 4-3 presents the XRD patterns of the coated samples at different current densities. XRD analysis showed the presence of *m*-ZrO_2 and low temperature aluminum oxide (γ-Al_2O_3) phases for all PEO treated samples. The *m*-ZrO_2 is incorporated from the electrolyte and γ-Al_2O_3 is formed by oxidation of the aluminum substrate. By increasing the PEO current density, formation of high temperature phases for both alumina and zirconia, (i.e., α-alumina and tetragonal, t, zirconia) is observed. At high PEO current densities, the formation of high temperature phases results from the prevailing high arcing energy and temperature. Phase

analysis results are consistent with the surface observations (Figure 4-2) regarding the incorporation of more zirconia in the coating at high current densities.

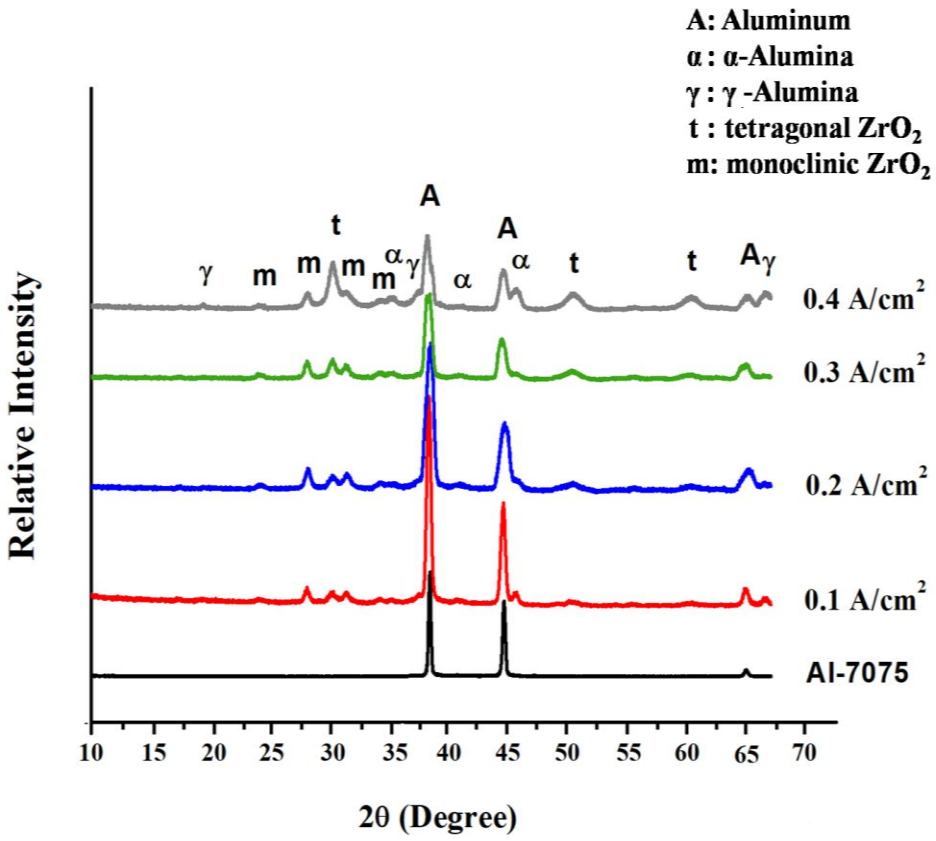

Figure 4-3 XRD patterns of untreated and treated samples at various current densities (a) 0.1 A/cm^2, (b) 0.2 A/cm^2, (c) 0.3 A/cm^2 and (d) 0.4 A/cm^2.

The cross-sectional morphologies of the coated layers produced at various PEO current densities are shown in Figure 4-4. By increasing the PEO current density from 0.1 A/cm^2 to 0.4 A/cm^2, the coating thickness was increased from 8 μm to 13 μm. SEM investigations demonstrated that the PEO coatings consist of two layers, i.e., an outer porous layer and a rather dense and thin inner layer. The inner layer, is shown as a dark layer between the substrate and coating. This dark layer can refer to the conventional nature of the PEO coated layers where the

substrate (aluminum alloy) converts to its oxide. Also, from the viewpoint of chemical composition, the bright areas in the porous layer could be related to the higher amounts of zirconia particles incorporated from the electrolyte by moving toward the surface. Regarding the coating growth mechanism, in the case of PEO coated Al substrate, an inward growth due to the melting of the Al substrate during the PEO process has been reported [17, 18]. At the same time, a mix of outward and inward growth has been reported by others [19, 20]. In the present case, the observed interface distortion in the samples coated at the higher PEO current density suggests substrate melting by intensive arcing and therefore an inward growth of the layers.

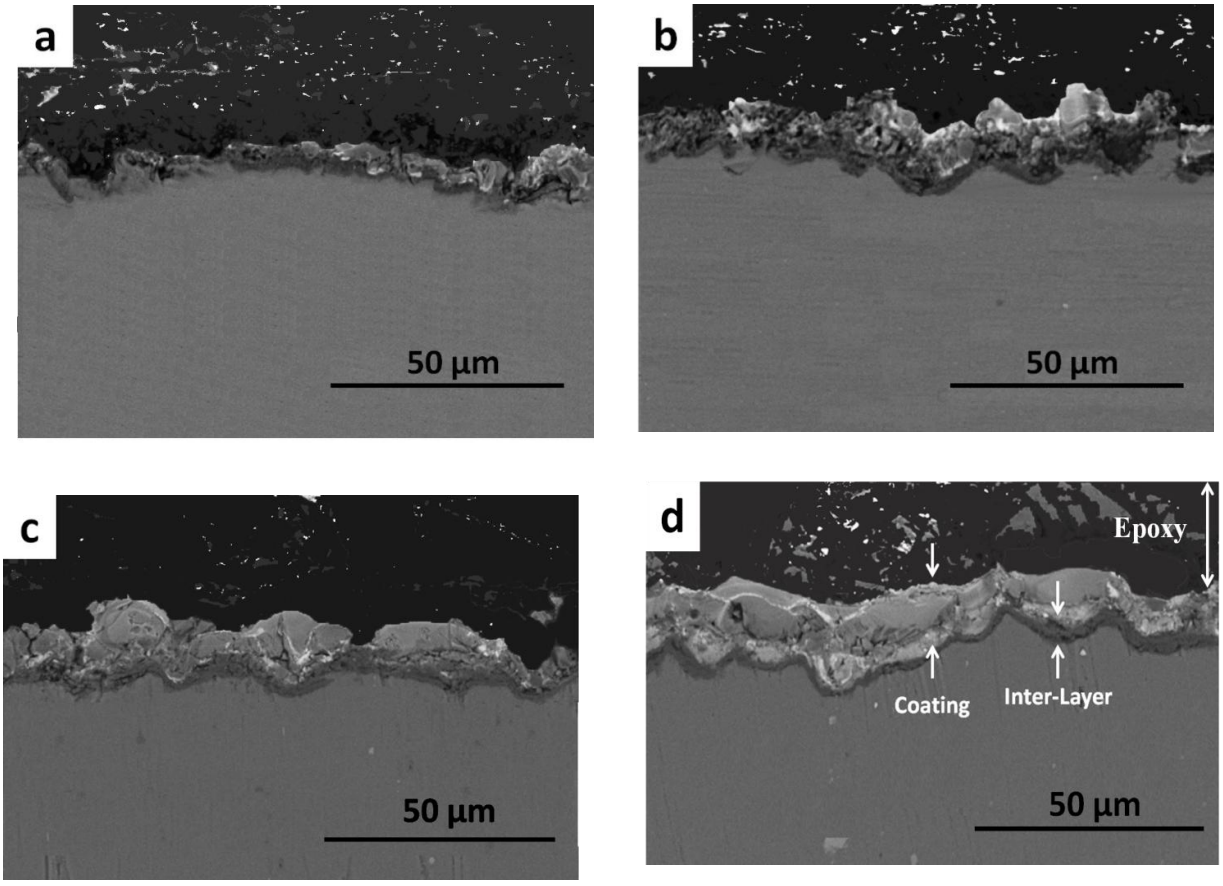

Figure 4-4 SEM cross-sectional images of the samples coated at various current densities (a) 0.1 A/cm^2, (b) 0.2 A/cm^2, (c) 0.3 A/cm^2 and (d) 0.4 A/cm^2.

Voltage-time (*V-t*) variations during PEO processing under various current densities in the galvanostatic mode are shown in Figure 4-5. The *V-t* response shows six identifiable regions during the PEO treatment. To study each stage, the total current density applied to the sample during the PEO treatment can be expressed as:

$$I_t = I_i + I_e \quad (4\text{-}1)$$

where I_t, I_i and I_e are the total current density, the ionic current density and the electron current density, respectively. Furthermore, based on Ohm's Law [21]:

$$V = IR \quad (4\text{-}2)$$

where R is the ohmic resistance attributes to the film resistance and hence, the thickness of the formed film. The first derivative of the voltage versus time ($\frac{dV}{dt}$) can be used to evaluate the slope of these curves at various stages:

$$\frac{dV}{dt} = \frac{dI}{dt}R + \frac{dR}{dt}I \tag{4-3}$$

Since a constant current density is used during processing, the $\frac{dI}{dt}R$ term is zero, therefore:

$$\frac{dV}{dt} = \frac{dR}{dt}I \tag{4-4}$$

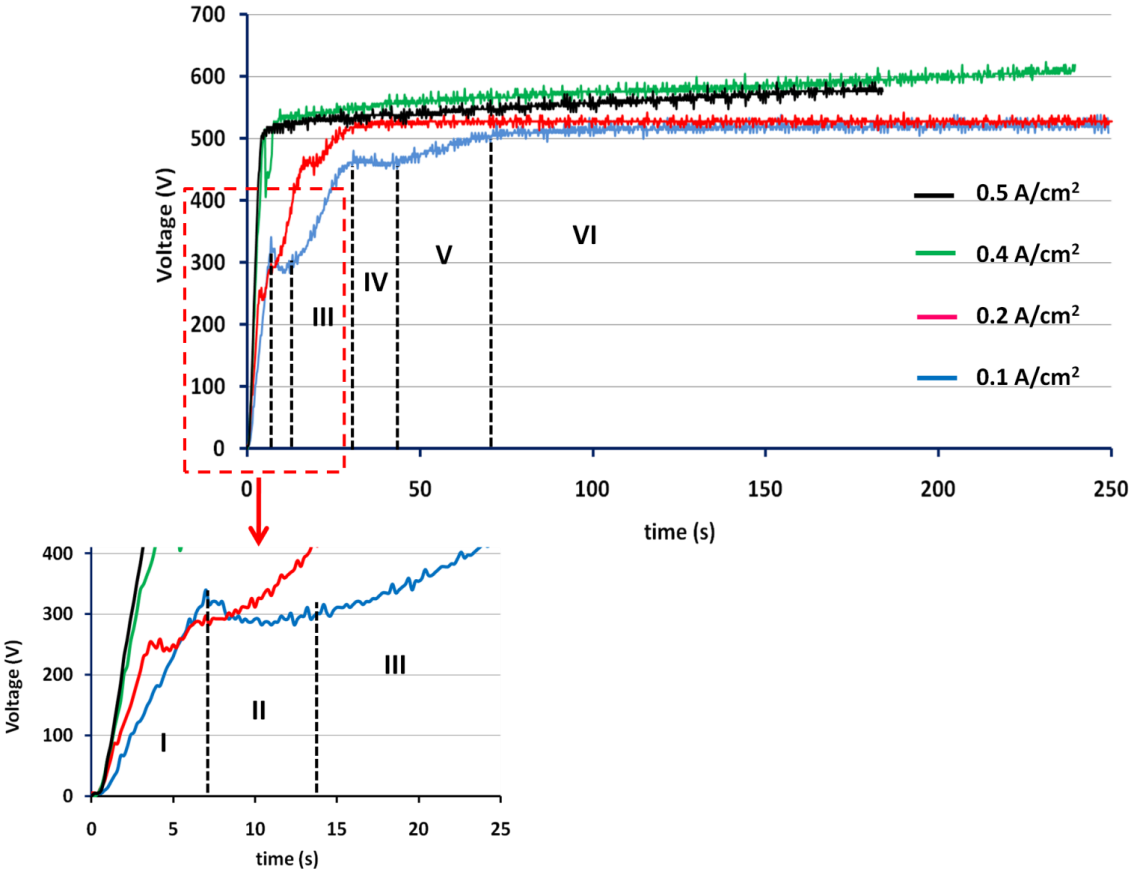

Figure 4-5Variation of voltage versus processing time for the samples treated at various current densities.

At the very first stage of the PEO processing, similar to the anodizing process, the oxidation reactions will form aluminum oxide on the Al substrate. In this region, the current passing through the oxide film is represented only by the ionic current ($I_t = I_i$). The steady increase in the voltage is correlated with the thickness growth which in turn increases the interface resistance ($\frac{dR}{dt}$). Furthermore, ZrO_2 charged particles in the electrolyte can be responsible for the latter increase in the resistant through their movement toward the substrate via an electrophoretic mechanism. The high resistivity leads to a continuous voltage increase to maintain the constant current density.

In the second stage, an almost horizontal *V-t* variation refers to the very low and almost zero $\frac{dR}{dt}$ which denotes a constant resistance and layer thickness. In this case, accumulation of particles by the electrophoresis force and the adsorbed anions and formed oxides can balance the growth rate and the detachment of chemical species. This balance maintains an almost constant resistance. XRD analysis for the sample treated up to this stage has been studied to explore the mechanism (Figure 4-6). The result show the existence of m-ZrO_2 and γ-Al_2O_3 phases with the former being deposited on the surface through the electrophoretic process. In addition, the γ-Al_2O_3 phase has been a product of anodizing during the first stages of this process. At the third stage, accumulation of electrons on the conduction band of the formed oxide and acceleration by the electric field produce avalanches by an impact ionization mechanism. In this region, both electron current (associated with dielectric breakdown, i.e., electron avalanche) and ionic currents are involved. Due to the avalanche, electronic current reaches a critical value and the dielectric breakdown and formation of small sparks occurs on the surface.

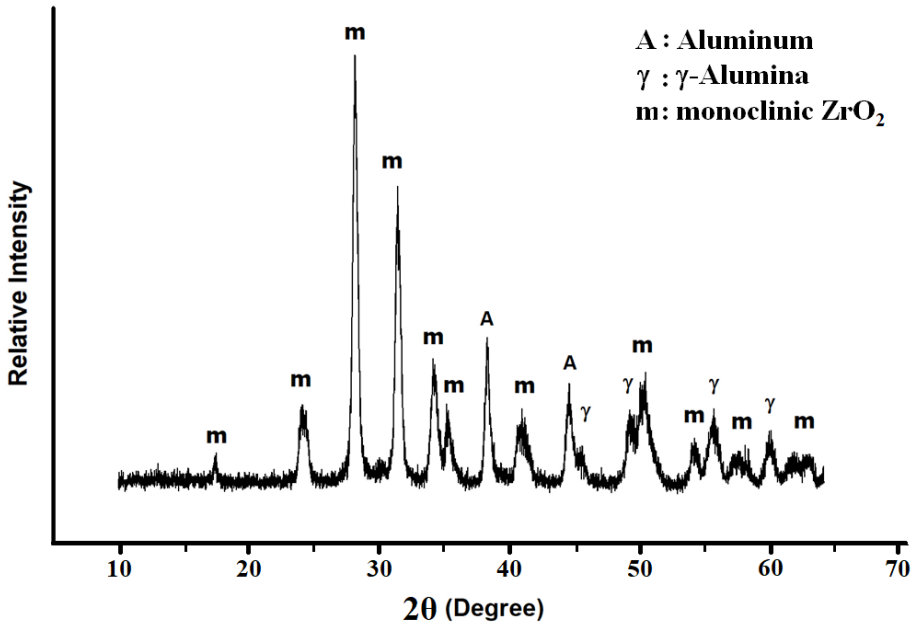

Figure 4-6 X-Ray diffraction pattern of the sample treated under 0.2 A/cm^2 for 20 s.

In stage III compared to stage I, a lower voltage increase ($\frac{dV}{dt}$) is required to maintain the same total current density since the electron current density is independent from the oxide layer thickness. Therefore, at this stage, the voltage continually increases but the voltage time slope, ($\frac{dV}{dt}$), decreases. Following this stage, the slope of the *V-t* curve is decreased to almost zero. This $\frac{dR}{dt}$ decrease can be related to the phase transformation of γ-Al_2O_3 to α-Al_2O_3. In this stage, the fraction of the electron current density in the total current density becomes dominant and the total current density is almost independent of the anodic oxide film thickness. In stage *V* where high voltages prevail, ZrO_2 particles in the electrolyte can gain sufficient energy to be adsorbed to the discharge channels. To keep the current constant in view of the incorporation of particles in pores, the resistivity and therefore the slope of the *V-t* curve are increased. At the longer PEO

processing time (stage VI), the voltage is not increasing anymore. The reason for this steady voltage-time response is attributed to the compensation of the applying energy on the surface for the m-ZrO_2 to t-ZrO_2 phase transformation. Since arcing is not uniformly distributed in this stage as it is in the second stage; the electron current is not playing the main role.

A typical emission spectrum of the sample undergoing PEO processing (200 s) is shown in Figure 4-7. The survey spectrum presented in Figure 4-7 (a) is dominated by four clearly pronounced spectral lines. Using NIST's atomic spectra database [22], each peak was assigned to a characteristic atomic transition. The atomic species involved in the arcing area identified by optical emission spectroscopy were Al, O and Zr. The results indicated the participation of elements from both the metal substrate and the electrolyte during the PEO treatment. The emission intensity evolution of the spectral lines at 396.1 nm (Al I), 466.3 nm (Al II), 777.2 nm (O I) and 360.1 nm (Zr I) during the PEO process is presented in Figure 4-7. The spectrum for each detected atomic wavelength has been recorded up to 200 s from the beginning of the process. Figure 4-7 (b) shows the variation of O presence during the coating process. Intensifying this specie at the mid time of the process denotes to the higher probability of the oxide formation in this time limit. Figure 4-7 (c) depicts the involvement of Al (I) from the initial stage of the PEO process showing that it can be related to the dissolution of the Al substrate even at the lower voltages. In the case of Al II, Figure 4-7 (d), the rather negligible intensity at the very first stages of the process refers to the absence of this ion due to the higher energy required for the ionization.

At the longer PEO treatment time, due to the initiation of the intensive arcing process, the ionization energy can be reached as shown by the presence of the related peaks. The evolution of Zr during the PEO process, Figure 4-7 (e), can illuminate the mechanism and involvement

process of a second phase in the composite coating. The evolution of Zr (I) during the PEO process suggests the formation and growth of ZrO_2 at the longer growth times. In other words, due to the existence of ZrO_2 particles in the electrolyte, high energy is required to move and deposit the zirconia particles. The required energy cannot be achieved at the first stages of the process, hence, zirconia particles are depositing at the latter stage of the process compared to the initial stage.

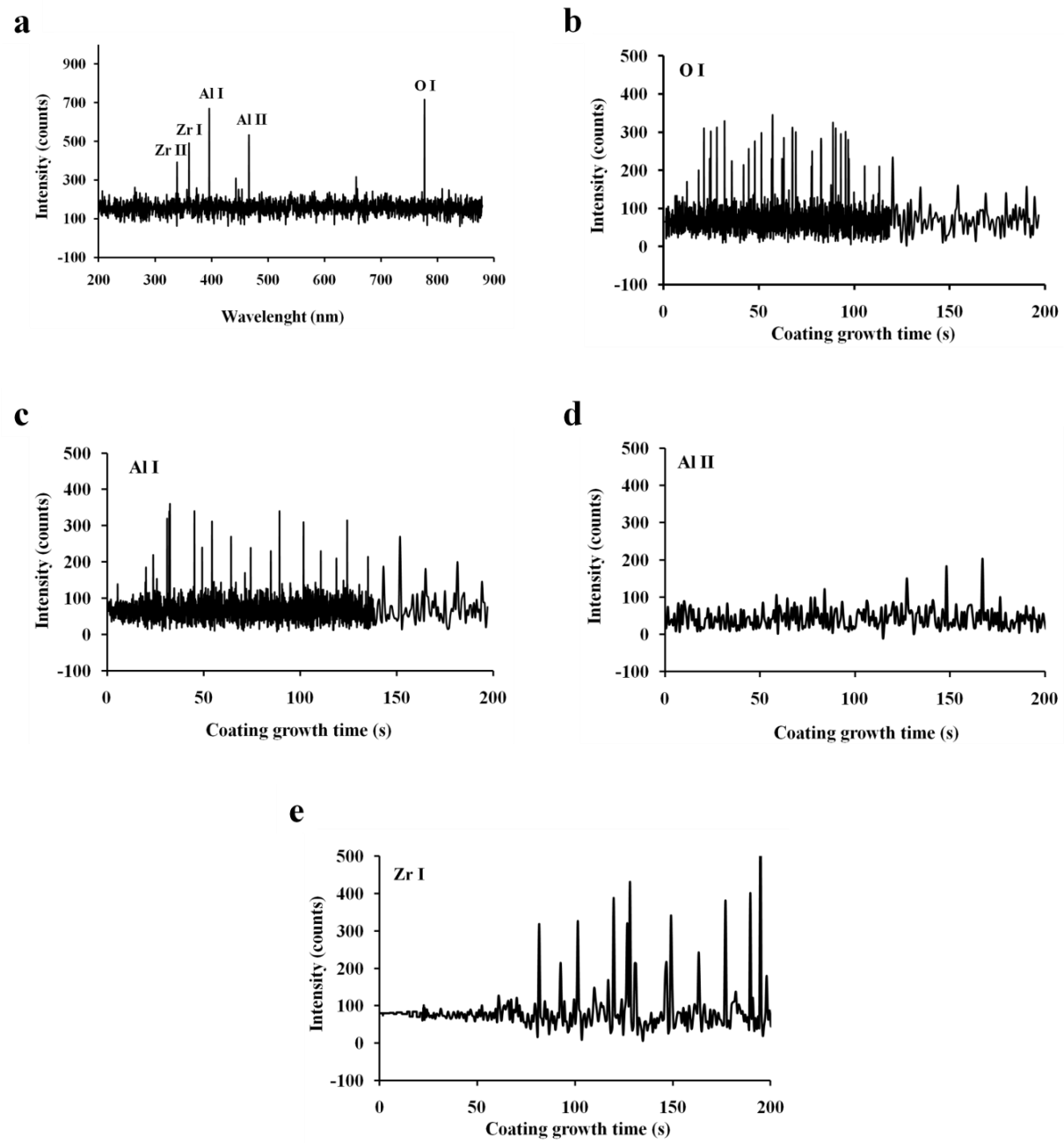

Figure 4-7 Optical spectroscopy of the sample treated at 0.4 A/cm^2 (a) survey spectra. Emission intensity during the PEO processing for (b) O I, (c) Al I, (d) Al II and (e) Zr I.

To gain additional insight of the coating mechanism and the nanoparticle incorporation process, high magnification SEM observations were conducted of the sample treated at 0.4 A/cm^2. Figure 4.8 shows accumulation of white particles around the pores. EDS analysis of

areas 1 and 2, Figure 4-8 (a), showed higher amounts of Al and Zr, respectively (Table 4-1). Higher amount of Zr in area 2 suggests higher probability for zirconia particles migrating toward pores and therefore deposition of zirconia inside and in the vicinity of pores. Figure 4-8(b) depicts the way of movement and absorbance of zirconia nanoparticles toward pores. In addition, Figure 4-8(c) demonstrates porosity filling by nano zirconia particles. In this regard, to discuss the process and observations, the electrophoretic process should be considered. By applying a voltage in this process, charged species in the electrolyte (zirconia nanoparticles) would experience an electrophoresis force. Particle movement in the electrophoretic process demand lower voltages compared to the plasma electrolytic process.

It can be concluded that at the early stages of the coating process, particle movement in the electrolyte toward the substrate is held by the electrophoretic mechanism as the main deposition mechanism. On the other hand, applying high energy via application of high voltages can result in intensive arcing and discharging. The resulting high temperatures can lead to the phase transformation of both the electrophoretically moved particles and the PEO formed oxides. Moreover, phase analysis of the treated layers revealed formation of γ and α-alumina phases by conversion and oxidation of the substrate via PEO. On the other hand, an electrophoretic process is resulting in zirconia nanoparticle involvement in the composite and indicates a hybrid of PEO and electrophoretic process as a coating method.

Table 4-1 EDS elemental composition of the coating produced at 0.4 A/cm^2.

Point	Al at. (%)	Zr at. (%)	O at. (%)
1	47.07	16.69	36.24
2	15.18	26.31	58.50

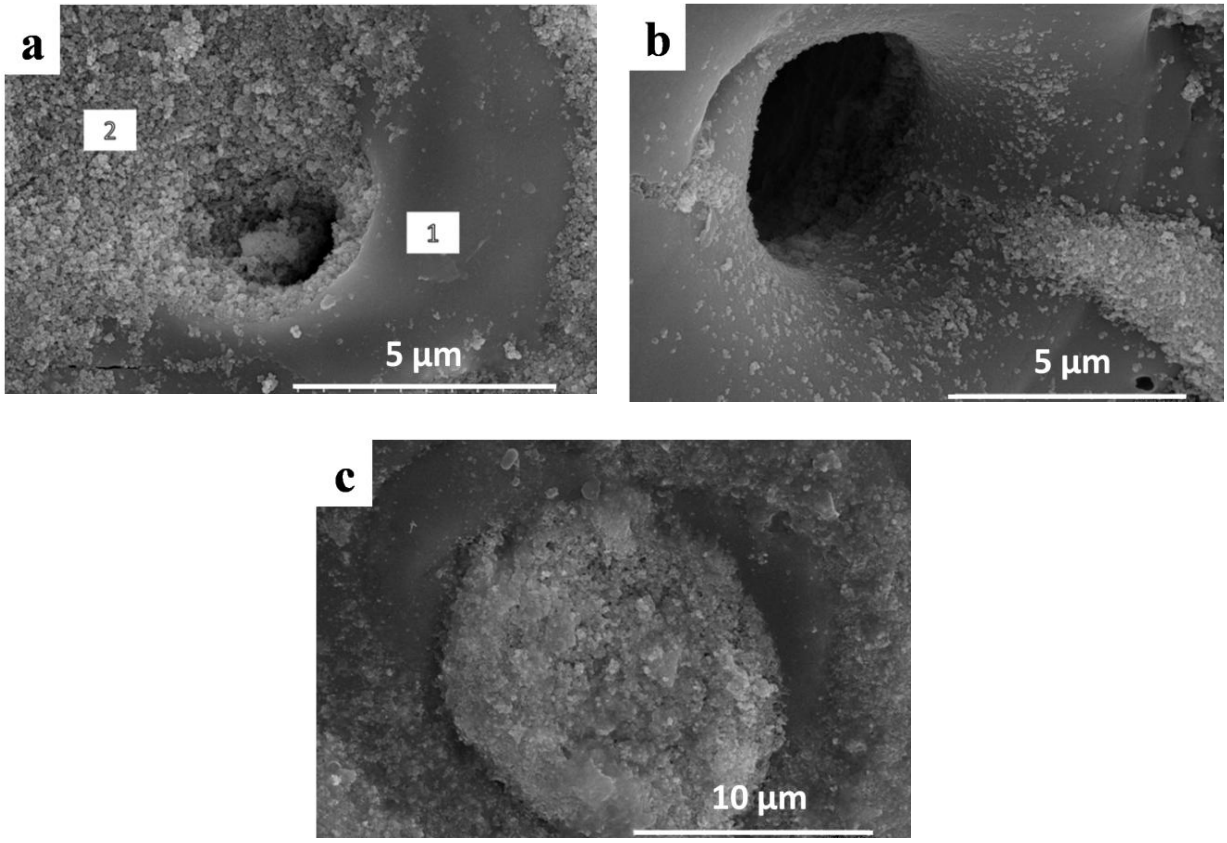

Figure 4-8 SEM images from the vicinity of pores for the sample coated under 0.4 A/cm^2 showing (a) accumulation of white particles around pores, (b) absorbance of zirconia nanoparticles toward pores and (c) porosity filling by nano zirconia particles.

Cross-sectional TEM analysis was conducted of the sample coated at 0.4 A/cm^2 current density is shown in Figure 4-9. The observations revealed four general areas in the coating microstructure. Starting from the substrate, sub-layer 1 shows a crystalline and dense structure. By going toward the top of the coating, sub-layer 2 is a mixture of a crystalline structure along with dispersed spherical particles. The volume fraction of the dark spherical particles is increasing by moving further towards the surface region (sub-layer 3). Finally, a thin amorphous layer is present at the very top portion of the coating at the surface (sub-layer 4) as confirmed by electron diffraction.

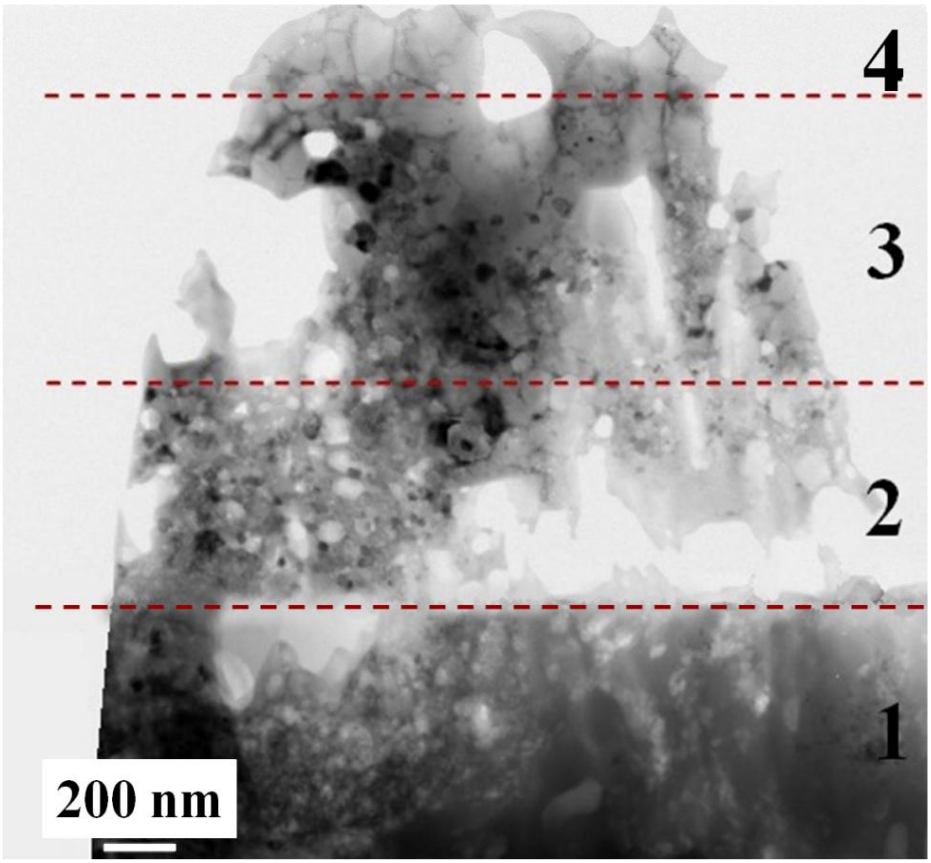

Figure 4-9TEM cross-sectional micrograph of the coating produced at 0.4 A/cm^2 showing formation of four sub-layers.

The HRTEM image of the sub-layer 1 presented in Figure 4-10 shows the presence of small round crystalline domains 2-3 nm in size embedded in long 20-40 nm crystalline structures. Measurements of d spacing (d = 2.3 Å) of the longer structures reveals existence of γ-Al_2O_3 (311) which is the main peak of this phase (JCPD, PDF# 47-1292) in area 1. Area 2 shows mainly presence of the small round crystalline structures with d = 2.57 Å consistent with the formation of α-Al_2O_3 (104) which is also the main peak of α alumina (PDF# 46-1212). Considering the alumina phase transformation temperature from amorphous to γ-Al_2O_3 (about 670 °C) and from γ- to α-Al_2O_3 (1100 °C), it is evident that the temperature in this region can be as high as 1100 °C and the α phase nucleates from within the γ phase. EDS analysis of this region, Figure 4-10 (b), confirms the formation of alumina. The results denote to the oxidation of the Al substrate and formation of an intermediate layer which was also visible during the SEM cross-sectional studies (Figure 4-4).

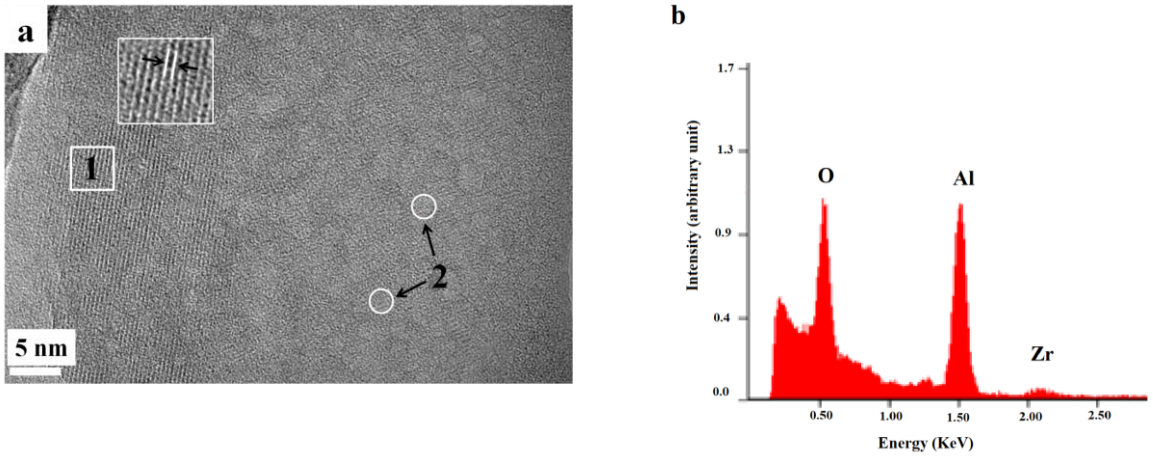

Figure 4-10 (a) Transmission electron micrograph of sub-layer 1 for the sample treated at 0.4 A/cm^2, and (b) EDS spectrum of sub-layer 1.

Figure 4-11(a) is a HRTEM image from a region in sub-layer 2. Lattice space analysis showed the presence of fringes of (011) *t*-ZrO_2 (area 1), (-111) *m*-ZrO_2 (area 2) and (111) γ-Al_2O_3 (area 3). Figure 4-11(b) presents another area of this sub-layer, which is composed of *t*-ZrO_2 (011) (area 1), α-Al_2O_3 (104) (area 2) and *m*-ZrO_2 (-111) (area 3). The presence of the aforementioned phases was also verified with electron diffraction analysis.

Figure 4-11(c) presents a selected area electron diffraction (SAED) pattern taken from a region in the sub-layer 2 showing a ring pattern characteristic of diffraction from a polycrystalline sample. The diffraction rings 2, 5 and 6 correspond to (011), (112) and (121) reflections of *t*-ZrO_2, respectively. In addition, the rings 3 and 4 are consistent with the (104) and (400) reflections of α-Al_2O_3, respectively, and rings 1 and 7 correspond to (-111) *m*-ZrO_2 and (440) γ-Al_2O_3 reflections, respectively. It should be noted that these findings are consistent with the XRD analysis conducted on this sample, Figure 4-3.

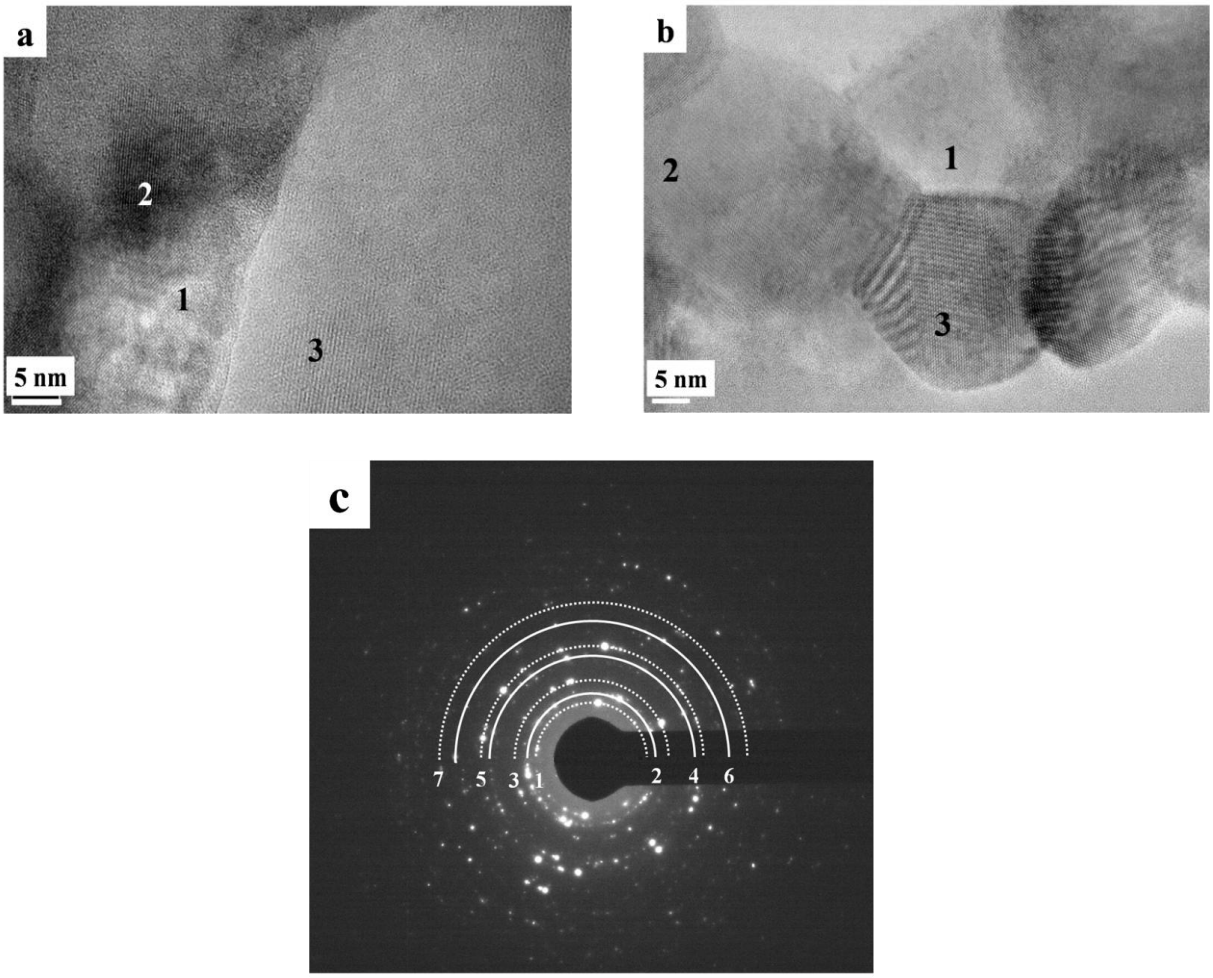

Figure 4-11 (a) and (b) HRTEM micrographs of sub-layer 2 from the sample treated at 0.4 A/cm^2 and (c) electron diffraction pattern from sub-layer 2.

Based on these results, the *m*-ZrO_2 particles can reach this sub-layer through the electrophoretic process and the phase transformation from monoclinic to tetragonal zirconia can be facilitated through the PEO process where high energies prevail. The temperature in this sub-layer is expected to be high enough for the monoclinic to tetragonal zirconia phase transformation. The nature of this transformation in sub-layer 2 was further investigated by high-resolution observations of the region around m-ZrO_2 particles. Figure 4-12 is a HRTEM image of a spherical m-ZrO_2 particle (dark particles in the center and up right side of the micrograph). It is interesting to note that t-ZrO_2 domains developed (areas 1 and 2) at the surface of the spherical

particle manifesting the monoclinic to tetragonal phase transformation. It should be noted that the monoclinic phase is stable up to 1170 °C, where it transforms to tetragonal phase. In this case, similar surface energy for m-ZrO_2 (1537 mJ/m^2) and *t*-ZrO_2 (1532 mJ/m^2) can further facilitate the phase transformation.

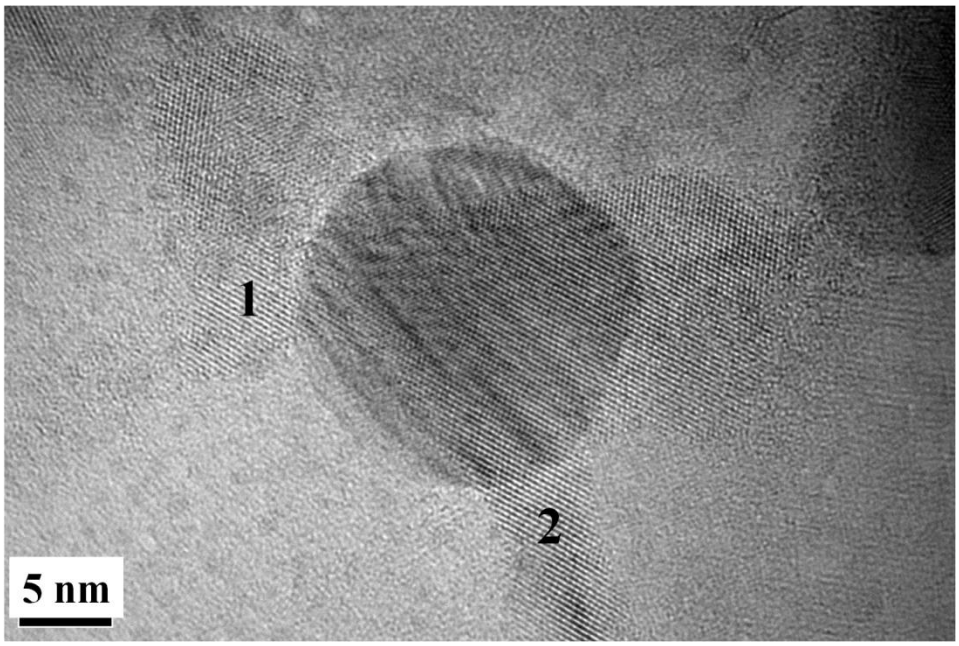

Figure 4-12HRTEM micrograph showing a partially transformed m-ZrO_2 particle.

TEM observations in the sub-layer 3 showed a distribution of dark nanoparticles in the range of 25-30 nm, Figure 4-13(a). Investigation of these particles via lattice space analysis revealed d = 3.73 Å which corresponds to (011) *m*-ZrO_2 (area 2 and 3). In addition, analysis in lighter areas (area 1) showed d = 4.49 Å which corresponds to (111) γ-Al_2O_3. HRTEM analysis of this region, Figure 4-13(b), also confirmed existence of (011) *m*-ZrO_2 (area 1 and 2) and (111) γ-Al_2O_3 (area 3). Finally, the top of the coating, sub-layer 4, exhibited an amorphous structure due to quenching effects from the electrolyte.

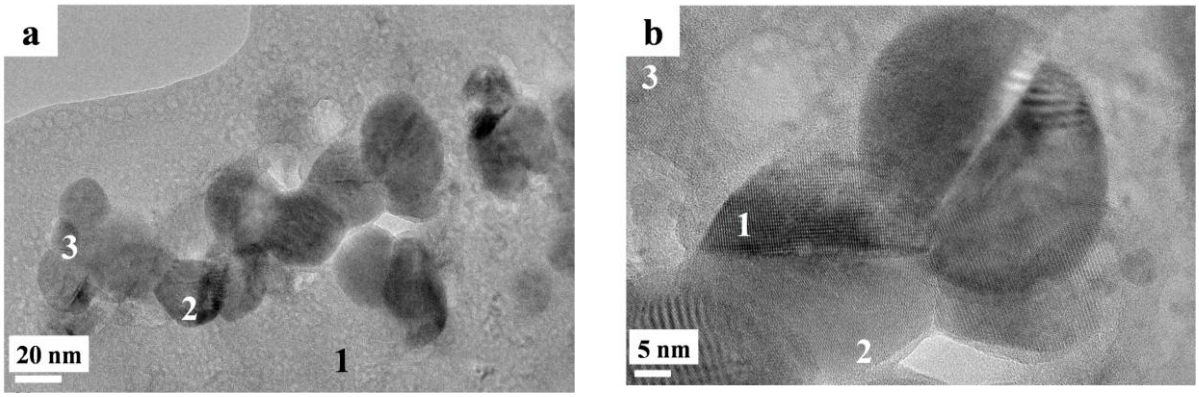

Figure 4-13 (a) and (b) Cross-sectional TEM images of sub-layer 3 showing formation of zirconia nanoparticles.

Based on the present findings, the coating formation and growth mechanism can be explained by interplay between oxidation of the Al substrate, transfer of zirconia particles from the electrolyte and arching and high temperature effects from processing. The evidence suggests that growth occurs via two simultaneously occurring processes. These are the (i) inward oxidation of the Al substrate where formation of dense α- and γ-Al_2O_3 prevails and (ii) transfer and deposition of zirconia particles from the electrolyte (outward growth). In this latter process, zirconia particles are deposited and intermixed with the existing alumina layer producing the observed nanocomposite microstructure. Depending on the energy input (based on the applied current density) during processing, the α-Al_2O_3 and *m*-ZrO_2 phases can transform to their high temperature γ-Al_2O_3 and *t*-ZrO_2 counterparts. Finally, the top coating layer remains amorphous due to the quenching effect from the electrolyte. It is evident that both the electrophoretic and PEO processes play a critical synergistic role. The first is transferring and depositing zirconia particles from the electrolyte while the second is oxidizing the substrate and provides the energy to produce desirable high temperature phases.

4.4 Conclusions

Alumina-zirconia nanostructured coatings were successfully deposited on Al 7075 alloy through a hybrid PEO-electrophoretic process. A nano zirconia containing electrolyte was used and a DC galvanostatic mode applied to coat the substrate. Microstructural properties of the coated layer were studied as a function of the processing current density. The coating primarily consisted of γ-alumina and monoclinic zirconia at low current densities, and α-alumina and tetragonal zirconia phases at high current densities.

TEM studies showed that the produced coatings were composed of four sub-layers. A dense sub-layer free from zirconia particles and composed of alumina phases was formed at the interface with the substrate. The next two sub-layers contained zirconia nanoparticles along with α and γ alumina, while the top sub-layer exhibited an amorphous structure. At the lower current densities, the electrophoretic process was dominant providing the driving force for nanoparticle incorporation in the coating from the electrolyte. At the higher current density, a PEO assisted electrophoretic process was prevailing for the formation of high temperature zirconia and alumina phases.

Chapter 5: Conclusions

- Alumina- zirconia nanocomposite coatings have been coated on Al-7075 alloy through PEO method in both zirconia incorporation routes of using Zr ions and zirconia particles in the electrolyte.
- High temperature phases with various microstructure and behavior have been produced by the PEO process.
- The composite layers have been formed with high growth rate of ~7 μm/min in this process.
- Tetragonal zirconia phase has been formed at room temperature in both experimental routes without using any stabilizer.
- In all coatings, polarization resistance and corrosion current density have been improved. The PEO coated layer in K_2ZrF_6 electrolyte and 300 s in particular showed the best behavior with 2.5 orders of magnitude lower corrosion current density than Al alloy.
- The alumina- zirconia PEO coatings have been affected the tribological behavior of Al alloy substrates. For the coatings produced under optimized conditions, friction coefficient of 0.14 and the mean wear rate of about 1.52×10^{-6} (mm^3N^{-1} m^{-1}) have been obtained, which are about 5 and 120 times lower than those for the Al substrate in the same test.

- Applying power in the galvanostatic mode has been resulted in more compact layers formation while in the potentiostatic mode, more high temperature phases could be formed.
- In the experimental route of applying coatings via Zr ions in the electrolyte, high temperature phases have been obtained by applying lower processing power. While in the route of adding nanoparticles in the electrolyte, higher energy has been needed to carry out the coating process, which can refer to the different coating mechanisms.
- In the case of tribological behavior, lower wear rate has been obtained for the coatings produced via K_2ZrF_6 electrolyte, while in the case of friction coefficient, the layers coated in the zirconia containing electrolyte have been shown better results.
- Study the coatings' microstructure by TEM showed development of four sub-layers. Incorporation of zirconia as a second phase has been discussed through a PEO assisted electrophoretic process. By approaching the surface from the substrate, high temperature phases were reduced while the incorporation of zirconia was increased.
- The mechanism of composite coating formation in case of applying coatings in a Zr containing electrolyte was oxidation of Al substrate to form alumina matrix and oxidation of Zr ions in the electrolyte to provide zirconia in the composite. In case of composite formation by adding zirconia nanoparticles to the electrolyte, the coating mechanism was an electrophoretic-PEO hybrid process. In this case, the electrophoretic process was responsible for zirconia particles movment in the electrolyte and PEO process was responsible for oxidation of Al substrate to form alumina.

Publications to date

[1] Nastaran Barati and Efstathios I. Meletis, 2018. Investigation of Al_2O_3-ZrO_2 nanocomposites coated on aluminum alloy by plasma electrolytic-electrophoretic hybrid process. Submitted to *ACS Applied Nano Materials*.

[2] Nastaran Barati, Aleksey Yerokhin, Farhad Golestanifard, Saeid Rastegari, Efstathios I. Meletis, 2017. Alumina- zirconia coatings produced by Plasma Electrolytic Oxidation on Al alloy for corrosion resistance improvement. *Journal of Alloys and Compounds, 724*, pp.435-442.

[3] Barati, N., Meletis, E.I., Golestani Fard, F., Yerokhin, A., Rastegari, S., Faghihi-Sani, M.A., 2015. Al_2O_3- ZrO_2 nanostructured coatings using DC plasma electrolytic oxidation to improve tribological properties of Al substrates. *Applied Surface Science, 356*, pp.927-934.

[4] Barati, N., Meletis, E.I., Golestani Fard, F., April 2017. Al_2O_3-ZrO_2 Composite coatings on aluminium through a hybrid Plasma Electrolytic-Electrophoretic process, 44th *International Conference on Metallurgical Coatings and Thin Films, 44th ICMCTF*, San Diego, California, USA.

[5] Nastaran Barati and Efstathios I. Meletis, May 2016. In-situ Formation of nanostructured Alumina-Zirconia converted layers on Al-7075 through plasma electrolytic technique. *3rd International Conference on Surfaces, Coatings and Nanostructured Materials*, University of Texas at Arlington, USA.

[6] Nastaran Barati, Farhad Golestanifard and Efstathios I. Meletis, June 2016.

Aluminum Zirconia nanocomposite coatings on aluminum via Plasma Electrolytic Oxidation, *5th International Conference from Nanoparticles and Nanmaterials to Nanodevices and Nanosystems, 5th IC4N*, Porto Heli, Greece.

References

[1] Abreu, C. M., Cristóbal, M. J., Figureueroa, R., Pena, G., 2015. Wear and corrosion performance of two different tempers (T6 and T73) of AA7075 aluminum alloy after nitrogen implantation. *Journal of Applied Surface Science, 327,* pp. 51-61.

[2] Zhang, Q., Wan, Y., Li, Y., Yang, S., Yao, W., 2013. Friction reducing behavior of stearic acid film on a textured aluminum substrate. *Journal of Applied Surface Science, 280,* pp.545-549.

[3] Gencer, Y., Gulec, A., 2012. The effect of Zn on the microarc oxidation coating behavior of synthetic Al-Zn binary alloys. *Journal of Alloys Compound, 525*, pp.159-165.

[4] McNiell, W., Gruss, L.L., 1966. *Anodic spark reaction processes and articles*, US Patent 3, 293, 158.

[5] Yerokhin, A. L., Shatrov, T. A., Samsonov, V., Shashkov, P., Pilkington, A., Leyland, A., Matthews, A., 2005. Oxide ceramic coatings on aluminum alloys produced by a pulsed bipolar plasma electrolytic oxidation process. *Surface and Coatings Technology, 199*, pp.150-157.

[6] Sabatini, G., Ceschini, L., Martini, C., Williams, J. A., Hutchings, I. M., 2010. Improving sliding and abrasive wear behavior of cast A356 and wrought AA7075 aluminum alloys by plasma electrolytic oxidation. *Materials and Design, 31*, pp. 816-828.

[7] Wen, L., Wang, Y., Zhou, Y., Ouyang, J., Guo, L., Jia, D., 2010. Corrosion evaluation of microarc oxidation coatings formed on 2024 aluminum alloy. *Corrosion Science, 5*2, pp. 2687-2696.

[8] Da Costa, C. E., Zapata, W.C., Velasco, F., Ruiz-Prieto, J. M., Torralba, J. M., 1999. Wear behavior of aluminum reinforced with nickel aluminide MMCs. *Journal of Materials*

Processing Technology, 92, pp.66-70.

[9] Chandrasekharaiah, T. M., Kori, S. A., 2009. Effect of grain refinement and modification on the dry sliding wear behavior of eutectic Al-Si alloys. *Tribology International, 42*, pp.59-65.

[10] Venkataraman, B., Sundararajan, G., 2000. Correlation between the characteristics of mechanically mixed layer and wear behavior of aluminum, Al-7075 alloy and Al- MMCs. *Wear 245*, pp.22-38.

[11] Wang, Z., Wu, L., Qi, Y., Jiang, Z., 2010. In situ formation of Al_2O_3-SiO_2-SnO_2 composite ceramic coating by micro arc oxidation on Al-20%Sn alloy. *Applied Surface Science, 256*, pp.3443-3447.

[12] Barati, N., Yerokhin, A., Golestanifard, F., Rastegari, S., Meletis, E. I., 2017. Alumina-zirconia coatings produced by Plasma Electrolytic Oxidation on Al alloy for corrosion resistance improvement. *Journal of Alloys and Compound, 724*, pp.435-442.

[13] Arunnellaiappan, T., Ashfaq, M., RamaKrishna, L., Rameshbabu, N., 2016. Fabrication of corrosion-resistant Al_2O_3-CeO_2 composite coating on AA7075 via plasma electrolytic oxidation coupled with electrophoretic deposition. *Journal of Ceramics International, 42*, pp.5897-5905.

[14] Basu, B., Vleugels, J., Van Der Biest, O., 2004. ZrO_2-Al_2O_3 composites with tailored toughness. *Journal of Alloys and Compound, 372*, pp.278-284.

[15] Zhang, Q., Wan, Y., Li, Y., Yang, S., Yao, W., 2013. Friction reducing behavior of stearic acid film on a textured aluminum substrate. *Applied Surface Science, 280*, pp.545-549.

[16] Fischer, A., Bobzin, K., 2011. Friction wear and wear protection. Wiley vch, Germany.

[17] Wang, H., Wang, H., 2007. Fabrication of self-lubricating coating on aluminum and its

frictional behavior. *Applied Surface Science, 253*, pp.4386-4389.

[18] Polat, A., Makaraci, M., Usta, M., 2010. Influence of sodium silicate concentration on structural and tribological properties of microarc oxidation coatings on 2017A aluminum alloy substrate. *Journal of Alloys and Compounds, 504*, pp.519-526.

[19] Sieber, M., Mehner, T., Dietrich, D., Alisch, G., Nickel, D., Meyer, D., Scharf, I., Lampke, T., 2014. Wear-resistant coatings on aluminum produced by plasma anodizing-A correlation of wear properties, microstructure, phase composition and distribution. *Surface Coating Technology, 240*, pp.96-102.

[20] Qin, X. W., Guo, Y., Xie, Z., 2008. Self-lubricative coating grown by microplasma oxidation on aluminum alloys in the solution of aluminate-graphite. *Applied Surface Science, 254*, pp.6395-6399.

[21] Hart L. D., Lense, E., 2006. *Alumina Chemicals: Science and Technology Handbook*, Wiley.

[22] Ighodaro, O. L., Okoli, O. I., 2008. Fracture Toughness Enhancement for Alumina Systems: A Review. *International Journal of Applied Ceramic Technology, 5*, 313-323.

[23] Badwal, S., Bannister, M., 1993. *Science and Technology of Zirconia V*, Technomic.

[24] Sōmiya, S., Yamamoto, N., Yanagida, H., 1986. *Science and Technology of Zirconia I*, American Ceramic Society.

[25] Reece, M. J., Tetlow, P. L., Galiotis, C., 1992. Phase transformation around indentations in zirconia. *Journal of Materials Science Letter, 11*, pp.575-577.

[26] Gupta, T. K., Bechtold, J. H., Kuznicki, R. C., Cadoff, L. H., Rossing, B. R., 1977. Stabilization of tetragonal phase in polycrystalline zirconia. *Materials Science, 12*, pp.2421-2426.

[27] Green, D. J., 1982. Critical Microstructures for Microcracking in Al_2O_3-ZrO_2 Composites, *Journal of American Ceramic Society, 65*, 610-614.

[28] Kerkwijk, B., 1999. *Wear and friction of nanostructured zirconia and alumina ceramics and composites*, Enschede: Department of Chemical Engineering, University of Twente.

[29] Basu, B., Vleugel, J., Biest, O., 2004. Microstructure–toughness–wear relationship of tetragonal zirconia ceramics. *Journal of European Ceramic Society, 24*, pp.2031-2040.

[30] Hutchings, I. M., 1992. Tribology: *Friction and Wear of Engineering Materials*, butterworth Heinemann, London.

[31] Hah, S. R., Fischer, T. E., Gruffel, P., Carry, C., 1995. Effect of grain boundary dopants and mean grain size on tribomechanical behavior of highly purified a-alumina in the mild wear regime. *Wear, 181-183*, pp.165-177.

[32] He, Y., Winnubst, L., Burggraaf, A. J., Verweij, H., 1996. Grain-size dependence of sliding wear in tetragonal zirconia polycrystals. *Journal of American Ceramic Society, 79*, pp.90-96.

[33] Wang, Y. S., He, C., Hockey, B. J., Lacey, P. I., Hsu, S. M., 1995. Wear transitions in monolithic alumina and zirconia-alumina composites. *Wear, 181-183*, pp.156-164.

[34] Esposito, L., Moreno, R., Herencia, A. J., Tucci, A., 1998. Sliding wear response of an alumina-zirconia system. *Journal of European Ceramic Society, 18 (1)*, pp.15-22.

[35] Keyvani, A., Saremi, M., Sohi, M. H., 2010. Microstructural stability of zirconia-alumina composite coatings during hot corrosion test at 1050 °C. *Journal of Alloys and Compounds, 506*, 103-108.

[36] Lianga, B., Liaob, H., Dinga, C., Coddet, C., 2005. Nanostructured zirconia-30 vol.% alumina composite coatings deposited by atmospheric plasma spraying, *Thin Solid Films, 484*, pp.225- 231.

[37] Naga, S. M., Kenawy, S. H., Awaad, M., Roos, E., Lyutovich, A., Ruoff, H., Krisch, R., 2011. Combined zirconia toughened alumina (ZTA) stacks obtained by electron beam physical vapour deposition. *Ceramic International, 37*, pp.771-777.

[38] Hao, Y., Li, J., Yang, X., Wang, X., Lu, L., 2004. Preparation of ZrO_2-Al_2O_3 composite membranes by sol-gel process and their characterization. *Materials Science Engineering A 367*, pp.243-247.

[39] Bjormander, C., 2006. CVD deposition and characterization of colored Al_2O_3/ZrO_2 multilayers. *Surface Coating Technology, 201*, pp.4032-4036.

[40] Chen, Y., Yang, Y., Chu, Z., Chen, X., Wang, L., Liu, Z., Dong, Y., Yan, D., Zhang, J., Kang, Z., 2018. Microstructure and properties of Al_2O_3-ZrO_2 composite coatings prepared by air plasma spraying. *Applied Surface Science, 431*, pp.93-100.

[41] Berghaus, J. O., Legoux, J., Moreau, C., Tarasi, F., Chra´ska, T., 2008. Mechanical and thermal transport properties of suspension thermal-sprayed Alumina Zirconia composite coatings. *Journal of Thermal Spray Technology, 17*, pp.91-104.

[42] Dejang, N., Limpichaipanit, A., Watcharapasorn, A., Wirojanupatump, A., Niranatlumpong, P., Jiansirisomboon, S., 2011. Fabrication and properties of plasma-sprayed Al_2O_3/ZrO_2 composite coatings. *Journal of Thermal Spray Technology, 20*, pp.1259-1268.

[43] Abdel-Samad, A., El-Bahloul, A. M. M., Lugscheider, E., Rassoul, S.A., 2000. A comparative study on thermally sprayed Alumina based ceramic coatings. *Journal of Materials Science, 35(12)*, pp.3127-3130.

[44] Ito, A., You, Y., Ichikawa, T., Tsuda, K., Goto, T., 2014. Preparation of Al_2O_3-ZrO_2 nanocomposite films by laser chemical vapor deposition. *Journal of the European Ceramic Society, 34(1),* pp.155-159.

[45] Wanga, X., Tiana, J., Yub, X., Shanb, Y., Liua, Z., Yin, Y., 2008. Effect of microstructure on the fracture behavior of micro-nano ZTA composite. *Materials Chemistry and Physics, 112 (1),* pp.213-217.

[46] Shanmugavelayutham, G., Kobayashi, A., 2007. Mechanical properties and oxidation behavior of plasma sprayed functionally graded zirconia-alumina thermal barrier coatings. *Materials Chemistry and Physics, 103*, pp.283-289.

[47] Filiaggi, M. J., Pilliar, R. M., Coombs, N. A., 1993. Post-plasma-spraying heat treatment of the HA coating/Ti-6Al-4V implant system. *Biomaterials Research, 27*, pp.191-198.

[48] Cheng, Y. H., Gupta, P., Meletis, E. I., 2010. Surface characteristics of 4340 steel treated by electro plasma processing. *Materials Science, 45*, pp.562-565.

[49] Meletis, E.I., Nie, X., Wang, F., Jiang, J.C., 2002. Electrolytic plasma processing for cleaning and metal-coating of steel surfaces. *Surface Coating Technology, 150*, pp.246-256.

[50] Yerokhin, A. L., Nie, X., Leyland, A., Matthews, A., Dowey, S. J., 1999. Review plasma electrolysis for surface engineering. *Surface Coating Technology, 122*, pp.73-93.

[51] Carpio, P., Salvador, M. D., Borrell, A., Sánchez, E, Moreno, R., 2016. Alumina-zirconia coatings obtained by suspension plasma spraying from highly concentrated aqueous suspensions. *Surface Coating, 72*, pp.713-719.

[52] Park, S. J., Choi, D. J., 2017. Synthesis of porous Al_2O_3/ZrO_2 nanocomposites by chemical vapor deposition. *Journal of Advanced Applied Ceramic, 116*, pp.236-241.

[53] Yan, Y., Han, Y., Huang, J., 2008. Formation of Al_2O_3-ZrO_2 composite coating on

zirconium by micro-arc oxidation. *Scripta Materialia, 59*, pp.203-206.

[54] Yan, Y., Han, Y., Li, D., Huang, J., Lian, Q., 2010. Effect of $NaAlO_2$ concentrations on microstructure and corrosion resistance of Al_2O_3/ZrO_2 coatings formed on zirconium by micro-arc oxidation. *Applied Surface Science, 256*, pp.6359-6366.

[55] Malinovschi, V., Marin, A., Negrea, D., Andrei, V., Coaca, E., Mihailescu, C.N., Lungu, C.P., 2018. Characterization of Al_2O_3/ZrO_2 composite coatings deposited on Zr-2.5Nb alloy by plasma electrolytic oxidation. *Applied Surface Science, 451*, pp.169-179.

[56] Zhang, L., Zhang, W., Han, Y., Tang, W., 2016. A nanoplate-like α-Al_2O_3 out-layered Al_2O_3-ZrO_2 coating fabricated by micro-arc oxidation for hip joint prosthesis. *Applied Surface Science, 361*, pp.141-149.

[57] Cheng, Y., Cao, J., Peng, Z., Wang, Q., Matykina, E., Skeldon, P., Thompson, G. E., 2014. Wear-resistant coatings formed on Zircaloy-2 by plasma electrolytic oxidation in sodium aluminate electrolytes. *Electrochimica Acta, 116*, 453-466.

[58] Luo, H., Cai, Q., He, J., Wei, B., 2009. Preparation and properties of composite ceramic coating containing Al_2O_3-ZrO_2-Y_2O_3 on AZ91D magnesium alloy by plasma electrolytic oxidation. *Applied Physics, 9*, pp.1341-1346.

[59] Arrabal, R., Matykina, E., Skeldon, P., Thompson, G. E., 2008. Incorporation of zirconia particles into coatings formed on magnesium by plasma electrolytic oxidation. *Journal of Materials Science, 43*, pp.1532-1538.

[60] Matykina, E., Arrabal, R., Skeldon, P., Thompson, G. E., 2008. Incorporation of zirconia nanoparticles into coatings formed on aluminum by AC plasma electrolytic oxidation. *Journal of Applied Electrochemistry, 38*, pp.1375-1383.

[61] Matykina, E., Arrabal, R., Monfort, F., Skeldon, P., Thompson, G.E., 2008. Incorporation of

zirconia into coatings formed by DC plasma electrolytic oxidation of aluminum in nanoparticle suspensions. *Applied Surface Science, 255*, pp.2830-2839.

[62] Shoaei-Rad, V., Bayati, M.R., Golestani-Fard, F., Zargar, H.R., Javadpour, J., 2011. Fabrication of ZrO_2-Al_2O_3 hybrid nano-porous layers through micro arc oxidation process. *Materials Letter*, *65*, pp.1835-1838.

[63] Sieber, M., Mehner, T., Dietrich, D, Alisch, G., Nickel, D., Meyer, D., Scharf, I., Lampke, T., 2014. Wear-resistant coatings on aluminum produced by plasma anodizing-A correlation of wear properties, microstructure, phase composition and distribution. *Surface Coating Technology*, *240*, pp.96-102.

[64] Wu, X., Qin, W., Guo, Y., Xie, Z., 2008. Self-lubricative coating grown by micro-plasma oxidation on aluminum alloys in the solution of aluminate-graphite. *Applied Surface Science*, *254*, pp.6395-6399.

[65] Naga, S. M., Kenawy, S. H., Awaad, M., Roos, E., Lyutovich, A., Ruoff, H., Krisch, R., 2011. Combined zirconia toughened alumina (ZTA) stacks obtained by electron beam physical vapor deposition. *Ceramics International*, *37*, pp.771-777.

[66] Hadraba, H., Drdlik, D., Chlup, Z., Maca, K., Dlouhy, I., Cihlar, J., 2012. Laminated alumina/zirconia ceramic composites prepared by electrophoretic deposition. *Journal of European Ceramics Society*, 32, pp.2053-2056.

[67] Zheng, Y., Li, H., Zhou, T., 2011. Microstructure and mechanism of Al_2O_3-ZrO_2 eutectic coating prepared by combustion-assisted thermal explosion spraying. *Applied Surface Science*, *258*, pp.1531-1534.

[68] Tang, M., Li, W., Liu, H., Zhu, L., 2012. Preparation Al_2O_3/ZrO_2 composite coating in an alkaline phosphate electrolyte containing K_2ZrF_6 on aluminum alloy by microarc oxidation. *Applied Surface Science, 258,* pp.5869-5875.

[69] Erokhine, A., Voevodin, A. A., Schmertzler, R. D., 1998. *Method for forming coatings by electrolyte discharge and coatings formed thereby*. US Patent No. 5720866, Feb.24.

[70] Dunleavy, C.S., Curran, J.A., Clyne, T.W., 2013. Time dependent statistics of plasma discharge parameters during bulk AC plasma electrolytic oxidation of aluminum. *Applied Surface Science, 268*, pp.397-409.

[71] Aliasghari, S., Skeldon, P., Thompson, G. E., 2014. Plasma electrolytic oxidation of titanium in a phosphate/silicate electrolyte and tribological performance of the coatings. Applied Surface Science, 316, pp.463-476.

[72] Zhang, Z., Gu, B., Zhang, W., Kan, G., Sun, J., 2012. The enhanced characteristics of osteoblast adhesion to porous Zinc-TiO_2 coating prepared by plasma electrolytic oxidation. *Applied Surface Science, 258,* pp. 6504-6511.

[73] Xue, W., Shi, X., Hua, M., Li, Y., 2007. Preparation of anti-corrosion films by microarc oxidation on an Al-Si alloy. *Applied Surface Science, 253,* pp.6118-6124.

[74] Shoaei-Rad, V., Bayati, M. R., Zargar, H. R., Javadpour, J., Golestani-Fard, F., 2012. In situ growth of ZrO_2 Al_2O_3 nano-crystalline ceramic coatings via micro arc oxidation of aluminum substrates. *Materials Research Bulletin, 47*, pp.1494-1499.

[75] Kern, F., Palmero, P., García Marro, F., Mestra, A., 2015. Processing of alumina-zirconia composites by surface modification route with enhanced hardness and wear resistance. Ceramics International, 41, pp.889-898.

[76] Wang, L., Chen, L., Yan, Z., Wang, H., Peng, J., 2010. The influence of additives on the

stability behavior of electrolyte, discharges and PEO films characteristics. Journal of Alloys and Compounds, 493, pp.445-452.

[77] Rudnick, L. R., 2009. *Lubricant Additives: Chemistry and Applications*, Second Edition, CRC Press.

[78] Aguilar, D. H., Torres-Gonzalez, L. C., Torres-Martinez, L. M., 2000. A study of the crystallization of ZrO_2 in the Sol-Gel system: ZrO_2-SiO_2. *Journal of Solid State Chemistry, 158*, pp.349-357.

[79] Cheng, Y., Wu, F., Dong, J., Wu, X., Xue, Z., Matykina, E., Skeldon, P., Thompson, G. E., 2012. Comparison of plasma electrolytic oxidation of zirconium alloy in silicate and aluminate-based electrolytes and wear properties of the resulting coatings. *Electrochimica Acta. 85*, pp.25-32.

[80] Rao, P.G., Iwasa, M., Tanaka, T., Kondoh, I., Inoue, T., 2003. Preparation and mechanical properties of Al_2O_3-15wt.%ZrO_2 composites. *Scripta Materialia*, *48*, pp.437-441.

[81] Palmour, H., Davis, R. F., Hare, T. M., 1978. Processing of Crystalline Ceramics, University conference on ceramic science, plenum press.

[82] Wu, Z., Yao, Z., Jia, F., Jiang, Z., 2010. Structure and property of micro arc oxidation ceramic coatings on Al alloy in K_2ZrF_6 solution. *Advanced Materials Research, 105*, 505-508.

[83] Curran, J. A., Clyne, T. W., 2005. Thermo-physical properties of plasma electrolytic oxide coatings. *Surface Coating Technology*, *199*, 168-176.

[84] Sreekanth, D., Rameshbabu, N., Venkateswarlu, K., 2012. Effect of various additives on morphology and corrosion behavior of ceramic coatings developed on AZ31 magnesium alloy by plasma electrolytic oxidation. *Ceramics International*, *38*, pp.4607-4615.

[85] Chen, H., Lv, G., Zhang, G., Pang, H., Wang, X. Q., Lee, H. J., Yang, S.Z., 2010. Corrosion performance of plasma electrolytic oxidized AZ31 magnesium alloy in silicate solutions with different additives. *Surface Coating Technology, 205*, pp.S32-S35.

[86] Raj, V., Ali, M. M., 2009. Formation of ceramic alumina nanocomposite coatings on aluminum for enhanced corrosion resistance. *Journal of Materials Processing Technology, 209*, pp.5341-5352.

[87] Menezes, P. L., Ingole, S. P., Nosonovsky, M., Kailas, S. V., Lovell, M. R., 2014. *Tribology for Scientists and Engineers*, Springer.

[88] Kerkwijk, B., Garcia, M., van Zyl, W. E., Winnubst, L., Mulder, E. J., Schipper, D. J., Verweij, H., 2004. Friction behaviour of solid oxide lubricants as second phase in α-Al_2O_3 and stabilised ZrO_2 composites. *Wear, 256*, pp.182-189.

[89] He, Y. J., Winnubst, A. J.A., Schipper, D. J., Burggraaf, A. J., Verweij, H., 1997. Effects of a second phase on the tribological properties of Al_2O_3 and ZrO_2 ceramics. *Wear, 210*, pp.178-187.

[90] Bartolom´e, J. F., Pecharrom´an, C., Moya, J. S., Mart´ın, A., Pastor, J. Y., Llorca, J., 2006. Percolative mechanism of sliding wear in alumina/zirconia composites. *Journal of European Ceramic Society, 26*, pp.2619-2625.

[91] Albert, C., Grard, M., Phillips, C. M., 2012. *Aluminum and its alloys, their properties, thermal treatment and industrial application*, Ulan Press.

[92] Park, G. H., Kim, J. T., Park, H. J., Kim, Y. S., Jeong, H. J., Lee, N., Seo, Y., Suh, J. Y., Son, H. T., Wang, W. M., Park, J. M., Kim, K. B., 2016. Development of lightweight Mg-Li-Al alloys with high specific strength. *Journal of Alloys and Compounds, 680*, pp.116-120.

[93] Shin, J., Kim, T., Kim, D., Kim, D., Kim, K., 2017. Castability and mechanical properties of new 7xxx aluminum alloys for automotive chassis/body applications. *Journal of Alloys and Compound, 698,* pp.577-590.

[94] Recloux, I., Mouanga, M., Druart, M., Paint, Y., Olivier, M. G., 2015. Silica mesoporous thin films as containers for benzotriazole for corrosion protection of 2024 aluminum alloys. *Applied Surface Science, 346,* pp.124-133.

[95] Groot, C., Peekema, R.M., 1955. *The corrosion of aluminum and its alloys*, Richland, Washington, Hanford Atomic Products Operation.

[96] Ji, S., Weng, Y., Wu, Z., Ma, Z., Tian, X., Fu, R. K.Y., Lin, H., Wu, G., Chu, P. K., Pan, F., 2017. Excellent corrosion resistance of P and Fe modified micro-arc oxidation coating on Al alloy. *Journal of Alloys and Compound, 710,* pp.452-459.

[97] Hu, W., Xu, J., Lu, X., Hu, D., Tao, H., Munroe, P., Xie, Z. H., 2016. Corrosion and wear behaviors of a reactive-sputter-deposited Ta_2O_5 nanoceramic coating. *Applied Surface Science*, 368, pp.177-190.

[98] Rahmati, B., Sarhan, A. A. D., Basirun, W. J., Abas, W. A. B. W., 2016. Ceramic tantalum oxide thin film coating to enhance the corrosion and wear characteristics of Ti-6Al-4V alloy. *Journal of Alloys and Compound, 676,* pp.369-376.

[99] Fatimah, S., Kamil, M.P., Kwon, J. H., Kaseem, M., Ko, Y.G., 2017. Dual incorporation of SiO_2 and ZrO_2 nanoparticles into the oxide layer on 6061 Al alloy via plasma electrolytic oxidation: Coating structure and corrosion properties. *Journal of Alloys and Compound, 707,* pp.358-364.

[100] Barati, N., Meletis, E.I., Golestani Fard, F., Yerokhin, A., Rastegari, S., Faghihi-Sani, M.A., 2015. Al_2O_3-ZrO_2 nanostructured coatings using DC plasma electrolytic oxidation to improve tribological properties of Al substrates. *Applied Surface Science, 356*, pp.927-934.

[101] Kim, D., Sung, D., Lee, J., Kim, Y., Chung, W., 2015. Composite plasma electrolytic oxidation to improve the thermal radiation performance and corrosion resistance on an Al substrate. *Applied Surface Science, 357*, pp.1396-1402.

[102] Fadaee, H., Javidi, M., 2014. Investigation on the corrosion behavior and microstructure of 2024-T3 Al alloy treated via plasma electrolytic oxidation. *Journal of Alloys and Compound, 604*, pp.36-42.

[103] Fatkullin, A. R., Parfenov, E. V., Yerokhin, A., Lazarev, D. M., Matthews, A., 2015. Effect of positive and negative pulse voltages on surface properties and equivalent circuit of the plasma electrolytic oxidation process. *Surface and Coatings Technology, 284*, pp.427-437.

[104] Duan, H., Yan, C., Wang, F, 2007. Effect of electrolyte additives on performance of plasma electrolytic oxidation films formed on magnesium alloy AZ91D, *Electrochimica Acta, 52*, pp.3785-3793.

[105] Cullity, B.D., 1978. *Elements of X-ray Diffraction*, Addison-Wesley Pub, Notre Dame.

[106] Galuskova, D., 2011. Corrosion of structural ceramics under sub-critical conditions in aqueous sodium chloride solution and in Deionized water. Part II: Dissolution of Al_2O_3-Based Ceramics. *Journal of American Ceramic Society, 94*, pp.3044-3052.

[107] Pareja, R. R., Ibáñez, R. L., Martín, F., Ramos-Barrado, J. R., Leinen, D., 2006. Corrosion behavior of zirconia barrier coatings on galvanized steel. *Surface and Coatings Technology, 200*, pp.6606-6610.

[108] Dean, J., Gu, T., Clyne, T.W., 2015. Evaluation of residual stress levels in plasma electrolytic oxidation coatings using a curvature method. *Surface and Coatings Technology, 269*, pp.47-53.

[109] Pabst, W., Gregorová, E., Malangré, D., Hostaša, J., 2012. Elastic properties and damping behavior of alumina–zirconia composites at room temperature. Ceramics International, 38, pp.5931-593.

[110] Lu, C., Liang, J., Zhou, J., Li, Q., Peng, Z., Wang, L., 2016. Characterization and corrosion behavior of plasma electrolytic oxidation coated AZ91-T6 magnesium alloy. *Surface and Coatings Technology, 304*, pp.179-187.

[111] Lou, B., Lin, Y., Tseng, C., Lu, Y., Duh, J., Lee, J., 2017. Plasma electrolytic oxidation coatings on AZ31 magnesium alloys with Si_3N_4 nanoparticle additives. *Surface and Coatings Technology, 332*, pp.358-367.

[112] Bian, G., Wang, L., Wu, J., Zheng, J., Sun, H., DaCosta, H., 2015. Effects of electrolytes on the growth behavior, microstructure and tribological properties of plasma electrolytic oxidation coatings on a ZA27 alloy. *Surface and Coatings Technology, 277*, pp.251-257.

[113] Bayati, M. R., Zargar, H. R., Talimian, A., Ziaee, A., Molaei, R., 2010. Characterization of Al_2O_3-TiO_2 nano porous solar absorbers derived via MAO/sol-gel hybrid process. *Surface and Coatings Technology, 205*, pp.2483-2489.

[114] K-Kęsik, A., Krok-Borkowicz, M., Dercz, G., Donesz-Sikorska, A., Pamuła, E., Simka, W., 2016. Multilayer coatings formed on titanium alloy surfaces by plasma electrolytic oxidation electrophoretic deposition methods. *Electrochimica Acta, 204*, pp.294-306.

[115] Liu, C., Liang, J., Zhou, J., Li, Q., Wang, L., Characterization of AZ31 magnesium alloy by duplex process combining laser surface melting and plasma electrolytic oxidation. *Applied Surface Science, 382*, pp.47-55.

[116] Arun, S., Arunnellaiappan, T., Rameshbabu, N., 2016. Fabrication of the nanoparticle incorporated PEO coating on commercially pure zirconium and its corrosion resistance. *Surface and Coating Technology, 305*, pp.264-273.

[117] Lu, X., Blawert, C., Huang, Y., Ovri, H., Zheludkevich, M. L., Kainer, K. U., 2016. Plasma electrolytic oxidation coatings on Mg alloy with addition of SiO_2 particles. *Electrochimica. Acta, 187*, pp.20-33.

[118] Hekmatfar, M., Moshayedi, S., Ghaffari, S.A., Rezaei, H.R., Golestani-Fard, F., 2011. Fabrication of HAp–8YSZ composite layer on Ti/TiO_2 nanoporous substrate by EPD/MAO method. *Materials Letters, 65*, pp.3421-3423.

[119] Van der Biest, O., Vandeperre, L. J., 1999. Electrophoretic deposition of materials, *Annual Review of Materials Science, 29*, pp.327-352.

[120] Barati, N., Yerokhin, A., Golestanifard, F., Rastegari, S., Meletis, E. I., 2017. Alumina-zirconia coatings produced by Plasma Electrolytic Oxidation on Al alloy for corrosion resistance improvement. *Journal of Alloys and Compounds, 724*, pp.435-442.

[121] Erkin Cura, M., Kim, S., Muukkonen, T., Varjus, S., Vaajoki, A., Söderberg, O., Suhonen, T., Kanerva, U., Wohn Lee, S., Hannula, S. P., 2013. Microstructure and tribological properties of pulsed electric current sintered alumina-zirconia nanocomposites with different solid lubricants. *Ceramics International, 39*, pp.2093-2105.

[122] Shoaei-Rad, V., Bayati, M. R., Golestani-Fard, F., Zargar, H. R., Javadpour, J., 2011. Fabrication of ZrO_2-Al_2O_3 hybrid nano-porous layers through micro arc oxidation process.

Materials Letters, *65*, pp.1835-1838.

[123] Liu, X., Zhu, L., Liu, H., Li, W., 2014. Investigation of MAO coating growth mechanism on aluminum alloy by two-step oxidation method. *Applied Surface Science, 293*, pp.12-17.

[124] Jiang, B. L., Wang, Y. M., 2010. Plasma electrolytic oxidation treatment of aluminum and titanium alloys. *Woodhead Publishing*, pp.110-154.

[125] Zhang, Y., Wu, Y., Chen, D., Wang, R., Li, D., Guo, C., Jiang, G., Shen, D., Yu, S., Nash, P., 2017. Micro-structures and growth mechanisms of plasma electrolytic oxidation coatings on aluminum at different current densities. *Surface and Coatings Technology, 321*, 236-246.

[126] Zhang, J., Fan, Y., Zhao, X., Ma, R., Du, A., Cao, X., 2018. Influence of duty cycle on the growth behavior and wear resistance of micro-arc oxidation coatings on hot dip aluminized cast iron. *Surface and Coatings Technology*, *337*, pp.141-149.

[127] Bakshi, U. A., Bakshi, V. U., 2010. *Elements of electrical engineering*. Technical Publications,1.

[128] NIST ASD Team, 2018. *NIST Atomic Spectra Database (version 5.5.6), National Institute of Standards and Technology*, Gaithersburg, MD, Available at: https://physics.nist.gov/asd.